PCCP

PERSPECTIVE

Computational electrochemistry: prediction of liquid-phase reduction potentials†

Cite this: *Phys. Chem. Chem. Phys.*, 2014, **16**, 15068

Aleksandr V. Marenich,*[a] Junming Ho,*[b] Michelle L. Coote,*[b] Christopher J. Cramer*[a] and Donald G. Truhlar*[a]

Received 11th April 2014,
Accepted 2nd June 2014

DOI: 10.1039/c4cp01572j

www.rsc.org/pccp

This article reviews recent developments and applications in the area of computational electrochemistry. Our focus is on predicting the reduction potentials of electron transfer and other electrochemical reactions and half-reactions in both aqueous and nonaqueous solutions. Topics covered include various computational protocols that combine quantum mechanical electronic structure methods (such as density functional theory) with implicit-solvent models, explicit-solvent protocols that employ Monte Carlo or molecular dynamics simulations (for example, Car–Parrinello molecular dynamics using the grand canonical ensemble formalism), and the Marcus theory of electronic charge transfer. We also review computational approaches based on empirical relationships between molecular and electronic structure and electron transfer reactivity. The scope of the implicit-solvent protocols is emphasized, and the present status of the theory and future directions are outlined.

1. Introduction

Many chemical reactions include steps involving actual or formal electron transfer from one reactant to another, resulting in oxidation or reduction. The tendency of a chemical species to lose or acquire electrons is quantitatively described by a key thermodynamic quantity called the reduction potential, which may be measured, for example, by cyclic voltammetry. However, in practice, the high reactivity of some interesting reagents (*e.g.*, organic radicals), or the irreversibility of a half-reaction, can make the direct experimental measurement of the corresponding reduction potentials difficult or unfeasible. Computational chemistry provides a valuable alternative to experiment in such cases. Recent advances have allowed for improved accuracy in predictions of many interesting equilibrium and kinetic chemical properties in the gas phase. Theoretical studies of condensed-phase processes have also become increasingly common and accurate, as a result of the development of more accurate continuum solvent models and combined quantum mechanical and molecular mechanical free energy methods. Therefore, well-chosen and validated combinations of theoretical models can now be used to make quantitative predictions of electrochemical quantities like reduction potentials. Indeed, comparisons of such predictions to experiment can now be useful for the assignment of specific chemical transformations to otherwise ambiguous observed potentials from voltammetry.

In Section 2, we will provide an overview of a number of fundamental electrochemical *concepts* widely used in computational electrochemistry. Then we will discuss various computational *methods* used for predicting reduction potentials in aqueous and nonaqueous solution (including ion-coupled electron-transfer reactions). Emphasis will be placed on the differences in the treatment of solvation effects by these techniques. In particular, we focus on three groups of methods.

The first group of methods (Section 3) is based on a quantum mechanical treatment of the solute combined with a dielectric continuum model of the solvent. In general, the standard reduction potential for the redox pair of interest in solution can be calculated from the standard-state Gibbs free energy of the corresponding half-reaction estimated, for example, based on a thermodynamic cycle that includes the free energies of products and reactants in the gas phase and their free energies of solvation.[1–4] Free energies of solvation can be calculated using implicit-solvent models, which are sometimes called continuum solvation models because the bulk electrostatic effects of the solvent are modeled as if the solvent were a continuous dielectric medium (that is, one uses a non-atomistic model of a molecular liquid) characterized by macroscopic properties (for example, dielectric constant and bulk surface tension at the solvent–air interface) and, sometimes, by microscopic properties (such as polarizability of the solvent

[a] *Department of Chemistry, Chemical Theory Center, and Supercomputing Institute, University of Minnesota, 207 Pleasant Street S.E., Minneapolis, MN 55455-0431, USA. E-mail: marenich@comp.chem.umn.edu, cramer@umn.edu, truhlar@umn.edu*

[b] *ARC Centre of Excellence for Electromaterials Science, Research School of Chemistry, Australian National University, Canberra ACT 0200, Australia. E-mail: junming.ho@yale.edu, michelle.coote@anu.edu.au*

† Electronic supplementary information (ESI) available: Computational and experimental data used for Fig. 1–3. See DOI: 10.1039/c4cp01572j

molecules and an effective solvent radius). By invoking this continuum approach, one reduces the electronic structure problem to the size of the solute of interest (in a field), so that the solute molecule can be treated at a higher theoretical level, for example, quantum-mechanically using density functional theory (DFT). The free energy of solvation can also be calculated by using more computationally expensive mixed discrete–continuum solvation models where one adds one or more solvent molecules to a bare solute molecule and treats only that portion of the solvent *not* explicitly included as a dielectric continuum.

The second group of protocols (Section 4) used for predicting reduction potentials is based on a quantum mechanical treatment of the solute with the solvent treated atomistically with its equilibrium ensemble of configurations sampled by means of molecular dynamics (MD) simulations or the Monte Carlo (MC) method. Note that the method commonly called MD is simply the classical trajectory method, and most often it is used simply as a means of ensemble averaging (justified by the assumption of ergodicity) rather than to calculate real-time dynamics. In typical MD and MC simulations, interactions between particles are described by using molecular mechanics (MM) force fields (which are the negative gradient fields of analytic potential energy functions written in internal coordinates). However, one may also employ direct dynamics, which means that the energies and forces are calculated as needed by electronic structure calculations rather than from an analytic potential energy function or from a fit to the results of electronic structure calculations. For example, direct dynamics may be carried out using Car–Parrinello extended-Lagrangian MD in which the wave function is propagated along with the nuclear coordinates[5] or by so called Born–Oppenheimer MD in which one solves for the fixed-nuclei electronic wave function at every time step.[6–10] The MM and direct dynamics approaches may also be combined by using a combined quantum mechanical/molecular mechanical (QM/MM) approach[11–24] where the solute molecule is treated quantum mechanically and the solvent molecules are treated using a MM force field. The QM region may also include one or more selected solvent molecules from the first and second solvation shells, although in such a case one may need to use an adaptive method[25–38] that allows solvent molecules to move between the QM subsystem and the MM subsystem. The computational protocols discussed in Section 4 treat all solvent particles explicitly, while the implicit-solvent models discussed in Section 3 use a mean-field approach.

The group of methods treated in Section 5 includes computational protocols that do not readily fit into either the first or the second group. For example, we will discuss computational approaches based on empirical relationships between molecular and electronic structure and electron transfer reactivity. Examples of such methods are the protocols that employ linear free energy relationships (LFERs) obtained by correlating computed or experimental reduction potentials to other computed properties or experimental observables.

We will also discuss in more detail some *examples* of applying the aforementioned computational methods to various classes of chemical systems in aqueous and nonaqueous solution (see Section 6). In particular, we will consider the studies of a number of inorganic (for example, nitrogen oxide species) and organic compounds, aqueous metal ions, and transition metal complexes (organometallic, metalorganic, or inorganometallic), and we will cover such currently heavily studied topics as electrocatalytic water oxidation.

We will focus on methodologies for prediction of liquid-phase redox potentials based on free energy calculations, and we will consider mainly the *thermodynamics* of redox processes in solution. Detailed analysis of kinetics or heterogeneous reactions is beyond the scope of the present article.

2. Fundamental electrochemical concepts

In this section we provide an overview of fundamental concepts used in computations of reduction potentials.

2.1. Standard states

Standard-state thermodynamic properties (such as the standard reduction potential) are denoted in the present paper by a superscript circle when they are defined to use the standard state of an ideal gas at a partial pressure of 1 bar for gases and the standard state of a solute in an ideal dilute solution with a formal solute concentration of 1 mol L^{-1} (sometimes called a 1 molar or 1 M ideal solution) for solutes. Alternative standard-state definitions used in the literature include a standard state of 1 atm ideal gas for gases and a standard state of 1 molal ideal solution for solutes. The free energy change of 1 mol of an ideal gas upon compression from 1 bar pressure to a pressure of 1 atm (*i.e.*, 1.01325 bar) is less than 0.04 kJ mol^{-1} at 298.15 K. The free energy difference due to a change from the 1 molar to the 1 molal ideal-solution standard state is also usually very small for aqueous solutions.

We note that the solvation literature sometimes employs a standard state of 1 mol L^{-1} for both the solute and the vapor, and this is sometimes denoted by a * rather than a °. The reason that this is convenient is that, as emphasized by Ben-Naim,[39] when the gas-phase concentration is the same as the liquid-phase concentration, the gas-phase entropy of translation is numerically the same as the liquid-phase entropy of liberation; thus the transfer of a solute from the gas-phase to the solute phase at fixed concentration equals the work of coupling the solute to the solvent, which is what is directly calculated by most solvation models.

2.2. Definition of the standard reduction potential

Consider the following reduction half-reaction,

$$O(s) + n_e e^-(g) \leftrightarrow R(s) \quad (1)$$

where O refers to an oxidized reagent, R refers to a reduced reagent, n_e is the number of electrons exchanged between the oxidized and reduced species, and "s" and "g" refer to species in solution and in the gas phase, respectively [at least one of O and R must be charged in the balanced chemical equation,

but their charge is not indicated explicitly in eqn (1)]. The free energy of the reaction, $\Delta_r G$, at temperature T can be expressed as

$$\Delta_r G(\mathrm{O}|\mathrm{R}) = \Delta_r G^{\circ}(\mathrm{O}|\mathrm{R}) + R_g T \ln \frac{a_R}{a_O} \quad (2)$$

where R_g is the gas constant, $\Delta_r G^{\circ}$ is the standard Gibbs free energy of the reaction, and the quantity a_X is the activity or effective concentration of X (where X is O or R) expressed for liquid-phase solutes as

$$a_X = \gamma_X \frac{c_X}{c^{\circ}} \quad (3)$$

where γ_X is the dimensionless activity coefficient of X, and c_X and c° are the bulk concentration of X and the standard concentration (in the same units), respectively. Hereafter we use the notation O|R which is equivalent to O/R and O → R sometimes to be used in the literature. A calculation of $\Delta_r G^{\circ}(\mathrm{O}|\mathrm{R})$ used in eqn (2) involves some thermochemical conventions on the treatment of the electron as discussed below.

If the species X is present in the gas phase then the activity a_X in eqn (2) should be replaced with the fugacity of X defined as

$$a_X = \phi_X \frac{P_X}{P^{\circ}} \quad (4)$$

where ϕ_X is a dimensionless fugacity coefficient of X, and P_X and P° are the partial pressure of X and the standard pressure (in the same units), respectively. In the present article, we use c° = 1 mol L^{-1} for solutes and P° = 1 bar for gases. The standard free energy of reaction (1) corresponds to the free energy $\Delta_r G$ obtained using $a_X = \gamma_X = 1$ for ideal liquid-phase reagents and $a_X = \phi_X = 1$ for ideal gas-phase reagents.

The absolute reduction potential E_{abs} corresponding to the half-reaction (1) is given by the Nernst equation[40,41] as

$$E_{abs}(\mathrm{O}|\mathrm{R}) = -\frac{\Delta_r G(\mathrm{O}|\mathrm{R})}{n_e F} = E^{\circ}_{abs}(\mathrm{O}|\mathrm{R}) - \frac{R_g T}{n_e F} \ln \frac{a_R}{a_O} \quad (5)$$

where F is the Faraday constant, and E°_{abs} is the standard reduction potential related to the standard free energy of reaction (1) by the following equation

$$\Delta_r G^{\circ}(\mathrm{O}|\mathrm{R}) = -n_e F E^{\circ}_{abs}(\mathrm{O}|\mathrm{R}) \quad (6)$$

Note that the quantity E°_{abs} defined above refers to the absolute standard reduction potential of a half-cell in which the redox reaction (1) occurs with all species present at their standard-state concentrations. However, experimental reduction potentials of half-cells are not measured in isolation but rather are measured relative to the potentials of other (reference) half-cells. Examples of common reference electrodes include the standard hydrogen electrode[42] (SHE), the saturated calomel electrode (SCE), and the silver chloride electrode (ACE). The modern electrode potential scale is based on the SHE, which is a hypothetical electrode immersed in a 1 M aqueous solution of H^+ with unit activity and no ionic interactions.[43–46] The SHE corresponds to the following half-reaction in aqueous (aq) solution:

$$\mathrm{H^+(aq)} + \mathrm{e^-(g)} \rightarrow \tfrac{1}{2}\mathrm{H_2(g)} \quad (7)$$

The reduction potential of the O|R couple can be defined relative to the SHE as

$$E^{\circ}_{rel,SHE}(\mathrm{O}|\mathrm{R}) = E^{\circ}_{abs}(\mathrm{O}|\mathrm{R}) - E^{\circ}_{abs}(\mathrm{SHE}) \quad (8)$$

where the subscript "rel,SHE" indicates a potential of a given redox couple or electrode determined relative to that of the SHE. The IUPAC recommended value of the absolute standard potential of the SHE in aqueous solution, $E^{\circ}_{abs}(\mathrm{SHE})$, is equal to 4.44 ± 0.02 V at 298.15 K,[44] whereas alternative reference values range from 4.05 to 4.42 V (see Section 2.4 for more details). The value of $E^{\circ}_{rel,SHE}(\mathrm{SHE})$ is conventionally set to zero for all temperatures for comparison of other electrodes to the SHE. The conversion constants between different reference electrodes in aqueous and organic solvents have been measured,[47] and these may be used to convert a reduction potential defined relative to the SHE into potentials relative to other reference electrodes. For example, the potential of the SCE relative to the SHE at 298 K in aqueous solution is 0.24 V.[48] Therefore, to convert values based on SHE to SCE, one needs to subtract 0.24 V from the calculation.

To facilitate comparison with experiment, theoretical calculations are typically carried out on either a half-cell reaction or on a full-cell reaction. Using the first approach, the reduction potential of a half-cell, $E^{\circ}_{rel,RE}(\mathrm{O}|\mathrm{R})$, in which the redox reaction (1) occurs is calculated relative to a particular reference electrode (RE) as

$$E^{\circ}_{rel,RE}(\mathrm{O}|\mathrm{R}) = E^{\circ}_{abs}(\mathrm{O}|\mathrm{R}) - E^{\circ}_{abs}(\mathrm{RE}) \quad (9)$$

where $E^{\circ}_{abs}(\mathrm{O}|\mathrm{R})$ is calculated using the standard Gibbs free energy of the corresponding half-reaction using eqn (6), and $E^{\circ}_{abs}(\mathrm{RE})$ is the absolute reduction potential of the reference electrode (other than the SHE) estimated as

$$E^{\circ}_{abs}(\mathrm{RE}) = E^{\circ}_{abs}(\mathrm{SHE}) + E^{\circ}_{rel,SHE}(\mathrm{RE}) \quad (10)$$

where the second term is a conversion constant between the SHE and the reference electrode RE that can be found in the literature.[48] Calculations of $E_{rel,RE}(\mathrm{O}|\mathrm{R})$ at arbitrary effective concentrations of oxidized and reduced species require in general a correction for the liquid junction potential.[49] When one calculates the potential of the full-cell reaction

$$\mathrm{O_1} + \mathrm{R_2} \leftrightarrow \mathrm{O_2} + \mathrm{R_1} \quad (11)$$

that involves the redox couples $O_1|R_1$ and $O_2|R_2$, the knowledge of absolute reduction potentials for these couples or for a reference electrode is not required. The potential of the cell can be expressed through the free energy of the reaction (11) as

$$E^{\circ}(\mathrm{cell}) = -\frac{\Delta_r G^{\circ}(\mathrm{cell})}{n_e F} = -\frac{\Delta_r G^{\circ}(\mathrm{O_1}|\mathrm{R_1}) - \Delta_r G^{\circ}(\mathrm{O_2}|\mathrm{R_2})}{n_e F} \quad (12)$$

The reduction potential of the $O_1|R_1$ couple relative to an arbitrary reference electrode (RE) can be expressed as

$$E^{\circ}_{rel,RE}(\mathrm{O_1}|\mathrm{R_1}) = E^{\circ}(\mathrm{cell}) + E^{\circ}_{rel,RE}(\mathrm{O_2}|\mathrm{R_2}) \quad (13)$$

where the second term can be further expressed as

$$E^{\circ}_{rel,RE}(\mathrm{O_2}|\mathrm{R_2}) = E^{\circ}_{rel,SHE}(\mathrm{O_2}|\mathrm{R_2}) - E^{\circ}_{rel,SHE}(\mathrm{RE}) \quad (14)$$

where the first term on the right-hand side is the reduction potential of the $O_2|R_2$ couple relative to the SHE, and the second term is a conversion constant between the SHE and the reference electrode RE.

The term ''standard reduction potential'' or simply standard potential is customarily reserved for potentials obtained by real extrapolation to infinite dilution, followed by ideal extrapolation to a standard state concentration, taken here as 1 mol L^{-1}. Furthermore, a standard potential refers to zero ionic strength. As a consequence, there are no non-ideal activity effects in a standard potential. In practice, infinite-dilution experimental potentials are obtained by assuming a functional form that models the dependence of the potential on ionic strength. A series of potential measurements is then carried out at different values of ionic strength and extrapolated to zero ionic strength where the activity coefficients approach unity.[50] In the determination of the standard potential of highly charged cations such as Fe^{3+}, obtaining accurate extrapolations to infinite dilution requires additional corrections for chemical effects such as hydrolysis of a first-shell water molecule coordinated to the Fe^{3+} ion, as well as accounting for non-unit activity coefficients of Fe^{3+}, Fe^{2+}, and H^+ under measurement conditions.[51] Most aqueous experimental reduction potentials have been extrapolated to infinite dilution and therefore these may be directly compared with theoretical calculations in which activity effects are ignored by assuming infinite dilution.

Many reported experimental potentials, especially in non-aqueous solvents, are measured at finite ionic strength or under the conditions where the actual species present might differ in protonation state or complexation state from the species to which the ideal standard potentials apply, or there might be ion pairing, which is non-ideal. Under these conditions, the activity is potentially much less than the bulk concentration, and the measured potential is referred to as the formal potential, $E^{o\prime}$,[41] which is related to the potentials E and E^o by the following equations

$$E(O|R) = E^{o\prime}(O|R) - \frac{R_g T}{n_e F}\ln\frac{c_R}{c_O} \quad (15)$$

$$E^{o\prime}(O|R) = E^{o}(O|R) - \frac{R_g T}{n_e F}\ln\frac{\gamma_R}{\gamma_O} \quad (16)$$

where the potentials may be either absolute or relative [compare eqn (15) to eqn (5)]. The formal potential is also called ''conditional'' to denote that it refers to specified conditions as opposed to standard conditions.[52] A formal potential can be defined as the potential observed experimentally in a solution containing equal numbers of moles of the oxidized and reduced substances together with other substances at specified concentrations. Accordingly, the formal potential incorporates activity effects associated with ionic strength, as well as chemical effects such as protonation, complexation, or other side reactions. The potential of the normal hydrogen electrode (NHE) (either absolute or relative) is based on a 1 mol L^{-1} concentration of the proton in a real (non-ideal) solution and is therefore a formal potential, as compared to the SHE defined using a 1 M ideal solution standard state for H^+. Of the two hydrogen electrodes, only the NHE is a working electrode because cannot be made in the laboratory because finite concentration and ideal behavior are mutually exclusive.[45] The difference between $E^{o\prime}$(NHE) and E^o(SHE) at 298 K is equal to −0.006 V, as estimated by using γ_O = 0.8 ($O = H^+$) for a 1 M solution of H^+ in water.[45]

When chemical effects are involved, additional corrections are required to convert the measured potential to the corresponding formal potential. For example, protonation is one of the most common chemical effects associated with redox reactions, particularly in aqueous solutions.[53] Proton transfer reactions often occur at a fast rate, and the measured potential is directly influenced by the prototropic equilibria.[54] For instance, it was necessary to consider two prototropic equilibria to obtain good agreement of theory and experiment for the reduction of nitroxide radicals in water.[55]

2.3. Thermochemical conventions for the electron and proton

The Gibbs free energy of the half-reaction (1) can be expressed in terms of the free energies of individual species, $G^o(X)$, where X refers to the oxidized or the reduced reagent or to the electron. The value of $G^o(e^-)$ depends on the statistical mechanical treatment of the electron. In eqn (1) and in eqn (7), the electron is treated as a gas-phase particle, but this is entirely a matter of formalism.[44,56] In fact, the solvated electron is an extremely reactive species with a short lifetime.[57,58] As such, a reduction half-reaction is in fact an irreversible process since it is very unlikely that the electron would exist in equilibrium with the reduction couple in the solution phase. The key reason that this is not an insuperable problem is that experimental reduction potentials are relative values (measured with respect to a reference electrode), and thus the contribution from the electron cancels out when the full reaction is considered. Thus, when the aim is to compare computed with experimental reduction potentials, it should not matter which reference state of the electron is used, or which statistical mechanical formalism is used, *as long as the choice is made consistently for both the reduction couple and the reference electrode*.

Related to this point, there has been significant experimental and theoretical research targeted at obtaining the absolute reduction potential of the standard hydrogen electrode, with the aim of establishing an absolute electrochemical scale.[44,58–62] In this context, the choice of value for the Gibbs free energy of the electron, as well as any assumptions regarding the state of the electron, would directly impact on the calculated absolute reduction potential. In the following section, we shall see that the choice of statistical mechanical formalism used to calculate the Gibbs free energy of the gaseous electron is small in comparison with the uncertainty associated with recent experimental and theoretical determinations of absolute reduction potential values for the SHE.

Before we proceed to discuss the statistical mechanical treatment used in the thermodynamics of free electrons, it is worth noting that there has been some confusion relating to the thermochemical conventions of the electron, namely the electron convention and the ion convention. The origin of these

two thermochemical conventions relates to how gas-phase ion chemists define the enthalpy of formation of ions. Under the electron convention (EC), which may also be called the stationary electron convention, the electron is defined as an element and therefore its formation enthalpy and Gibbs free energy are zero at all temperatures. On the other hand, the ion convention (IC) defines the formation enthalpy of the electron to be equal to its integrated heat capacity ($H_T^o - H_0^o$) with the consequence that the resulting formation enthalpies of ions differ by $H_T^o - H_0^o$ under the two conventions.[63] Nevertheless, the enthalpy of the reaction (1) is the same under both conventions. In his seminal work,[64] Bartmess inconsistently used the stationary electron convention instead of the ion convention where the formation enthalpy, integrated heat capacity and entropy (and hence Gibbs free energy) of the electron were assigned a zero value at all temperatures.[65] As a consequence, the resulting entropy (S^o) and integrated heat capacity of the electron ($H_T^o - H_0^o$) differ significantly from those under the electron convention (see Table 1). This also resulted in disagreement between the enthalpy and entropy of ionization of the hydrogen atom under the two conventions (these should be independent of convention). Fortunately, the error in the Gibbs free energy of the electron due to this inconsistency is relatively small (<0.1 kJ mol^{-1}).

Under the EC-B and IC-B conventions, the thermodynamics of the electron and the proton were calculated by assuming ideal gas behavior and following Boltzmann statistics; however, as Bartmess also pointed out, electrons and protons are fermions and therefore Fermi–Dirac statistical mechanics is the more physically appropriate treatment to use.[64] The data calculated using Fermi–Dirac statistics are shown in Table 1 and a notable difference is observed (~ 4 kJ mol^{-1}) for the Gibbs free energy of the electron and the formation free energy of the proton as compared to the values calculated without this quantum mechanical consideration. The Fermi–Dirac values are the most rigorous and are recommended when accurate treatment of the electron is sought. However, as noted above, in calculating a *relative* reduction potential it is only pertinent that one uses a convention for the Gibbs free energy of the electron that is the same as that used for the absolute potential of the reference electrode.

Table 1 Thermodynamic functions of the electron and the proton under various thermochemical conventions[a]

Quantity	EC-B	IC-B[b]	IC-B	EC-FD	IC-FD
Electron					
$\Delta_f H^o$	0	0	6.20	0	3.15
$\Delta_f G^o$	0	0	0	0	0
S^o	20.98	0	20.98	22.73	22.73
$H_T^o - H_0^o$	6.20	0	6.20	3.15	3.15
G^o	−0.05	0	−0.05	−3.62	−3.62
Proton					
$\Delta_f H^o$	1536.20	1530.00	1530.0	1533.10	1529.95
$\Delta_f G^o$	1516.96	1517.01	1516.96	1513.32	1513.32
S^o	108.95	108.95	108.95	108.95	108.95
$H_T^o - H_0^o$	6.20	6.20	6.20	6.14	6.14
G^o	−26.27	−26.27	−26.27	−26.33	−26.33
Ionization process, $H \rightarrow H^+ + e^-$					
ΔH_{ion}^o	1318.25	1312.05	1318.25	1315.14	1315.14
ΔS_{ion}^o	15.22	−5.76	15.22	16.97	16.97
ΔG_{ion}^o	1313.71	1313.77	1313.71	1310.08	1310.08

[a] All quantities are given at $T = 298$ K using reference data.[64] Enthalpies and free energies are in kJ mol^{-1}, entropies are in J (mol K)$^{-1}$. EC refers to the electron convention, IC refers to the ion convention, B refers to the use of Boltzmann statistics, and FD refers to the use of Fermi–Dirac statistics. [b] IC-B values obtained[64] with an additional assumption that the thermodynamic functions of the electron listed in this table are equal to zero at all temperatures.

2.4. The absolute reduction potential of the SHE

The absolute reduction potential $E_{abs}(O|R)$ computed using eqn (5) and (6) cannot be directly compared to experimental data because the corresponding experimental potential, $E_{rel,RE}(O|R)$, is not absolute but measured relative to the potential of some reference electrode (RE) (for example, SCE). The experimental value $E_{rel,RE}(O|R)$ at arbitrary activities of O and R can then be converted to the potential $E_{rel,SHE}(O|R)$ defined relative to the SHE by equation

$$E_{rel,SHE}(O|R) = E_{rel,RE}(O|R) + E^o_{rel,SHE}(RE) \quad (17)$$

provided the conversion constant $E^o_{rel,SHE}(RE)$ is known from the reference literature. The theoretical value of $E_{rel,SHE}(O|R)$ can be computed from $E_{abs}(O|R)$ by subtracting a reference value for the absolute standard reduction potential of the SHE, $E^o_{abs}(SHE)$. Therefore, the accuracy of $E^o_{abs}(SHE)$ conditions the accuracy of $E_{rel,SHE}(O|R)$.

There have been a number of theoretical and experimental determinations of $E^o_{abs}(SHE)$ (unless noted otherwise, the rest of this section refers to the SHE in aqueous solution). However, the scatter in the data is rather large, ranging from 4.05 to 4.44 V. Selected recommended values are compiled in Table 2. This raises the question of which value of $E^o_{abs}(SHE)$ should be used in conjunction with theoretical calculations for predicting reduction potentials. The value of $E^o_{abs}(SHE)$ under standard conditions can be derived based on a thermodynamic cycle shown in Scheme 1 by the following equation:

$$E^o_{abs}(SHE) = [\Delta G^o_S(H^+) + \Delta G^o_{ion} + \Delta G^o_{at}]/F$$
$$= [\Delta G^o_S(H^+) + \Delta_f G^o(H^+)]/F \quad (18)$$

Table 2 Reference values of the absolute potential of the SHE in water[a]

$E^o_{abs}(SHE)$	$\Delta G^o_{ion}(H^+)$	Surface potential	$\Delta_f G^o(H^+)$	Ref.
4.44	−1088	Yes	1517	Trasatti[44]
4.42	−1091	Yes	1517	Fawcett[60]
4.28	−1105[b]	No	1517	Kelly *et al.*[59,74]
4.28	−1101	No	1513[c]	Isse and Gennaro[76]

[a] The first column shows reference values of the absolute potential of the SHE in water (in V), the second column shows reference values of the solvation free energy of H^+ in water (in kJ mol^{-1}), the third column indicates whether this solvation energy includes the surface potential (see the text for more detail), the fourth column shows reference values for the free energy of formation of H^+ in the gas phase (in kJ mol^{-1}). All the quantities reported here correspond to standard conditions (298 K, ionic and neutral solutes at 1 M, ideal gases at a partial pressure of 1 bar), as denoted by a small circle. Unless noted otherwise, the proton and the electron are treated using Boltzmann statistics (see Table 1). [b] The same as the value obtained by Tissandier *et al.*[73] using cluster approximation calculations. [c] The proton and the electron are treated using Fermi–Dirac statistics.

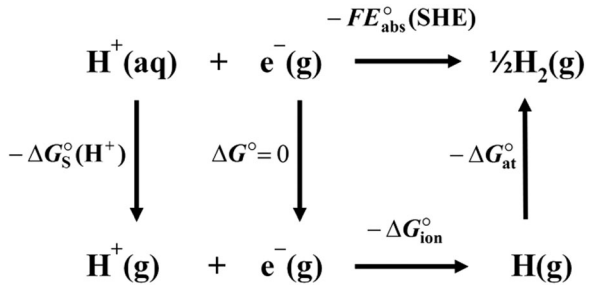

Scheme 1 Thermodynamic cycle for the absolute potential of the SHE.

where $\Delta G^{o}_{S}(H^+)$ is the solvation free energy of the proton in water, ΔG^{o}_{ion} is the gas-phase ionization free energy of H, ΔG^{o}_{at} is the gas-phase atomization free energy of H_2, and $\Delta_f G^{o}(H^+)$ is the gas-phase free energy of formation of H^+, with all quantities given at 298 K.

The discrepancies between the reference values of E^{o}_{abs}(SHE) stem from the different values employed for $\Delta G^{o}_{S}(H^+)$ and (to a lesser extent) from the different values of $\Delta_f G^{o}(H^+)$. The latter values depend on the statistical mechanical formalism for the treatment of the proton and the electron (*i.e.*, either Boltzmann or Fermi–Dirac statistics).

The reference values of $\Delta G^{o}_{S}(H^+)$ (Table 2) depend on the definition of a solvation free energy of a charged species. There is a distinction between the *real* solvation free energy,[66] ΔG^{o}_{S} (real), and the absolute or *intrinsic* solvation free energy, ΔG^{o}_{S} (intr.).[67] The former corresponds to the Gibbs free energy change associated with moving a single ion from the gas phase into a solution, which includes a contribution from the difference between the inner electric potential of the medium and the inner electric potential of the vacuum [see, for example, eqn (16) in Fawcett's article[60]]. This potential difference is due to a difference in solvent structure effects inside the medium and at its surface, and it is called the surface potential.[67] The intrinsic solvation free energy ΔG^{o}_{S}(intr.) is a purely chemical free energy change from which this electrical contribution is removed (or is not present to begin with), and therefore it differs from the real solvation free energy by the product of the charge of the ion and the inner potential of the medium according to the following equation for an ion $M^{z\pm}$:

$$\Delta G^{o}_{S}(M^{z\pm}, \text{real}) = \Delta G^{o}_{S}(M^{z\pm}, \text{intr.}) \pm zF\chi \qquad (19)$$

where χ is the surface potential, and ΔG^{o}_{S}(intr.) is the intrinsic standard-state free energy of solvation defined as a free energy of transfer from an ideal gas at a partial pressure of 1 bar to a 1 M ideal solution.

The surface potential contribution for a singly charged ion has recently been estimated to be $\sim$0.145 V (14 kJ mol^{-1}) for water,[60] but values ranging from −1.1 to +0.5 V have also been reported.[67–72] Trasatti's value of E^{o}_{abs}(SHE) (Table 2) is based on the real solvation free energy of the proton being equal to −(1088 ± 2) kJ mol^{-1}.[44] Fawcett's value of E^{o}_{abs}(SHE) corresponds to a slightly different value of ΔG^{o}_{S}(real) (−1091 kJ mol^{-1}).[60]

Tissandier *et al.*[73] and Kelly *et al.*[59,74] have employed the cluster pair approximation to obtain an estimate of the solvation free energy of the proton, −(1105 ± 8) kJ mol^{-1}. This value is considered to be the intrinsic (rather than real) solvation free energy, ΔG^{o}_{S}(intr.), because the solvated ion clusters used in these calculations contain only up to six water molecules, which is not enough to produce the surface potential. The value[59,74] of E^{o}_{abs}(SHE) = 4.28 V (Table 2) obtained using ΔG^{o}_{S} (intr.) = −1105 ± 8 kJ mol^{-1} was supported by Camaioni and Schwerdtfeger,[75] and it was also reproduced in the work of Isse and Gennaro.[76] Donald *et al.*[58,61,62,77] made an estimate of E^{o}_{abs} (SHE) in the range between 4.05 and 4.21 V derived from nanocalorimetric measurements involving nanodroplets of water containing transition metal ions.

As noted elsewhere,[78] the contribution due to the surface potential cancels out in a chemically balanced chemical reaction that occurs in a single phase because the total charge is conserved in that reaction. In the case of a calculation of equilibrium reduction potentials involving a single phase, it should not matter whether the contribution from surface potential is included in the solvation free energy, as long as this is done consistently for all reacting species and products.[78] Furthermore, the concept of surface potential applied to the standard hydrogen electrode is quite controversial because by its modern definition[45] the SHE (in contrast to the typical working NHE) is a theoretical (hypothetical) electrode in a 1 M ideal solution, with no ionic interactions, which implies that there is no surface potential.

In addition, the choice of the reference value of E^{o}_{abs}(SHE) depends on whether a particular computational protocol was designed to predict real or absolute solvation free energies. Concerning implicit-solvent models, they generally contain parameters that have been optimized to reproduce reference solvation free energies of ionic species derived with use of a certain reference value of $\Delta G^{o}_{S}(H^+)$. More specifically, reference solvation free energies of ions are indirectly obtained *via* thermochemical cycles involving, for example, the solvation free energy of the proton, aqueous pK_a values, and gas-phase reaction energies.[59] Therefore, one should choose the reference value of E^{o}_{abs}(SHE) corresponding to the same value of $\Delta G^{o}_{S}(H^+)$ used in the parametrization of a given solvation model.

Table 3 shows the aqueous standard reduction potentials for several redox couples derived with the use of reference solvation energies of ionic species[79,80] that are based on the reference value of $\Delta G^{o}_{S}(H^+)$ in water equal to −1105 kJ mol^{-1}.[73] The gas-phase reaction energy and the solvation free energy of neutral species were obtained using the G3(MP2,CC)(+) composite method[81] and the SMD implicit-solvent model,[82] respectively. When the computed standard reduction potentials are expressed relative to the SHE using the reference value[59] of E^{o}_{abs}(SHE) = 4.28 V, which is consistent with $\Delta G^{o}_{S}(H^+)$ = −1105 kJ mol^{-1} (see Table 2), the mean unsigned error relative to the experimental values[83–85] of $E^{o}_{rel,SHE}$(O|R) is 0.08 V. The error increases to 0.20 V if one uses the reference value[60] of E^{o}_{abs}(SHE) = 4.42 V, which is *not* consistent with $\Delta G^{o}_{S}(H^+)$ = −1105 kJ mol^{-1}.

Table 3 Calculated aqueous standard reduction potentials of selected redox couples relative to different reference values of the absolute potential of the SHE (in V)[a]

	$E^{o}_{rel,SHE}(O\|R)$		
O|R	E^{o}_{abs}(SHE) = 4.28	E^{o}_{abs}(SHE) = 4.42	Experiment
$HOO^{\bullet}\|HOO^{-}$	0.56	0.42	0.76
$HS^{\bullet}\|HS^{-}$	1.06	0.92	1.15
$CH_3S^{\bullet}\|CH_3S^{-}$	0.69	0.55	0.73
$PhS^{\bullet}\|PhS^{-}$	0.73	0.59	0.69
$PhO^{\bullet}\|PhO^{-}$	0.69	0.55	0.79
$OH–PhO^{\bullet}\|OH–PhO^{-}$	0.50	0.36	0.45
$NO_2–PhO^{\bullet}\|NO_2–PhO^{-}$	1.15	1.01	1.22
Mean unsigned error	0.08	0.20	

[a] See the text for details.

Table 4 Reference values of the absolute potential of the SHE in nonaqueous solvents[a]

Solvent	E^{o}_{abs}(SHE)	$\Delta G^{o}_{S}(H^{+})$	Surface potential	Note
Acetone	4.13	−1118	Yes	*b*
Acetonitrile	4.60	−1074	Yes	*b*
Acetonitrile	4.59	−1074	Yes	*c*
Acetonitrile	4.52	−1081	No	*d*
DMSO	3.83	−1147	Yes	*c*
DMSO	3.96	−1136	No	*d*
Ethanol	4.21	−1111	Yes	*b*
Ethanol	4.24	−1108	Yes	*c*
Formamide	4.29	−1103	Yes	*b*
Methanol	4.19	−1113	Yes	*b*
Methanol	4.17	−1114	Yes	*c*
Methanol	4.38	−1095	No	*d*

[a] DMSO stands for dimethyl sulfoxide. See footnote *a* in Table 2 and the text for further details. [b] See ref. 66 for details. [c] See ref. 60 for details. [d] Using the cluster-pair approximation for calculating the absolute solvation free energy of the proton and Boltzmann statistics for the proton and the electron in the gas phase; see ref. 74 for further details (see footnote *e* in Table 8 there).

Selected reference values of the absolute reduction potential of the SHE in nonaqueous solvents are summarized in Table 4. The surface potential contribution for H^+ in nonaqueous solvents varies from −0.1 V in acetonitrile to −0.34 V in acetone.[66] In the case of nonaqueous solvents, one can consider reference electrodes other than the SHE, *e.g.* the ferricenium/ferrocene ($Fc^+|Fc$) redox couple. The absolute potential of the $Fc^+|Fc$ half-reaction has been recently estimated to be 4.99, 4.93, and 5.04 V in acetonitrile, 1,2-dichlorethane, and DMSO, respectively.[86]

While it is important to make a consistent choice of the reference value of E^{o}_{abs}(SHE) for a particular protocol, we also note that the values of E^{o}_{abs}(SHE) used in the literature (Tables 2 and 4) vary within 0.2 V or ∼20 kJ mol^{-1} for the same solvent, which is comparable with typical errors in the free energies of solvation for ions computed using implicit-solvent models.[82]

3. Protocols based on implicit-solvent models

In this section we review various theoretical protocols that utilize dielectric continuum solvation models for predicting reduction potentials. We begin with a theoretical overview of these methods and continue to an overview of their applications.

3.1. Theoretical background

As discussed above, a condensed-phase reduction potential can be evaluated from the standard-state Gibbs free energy of the corresponding reaction or half-reaction. The reaction free energy is computed as a difference in the free energies of products and reactants, with the free energy of each reagent being computed as a sum of the gas-phase free energy and the free energy of solvation. These free energies have several components: the equilibrium values of the Born–Oppenheimer potential energies, the entropy due to electronic degeneracy (including spin), zero-point vibrational energy, and thermal contributions to the free energy, where the thermal contributions may be further partitioned into subcomponents, with different theoretical methods possibly being employed for some of the components or subcomponents. The Born–Oppenheimer energy is the ground-state electronic energy including nuclear repulsion. The gas-phase subcomponents of the thermal contributions are due to electronic excitation, multiple conformations (if present), vibrational and rotational excitations, and translational motion. Internal rotations are included in the vibrational and/or conformational terms. The liquid-phase subcomponents are the same except that librations replace rotations and liberational contributions replace translational ones. In the present section, we emphasize a calculation of the solvation part by continuum solvation models in which the bulk electrostatic effects of the solvent are treated using the dielectric continuum approximation.

In calculating the standard free energy of the reaction from the standard free energies of participating species, it is convenient to write the standard free energy of an individual compound X in solution, G^{o}, using explicit Boltzmann averaging over multiple molecular conformations of a given species as follows

$$G^{o}(X) = -R_g T \ln\left(\sum_{k\in\{C\}} e^{-G^{o}_{k}(X)/R_g T}\right) \qquad (20)$$

where $G^{o}(X)$ is averaged over a set C of low-energy conformers k in solution, and $G^{o}_{k}(X)$ is the free energy of conformer k that is usually expressed as

$$G^{o}_{k}(X) = G^{o}_{g,k}(X) + \Delta G^{o}_{S,k}(X) \qquad (21)$$

where the first term on the right side is the gas-phase free energy of structure k and the second term is the solvation free energy of k defined as the free energy of transfer of the solute from the ideal-gas state at a solute partial pressure of 1 bar to a 1 M ideal solution. This is often assumed to be independent of k. More details on a computation of ΔG^{o}_{S} will be provided below.

The gas-phase free energy of structure k can be expressed as

$$G^{o}_{g,k}(X) = E_k(X) - R_g T \ln d + \varepsilon_{ZPE,k}(X) + G^{o}_{thermal,T,k}(X) \qquad (22)$$

where the first term on the right side is the equilibrium potential energy equal to the electronic energy (which is always taken to include nuclear repulsion) in the gas phase using either gas-phase or liquid-phase solute geometries, d is the degeneracy

of the ground electronic state, the third term is the zero-point vibrational energy (ZPE), and the fourth term is the thermal contribution to Gibbs free energy for conformer k (at temperature T). The latter includes only translation (which is independent of k) and electronic excitation and vibrational–rotational contributions of a single structure.

If the liquid-phase solute geometry is expected to be close to the gas-phase one a calculation of eqn (21) can be performed at the fixed gas-phase geometry and by using only gas-phase frequencies. In many cases, the use of solution-phase vibrational frequencies is expected to cause only a small change.[87]

Often, the ZPE and thermal contributions are based on the ideal-gas, harmonic-oscillator, rigid-rotator approximation. The resulting ZPE and thermal contributions may thus have errors associated with limitations of such an approximation in addition to systematic errors due to limitations of the employed electronic structure methods. The errors due to anharmonicity of high-frequency vibrational modes can be mitigated by scaling the frequencies using empirically determined factors.[88] This may be called a quasiharmonic treatment (defined as using the harmonic oscillator formulas but with effective frequencies).

The breakdown of the harmonic oscillator model for the free energies of low-frequency vibrational modes (*e.g.*, the internal rotation around a carbon–carbon single bond and the case of mixed internal rotations and low-frequency bending modes) is harder to correct. Torsions are the most common source of the multiple structures of eqn (20), and when the multiple structures can be accounted for by a single torsion or by separable torsions, one may treat the problem by using a single structure with the harmonic potentials of torsional modes replaced by one-dimensional hindered rotor potentials,[89,90] but in the case of multiple torsions a coupled torsional treatment is recommended.[91,92]

Calculating the standard free energy of an arbitrary chemical reaction in solution from the ensemble-averaged standard free energies of individual compounds using eqn (20) and (21) accounts for the entropy associated with including multiple alternative structures as well as for the relaxation of the solute geometry in solution.

3.2. Thermochemical cycles

The standard free energy of a reaction in solution can be related to the standard free energy of the same reaction in the gas phase in terms of a thermochemical (Born–Haber) cycle shown in Scheme 2. By considering only a single conformation for each reagent (the index k is omitted in this case), we have

$$\Delta_r G_S^\circ(\mathrm{A|B}) = \Delta_r G_g^\circ(\mathrm{A|B}) + \sum_i \Delta G_S^\circ(B_i) - \sum_i \Delta G_S^\circ(\mathrm{A}_i) \quad (23)$$

where the index i runs over all reactants A and all products B, and $\Delta_r G_g^\circ$ is the standard free energy of the gas-phase reaction expressed through the gas-phase standard free energies of individual species as

$$\Delta_r G_g^\circ(\mathrm{A|B}) = \sum_i G_g^\circ(\mathrm{B}_i) - \sum_i G_g^\circ(\mathrm{A}_i) - G_g^\circ(\mathrm{e}^-) \quad (24)$$

where $G_g^\circ(\mathrm{X})$ (X = A_i or B_i) is given by eqn (22).

$$\begin{array}{ccc} \sum_i \mathrm{A}_i(\mathrm{s}) + n_e\,\mathrm{e}^-(\mathrm{g}) & \xrightarrow{\Delta_r G_s^\circ(\mathrm{A|B})} & \sum_i \mathrm{B}_i(\mathrm{s}) \\ \Big\downarrow -\sum_i \Delta G_S^\circ(\mathrm{A}_i) & \Big\downarrow \Delta G^\circ = 0 & \Big\uparrow \sum_i \Delta G_S^\circ(\mathrm{B}_i) \\ \sum_i \mathrm{A}_i(\mathrm{g}) + n_e\,\mathrm{e}^-(\mathrm{g}) & \xrightarrow{\Delta_r G_g^\circ(\mathrm{A|B})} & \sum_i \mathrm{B}_i(\mathrm{g}) \end{array}$$

Scheme 2 Thermochemical cycle relating the standard free energy of the redox reaction in solution, $\Delta_r G_S^\circ$, to the standard free energy of the gas-phase reaction, $\Delta_r G_g^\circ$, using the solvation free energies of the reactants (A) and the products (B). The symbol "g" denotes gas-phase processes and particles, and the symbol "s" denotes those in solution. The upper-case subscript "S" refers to the free energy of solvation. The electron is treated as a gas-phase particle.

The resulting standard reduction potential relative to the SHE can be expressed as

$$E_{\mathrm{rel,SHE}}^\circ(\mathrm{A|B}) = -\frac{\Delta_r G_S^\circ(\mathrm{A|B})}{n_e F} - E_{\mathrm{abs}}^\circ(\mathrm{SHE}) \quad (25)$$

where the last term is the absolute potential of the standard hydrogen electrode. One can use a reference value of $E_{\mathrm{abs}}^\circ(\mathrm{SHE}) = 4.28$ V determined in earlier work[59] employing the integrated heat capacity and entropy of the electron from Boltzmann statistics, which corresponds to $G_g^\circ(\mathrm{e}^-) = 0.00$ eV to be used in eqn (24). One advantage of using this reference value is that the contribution from the surface potential (see Section 2.4) need not be evaluated.

3.3. Electronic structure calculation

In regard to computing the electronic energy of individual reactants and products [the first term on the right-hand side of eqn (22)], the electronic energy may be calculated at a very high level of wave function theory[93] (*e.g.*, coupled cluster theory with singles and doubles with a perturbative correction for triple excitations, *i.e.*, CCSD(T)) employed with nearly complete basis sets in order to achieve chemical accuracy (which is roughly associated with an error of 4 kJ mol^{-1} or less) but only in the case of small molecules (having ten or fewer non-hydrogen atoms). Such computations become prohibitively time-consuming (or computer memory consuming) for larger systems. A recent major advance is the introduction of practical explicitly correlated methods (especially the F12 method)[94–97] and basis sets[98a] to mitigate the slow convergence of the correlation energy with basis set size. The recent introduction of the incremental method has greatly increased the size of systems that can be treated at the converged basis-set-limit of CCSD(T).[98b–d] Nevertheless, the associated computational cost scales at least as the 7th power of the size of the system. One way of cutting the cost and decreasing this high-power scaling for large systems is to use localized orbitals and treat the correlation energy of subsystems independently in terms of these localized orbitals;[99,100] the fragment methods considered at the end of this subsection provide an alternative divide-and-conquer approach to treating large systems.

Early attempts to overcome the slow brute force convergence of the correlation energy involved extrapolation[101] and scaling,[102,103]

and second-generation methods attempts include a number of cost-effective composite methods of reasonably high accuracy. Examples of composite methods include methods such as G3S,[104] G3SX,[105] G4,[106] and other Gaussian-*n* (G*n*) theories,[104,107,108] multicoefficient correlation methods,[109–116] CBS-X procedures (*e.g.*, X = QB3[117]), and the correlation-consistent composite approach (CCCA).[118,119] For instance, the G*n* methods were originally designed to approximate the QCISD(T) energies obtained using large triple-zeta basis sets with the energies from more computationally affordable QCISD(T)/6-31G(d) calculations in combination with additivity corrections, obtained at the MP2 or MP4 levels of theory.

The mean absolute deviation relative to reference energies is 3.5 kJ mol^{-1} for G4 electron affinity calculations and 3.8 kJ mol^{-1} for G4 ionization energy calculations.[106] The BMC–CC composite method[120] gives a slightly higher mean absolute deviation in electron affinities, 5.4 kJ mol^{-1}, but at a cost savings of two or more orders of magnitude.

Kohn–Sham density functional theory[121] can provide a cost-effective alternative for calculating the gas-phase reaction energies; however, the performance of DFT depends on the choice of exchange–correlation functional.[122–128] For example, a number of exchange–correlation functionals failed to provide an accurate description of the energetics of a test set of radical reactions when compared with benchmark G3(MP2)-RAD values, with all methods tested showing unpredictable deviations of up to 40 kJ mol^{-1} or more in some cases.[124] However, more recent exchange–correlation functionals such as M05-2X and M06-2X are quite accurate for radicals,[125,129,130] and several newer functionals have broader accuracy than many older functionals.[125,131–136]

For comparison with mean unsigned errors in electron affinities given above, we note that density functional theory has been shown to yield mean unsigned errors in electron affinities of 5.5 kJ mol^{-1} with the M08-HX exchange–correlation functional and a minimally augmented multiply polarized valence triple-zeta basis set[128] and 16.2 kJ mol^{-1} with the mPW1PW exchange–correlation functional and a very small basis set.[137]

For large systems, a multilayer approximation, such as the ONIOM approximation,[16–18,24] can be employed. The ONIOM method partitions a system into layers (like the layers of an onion) with the inner layers treated at a higher level than the outer layers. Note that ONIOM represents a multi-layer extension of older[12,138,139] two-layer methods. The innermost layer may be defined to include the reaction center plus its directly bonded substituents so that the chemistry of the reaction is modeled accurately. In a prior benchmarking calculation of the enthalpies of a number of radical reactions by one of us, a two-layer ONIOM approach that uses the composite G3(MP2)-RAD method for the innermost layer and large basis set R(O)MP2 for the outer layer was shown to reproduce the corresponding standard G3(MP2)-RAD calculations for a test set of 112 different radical reactions to within a mean absolute deviation of 1.2 kJ mol^{-1}.[124] The approach as a whole has been shown to reproduce experimental thermochemistry and kinetics to within chemical accuracy for a broad range of radical reactions including one-electron reduction and oxidation potentials.[55,140–143] The reader should note that the above-mentioned ONIOM protocol[124] is in fact a QM/QM method where all the layers are treated using quantum mechanical methods, but with lower-level quantal methods for outer layers so that the treatment is applicable to moderate-sized systems.

For very large systems containing hundreds to thousands of non-hydrogen atoms, *e.g.* enzymes and other bio-macromolecules, the outermost layer of an ONIOM approach is typically treated using a molecular mechanics (MM) force field. Such a combination is commonly referred to as a combined QM/MM method. For example, the effective fragment potential (EFP) method is a model potential that is derived from quantum mechanical calculations and has been designed to model intermolecular interactions. The model (known as EFP1)[144] was originally designed to model aqueous solvation effects on chemical and biomolecular reactions and was later generalized to study non-bonded intermolecular interactions (yielding a method called EFP2).[145,146] This approach has been successfully applied to predict the reduction potentials and pK_a's of substrates in complex environments such as an enzyme active site where the reaction center is treated by wave function theory, and the remainder of the system is represented by an EFP separated from the wave function part by a buffer region.[147,148] Other QM/MM methods have also been developed.[11,13–15,19–24]

The development of other fragment-based methods is presently a very active area of research. In these approaches, a large molecule or molecular system is made more computationally tractable by explicitly considering only one part (fragment) of the whole in any particular calculation. A variety of such methods have been developed, including the fragment molecular orbital (FMO) method[149–152] and the explicit polarization potential (X-Pol) method,[153,154] as well as various energy-based systematic fragmentation approaches,[145,155–163] and they are intended for extending traditional correlated calculations to study very large systems. Various classifications of fragment methods have been proposed.[158,160–166] One particularly general classification is based on labeling the smallest subsystems used to define fragments as monomers and recognizing (i) that in the various fragment methods the monomers are distributed among fragments in different ways and (ii) that in some methods that fragments are treated as isolated systems whereas in other methods they are embedded in an electrostatic potential due to the un-included monomers. The FMO and X-Pol methods are examples of electrostatically embedded methods where each monomer appears in at most one fragment or at a single fragment–fragment boundary, whereas the electrostatically embedded many-body method,[155] the generalized energy-based fragmentation approach,[164] the many-overlapping-body expansion,[160] and the electrostatically embedded molecular tailoring approach[163] are examples of methods where a given monomer appears in two or more fragments. It is envisaged that the development of such methods should eventually expand the scope of traditional correlated methods to very large systems.[167]

3.4. Solvation energy calculation

Here we consider the computation of the standard-state free energy of solvation, ΔG_S^o, in more detail. The standard-state free

energy of solvation is usually expressed through the fixed-concentration solvation energy, ΔG^*_S, as follows

$$\Delta G^o_S = \Delta G^*_S + R_g T \ln(R_g T / p^o V^o) \quad (26)$$

where the fixed-concentration free energy of solvation is equal to the free energy of transfer of the solute from the ideal-gas state with the same concentration as the standard-state solute concentration. Using $V^o = 10^{-3}$ m^3 mol^{-1} (*i.e.*, 1 L mol^{-1}) and $p^o = 10^5$ Pa (*i.e.*, 1 bar), the second term of eqn (26) is defined as the free energy change of 1 mol of an ideal gas upon compression from 1 bar pressure to 1 M concentration. At $T = 298$ K, this term equals ~ 8 kJ mol^{-1}. In fact, many popular computational programs such as Gaussian 09[168] conventionally produce values of ΔG^*_S, and an appropriate correction should be made when a value of ΔG^o_S is required instead.

As mentioned above, the reason why ΔG^*_S becomes involved is that when the concentration is fixed, the liberational free energy in solution is the same as the translational free energy in the gas-phase, and for a dilute (ideal) solution, the free energy of solvation is equal to the work of coupling the solute to the solvent. Within the dielectric continuum model, this work may be written as

$$\Delta G^*_S = \Delta G_{EP} + G_{NBE} + \Delta G_N \quad (27)$$

where the first term on the right-hand side is the bulk electrostatic (BE) component, the second term accounts for non-bulk-electrostatic (NBE) effects (which should be parsed as effects that are not bulk electrostatic effects, not as electrostatic effects that differ from bulk ones; see the next section for more details), and the third term refers to the change in ΔG^*_S due to a change in the solute's geometry upon solvation, provided that the first and the second term are calculated at the gas-phase geometry.

The G_{EP} energy is usually obtained from a self-consistent reaction field (SCRF) quantum-mechanical calculation at a fixed geometry, and it can be expressed using the following equations:

$$\Delta G_{EP} = \Delta E_E + G_P \quad (28)$$

$$\Delta E_E = \langle \Psi | H^{(g)} | \Psi \rangle - \langle \Psi^{(g)} | H^{(g)} | \Psi^{(g)} \rangle \quad (29)$$

$$G_P = \left\langle \Psi \left| -\frac{e}{2}\phi \right| \Psi \right\rangle + \frac{e}{2}\sum_k Z_k \phi_k \quad (30)$$

where $H^{(g)}$ and $\Psi^{(g)}$ are the solute electronic Hamiltonian and electronic wave function, respectively, in the gas phase, Ψ is the polarized solute electronic wave function in solution, e is the elementary charge, k runs over all atoms in the solute molecule, ϕ is the reaction field as a function of position $\mathbf{r}$ inside the cavity defined by the solute–solvent boundary, ϕ_k is the same reaction field evaluated at atom k, and Z_k is the atomic number of atom k. In the SCRF calculation, one solves for the orbitals of the polarized Ψ in a field that represents both the self-consistent relaxation of the other orbitals of the explicit subsystem and also the self-consistent relaxation of the solvent to the polarized implicit subsystem. This represents a quantum mechanical version of the classical SCRF model of Onsager.[169]

The EP term is a sum of the change in the solute's internal electronic energy (ΔE_E) in transferring from the gas phase to the liquid phase at the same gas-phase geometry and the polarization free energy (G_P) of the solute–solvent system when the solute is inserted. The polarization free energy includes a negative (favorable) term due to the favorable mutual polarization of the solute and the solvent (solute–solvent induction forces) minus the work required to polarize the solvent (the work required to polarize the solute is the already mentioned ΔE_E). The work to polarize the solvent is usually estimated by the linear response approximation, in which case it is one half of the magnitude of solute–solvent interaction energy; this reduces the effect of the polarization by a factor of one half, which is already reflected in eqn (30).[170]

The reaction field ϕ used in eqn (3) can be obtained by solving the nonhomogeneous-dielectric Poisson equation (NPE)[171,172] for bulk electrostatics,

$$\nabla\cdot(\varepsilon\nabla\Phi) = -4\pi\rho \quad (31)$$

where ε is the solvent's relative permittivity, ρ is the charge density of the solute molecule obtained from the solute's electronic wave function in solution (the charges of the medium, called bound charges, do not appear explicitly), Φ is the total electrostatic potential equal to a sum of the electrostatic potential of the solute and the reaction field ϕ. The relative permittivity ε is a function of position in general (*i.e.*, the medium is nonhomogeneous); in practice, ε is usually set equal to the bulk dielectric constant of the solvent outside the solute electrostatic cavity, and it is set to unity inside the cavity because the polarization is treated explicitly inside the cavity in terms of the deviation of Ψ from $\Psi^{(g)}$.

The reaction field that represents the solvent can also be modeled by using alternative approaches,[172,173] for example, the generalized Born (GB) approximation[174–179] (a generalization to charged and neutral molecules of the Born approximation,[174] which applies only to atomic ions). The GB approximation employs a representation of the solute as a set of partial atomic charges modeled as point charges at the nuclear positions. The interaction of the partial atomic charges of the solute in the solvent and with each other is dielectrically screened by the polarized solvent and descreened by other parts of the solute.[173,179,180]

The NPE approximation has the disadvantage that it is almost always applied with an unrealistic model boundary between solute (inside of which the dielectric constant is unity in SCRF methods, because polarization is included explicitly) and the solvent (where the dielectric constant has the bulk liquid value). This unrealistic partition is also used in the dielectric screening model of the GB approximation, and as a results the bulk electrostatic energy of either the NPE or GB method is sensitive to the atomic radii that are used to define the position of this model boundary.[181]

The ΔG_N term in eqn (27) is equal to the change in the computed solvation free energy due to a change in nuclear coordinates when transferring from the gas phase to the liquid phase (nuclear relaxation). In many cases, the ΔG_N term is small,

and it can be safely neglected by using only gas-phase geometries in all calculations. The issue is discussed elsewhere.[182]

Several different methods have been employed to handle the electrostatic portions of the SCRF calculations. Examples of SCRF solvation models that utilize the continuous charge density of the solute and solve the NPE for bulk electrostatics in a dielectric continuum include the model of Rivail and Rinaldi in which the solvent is polarized by solute multipole moments[183,184] and the polarizable continuum model of Miertuš, Scrocco, and Tomasi (MST)[185] based on an apparent surface charge on the solute's surface (*i.e.*, on an assumed boundary between the solute and the solvent). The latter model is usually abbreviated as PCM[185] but is now called dielectric PCM (D-PCM) to emphasize that the continuum solvent is treated as a polarizable dielectric. Similar models include the conductor-like version of PCM (C-PCM)[186,187] and the integral-equation-formalism version of PCM (IEF-PCM).[188] Methods with similar physical content in the electrostatics include the Jaguar solvation model,[189–191] the conductor-like screening model (COSMO)[192] (which is similar to C-PCM), and COSMO for real solvents (COSMO-RS).[193] Other models that can be considered as an extension of the PCM for the electrostatic part include the electrostatic parts of the MST model[194,195] of Luque *et al.* and of the solvation model based on density (SMD).[82] Examples of solvation models that utilize the GB approximation for bulk electrostatics include SM8,[196] SM8AD,[197] SM12,[198] and others.[199–201] Solvation models that utilize other approaches for bulk electrostatics are reviewed elsewhere.[172]

3.5. Non-bulk-electrostatic effects in implicit-solvent models

Dielectric continuum solvation models used in the literature[79,82,172,173,180–204] differ from each other not only in the way that they treat bulk electrostatics but also in the way that they treat non-bulk-electrostatic effects. It is usually assumed that beyond the first solvation shell, the solvent contributions are well modeled by the bulk dielectric model, so the non-bulk-electrostatic effects are sometimes called first-solvation-shell effects.

In the models developed at the University of Minnesota such as SMD[82] and other SM*x* models where $x = 1–12$,[79,173,180,198] the G_{NBE} term in eqn (27) is treated as a sum over empirical atomic surface tension terms[180] called CDS terms that nominally account for cavity formation (C), dispersion (D), and solvent-structure (S) effects. Using this approach, the G_{NBE} term is expressed in general as

$$G_{NBE} = \sum_k \sigma_k A_k \quad (32)$$

where k runs over all atoms, A_k is the solvent accessible surface area of atom k, and σ_k is a function that depends on the atomic number of atom k and the solute's geometry and that includes model parameters optimized with the use of experimental data. In practice, "solvent structure" includes many effects, including those associated with hydrogen bonding, the hydrophobic effect, exchange repulsion of solute and solvent, and the deviation of the microscopic dielectric constant of the first solvation shell from the bulk dielectric constant. Careful parametrization of G_{NBE} is essential for a quantitatively accurate theory for neutral solutes.[203,204]

The model boundary between the solute and the solvent in implicit-solvent models is typically offset from the van der Waals surface of the solute (*i.e.*, of the explicit subsystem) by an effective solvent radius, so one has to choose solute atomic radii (called Coulomb radii in this context) that determine the van der Waals surface and also choose an effective solvent radius. The results are very sensitive to the position of this surface, and this sensitivity shows up as the sensitivity mentioned above to the model radii.[175,205] But the solute–solvent boundary is intrinsically ambiguous because in the real system, the dielectric constant does not change suddenly at a well-defined boundary, and in the first solvation shell the dielectric constant is not equal to the bulk value.[206–210] Treatments of the non-bulk-electrostatic effects that do not take account of the ambiguity of the bulk electrostatics due to the ambiguity in the placement of this boundary, such as the cavity-dispersion–repulsion contributions in PCM models[172] do not yield quantitatively accurate solvation energies.[204] A key advantage of the SMD and SM*x* approaches is that the NBE terms are parametrized to be consistent with a given choice of solute radii. If the solute radii are changed and the parametrization repeated, one obtains similar results; thus the sensitivity to the choice of radii is diminished, at least for neutral solutes.[203–205] The SM*x* approach[180] of parameterizing the first-solvation-shell effects to be consistent with a given electrostatic model has also been adopted in the MST model of Luque *et al.*[194,195] and in Jaguar[190,191] solvation models.

3.6. Accuracy of implicit-solvent models

This section reviews applications of computational protocols that involve a computation of the free energy of a target reaction or half-reaction in solution using high-level quantum mechanical calculations in combination with the dielectric continuum approximation for treatment of solvation effects. Such computational protocols typically include the use of thermochemical cycles that relate the standard free energy of the redox reaction in solution to its gas-phase counterpart through the solvation free energies of the reactants and the products (see Scheme 2). Such an approach, which is also commonly used to predict pK_a values,[126,211] has been shown in several instances to predict reduction potentials accurate to within 50 mV (equivalent to predicting free energies of reaction to 5 kJ mol^{-1}) of experiment for various classes of compounds.[55,86,140,212–223]

In one study, Baik and Friesner[224] computed the standard redox potentials of selected organic molecules, metallocenes, and inorganic transition metal ions supported by bipyridine ligands in water, acetonitrile, dimethylformamide, and dichloromethane using the B3LYP[225,226] exchange–correlation functional along with augmented triple-zeta quality basis sets and in combination with a self-consistent reaction field continuum solvation model for solving the NPE for bulk electrostatics, and they obtained a mean unsigned error (MUE) of 150 mV in the computed standard redox potentials (relative to available experimental data) for species in both water and organic solvents. Similarly, Fu *et al.*[212] combined the B3LYP exchange–correlation

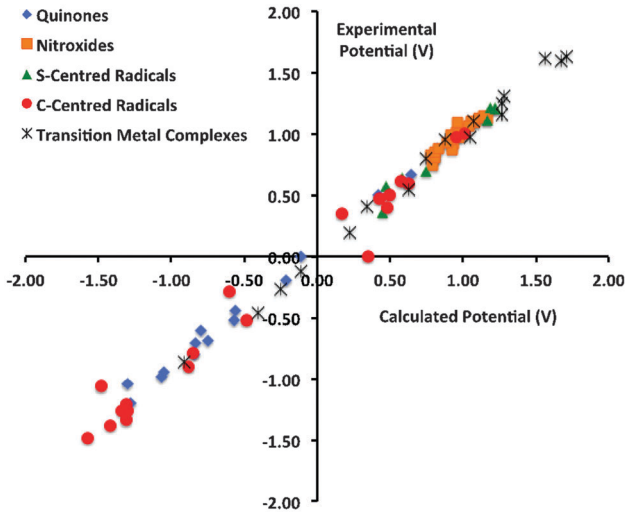

Fig. 1 Theoretical reduction potential *versus* experimental one for 84 chemical compounds of various classes.[140,212,213,215,217,219–221]

functional with the dielectric version of the polarizable continuum model of Tomasi *et al.* (D-PCM)[172,185] to estimate reduction potentials for 270 organic molecules in acetonitrile with a MUE of 170 mV. Sviatenko *et al.*[227] have recently studied the standard reduction potentials for a number of functionalized organic compounds including quinones and nitro and azacyclic compounds by testing several exchange–correlation functions, basis sets, and continuum solvation models. In particular, they have found that a combination of the M05-2X[129] exchange–correlation functional used with triple-zeta quality basis sets and the SMD continuum solvation model[82] results in an MUE of 120 mV.

We have combined the data from several different studies[140,212,213,215,217,219–221] to compare calculated *versus* experimental reduction potentials for a variety of systems, including O-, S- and C-centered radicals, and transition metal complexes, in both aqueous and nonaqueous solvents. Fig. 1 shows the reduction potentials for a sample of 84 compounds, and for this sample of compounds the mean unsigned error in the computed data relative to experiment is about 65 mV (or 6 kJ mol^{-1}), which we consider to be remarkably small in light of the diverse range of compounds in the test set. Excellent results on the prediction of reduction potentials (to within 50 mV) that may be sometimes found in the literature are usually specific to a particular class of compounds. However, more realistic errors (especially, when larger and more diverse test sets are considered) can be much larger. Recall that there are actually a considerable number of parameters [*e.g.*, a level of theory, solvent model, choice of the reference values for $\Delta G^{o}_{S}(H^{+})$ and E^{o}_{abs}(SHE)] that can significantly impact the accuracy of the prediction. Results obtained using implicit-solvent models such as PCM can also differ due to different scaling factors for atomic Coulomb radii used by default in popular computational programs or chosen by the user.[222] In the numerous studies that report highly accurate results, different combinations of the aforementioned parameters and settings are often used and are usually restricted to specific classes of compounds and therefore the performance of these methods with respect to *general* prediction of reduction potentials still requires further investigation.

Electrochemical half-reactions necessarily involve the consumption or generation of charged species, the solvation free energies for which, experimental or calculated, have relatively large uncertainties. For example, there is some ambiguity concerning whether the experimental solvation free energies of ionic species, used to parameterize continuum solvent models, include the contribution associated with the surface potential of the solvent,[67] the contribution of which has been estimated in various ways, for example recent studies gave about 13–14 kJ mol^{-1} for water as solvent.[60,67] In comparison with experiment, there are additional considerations concerning the conversion constants between different reference electrodes in different solvents and whether the effect of liquid junction potentials is likely to be significant, in addition to choosing the reference solvation free energy of the proton and the corresponding absolute potential of the reference electrode. For these reasons, calculating a reduction potential with 50 mV accuracy may be regarded as a very challenging task.

To this end, we have carried out a systematic assessment study with the view to identifying optimal combinations of level of theory, solvation model, and thermodynamic cycle, which are suitable for *accurate* and *general* prediction of reduction potentials in the gas and aqueous phase. The calculations were carried out using ADF,[228] Gaussian 09,[168] and Molpro.[229,230] Further details including experimental reference data[53,84,85,231–247] used in the assessment study are given in the ESI.†

Fig. 2 compares the performance of various DFT methods (B3LYP, BMK, B97-1, M05-2X and M06-2X) and high-level composite procedures such as G3(MP2,CC)(+), G3MP2B3 and ROCBS-QB3 for the calculation of 72 adiabatic ionization potentials and 21 electron affinities respectively encompassing a broad range of organic compounds. As shown, the three composite procedures

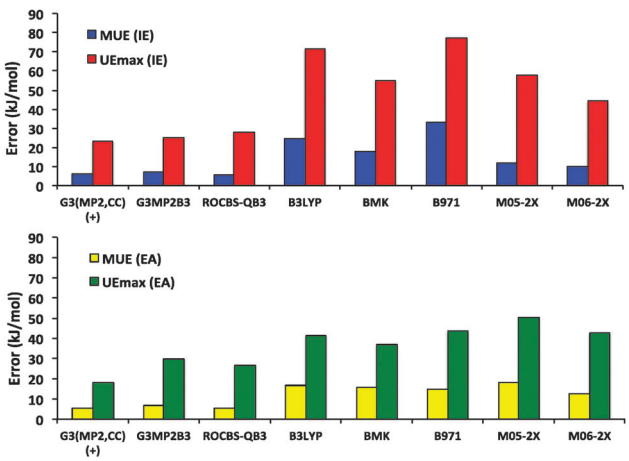

Fig. 2 Performance of various composite procedures and DFT methods in calculating the gas-phase ionization potentials (top) and electron affinities (bottom). Mean unsigned errors (MUE) and maximum unsigned error (UE_{max}) are in kJ mol^{-1}.

perform consistently well for both target calculations with mean unsigned errors (MUEs) of about 60 mV (or 6 kJ mol^{-1}) whereas DFT methods generally incur much higher errors (> 20 kJ mol^{-1}) with the exception of M05-2X and M06-2X where the MUEs are about 12 and 10 kJ mol^{-1}, respectively. It is also interesting to note that some DFT methods such as B97-1 perform reasonably well for the calculation of electron affinities (MUE = 15 kJ mol^{-1}) but the corresponding error for ionization potentials is two-fold larger (30 kJ mol^{-1}). In this regard, the M06-2X method performs much more consistently, having errors for both ionization potentials and electron affinities of 10 and 13 kJ mol^{-1}, respectively. Additionally, it is also worth noting that the largest unsigned errors (UE_{max}) for the composite procedures are generally smaller than those observed for the DFT methods examined in this study by a factor of two or more.

Based on the above results, we have selected the G3(MP2,CC)(+) method for gas-phase calculations in conjunction with the C-PCM (UAHF/UAKS), SMD, and COSMO-RS continuum models for calculating aqueous standard reduction potentials for a collection of 53 organic molecules incorporating a variety of functionalities (nitroxides, phenols, hydroquinones, aliphatic amines, anilines, indoles and organosulphur compounds). As noted in Section 2.4, reduction potentials should be calculated using a reference value of E^{o}_{abs} for the SHE that is based on the same value of $\Delta G^{o}_{S}(H^{+})$. As such, all calculated reduction potentials are with respect to E^{o}_{abs} (SHE) = 4.28 V, except for the CPCM-UAHF calculations where the value of E^{o}_{abs}(SHE) = 4.47 V is employed.[78] The results are summarized in Fig. 3.

One can see from Fig. 3 that the performance of implicit-solvent models can vary considerably depending on the type of compound under study. For instance, all continuum solvation models perform very well for nitroxides and amines where the MUE ranges from 50 to 200 mV. On the other hand, the corresponding errors for alcohols range from 200 to 350 mV. Overall, the MUEs are 190, 230, 210 and 190 mV for the CPCM-UAHF, CPCM-UAKS, SMD and COSMO-RS models, respectively. The smaller errors observed in selected classes of compounds might be attributed to systematic cancellation of errors, and/or similarity to the types of compounds used to parameterize the implicit-solvent models. At the same time, it is worth noting that the oxoammonium reductions (*i.e.*, nitroxide radical oxidations) are simple one-electron processes for which theory and experiment can be compared directly, whereas the one-electron reduction of the amines and phenols also involve changes in the protonation state. The experimental one-electron reduction potentials are thus not direct measurements but are derived from experimental data for proton-coupled electron transfer processes using additional data (such as pK_a values and/or bond dissociation free energies). Hence in such cases, the greater deviations of theory and experiment may also actually reflect greater uncertainty in the experimental results.

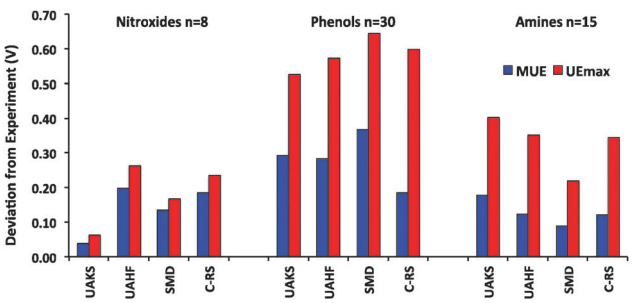

Fig. 3 Performance of various continuum solvent models in conjunction with the G3(MP2,CC)(+) method in calculating the aqueous reduction potentials of a range of compounds that have been broadly categorized as nitroxides, alcohols and amines (*n* = number of compounds in a dataset). C-RS means COSMO-RS.

A related study was reported earlier by Guerard and Arey.[248] They studied aqueous single-electron oxidation potentials of a smaller test set of 22 neutral organic compounds for which accurate experimental oxidation potential and gas-phase ionization energy data were available. They found mean unsigned errors of 270 to 500 mV, depending on the model, with the best results obtained with the SMD solvation model. The larger average errors observed in the latter study is presumably because some of the implicit-solvent models were applied using atomic radii, scaling factors and/or levels of theory that were not optimized for some of the implicit-solvent models. Nonetheless, these studies indicate (assuming one uses a chemically accurate level of theory) that a realistic error estimate for the general prediction of *aqueous* absolute reduction potentials would be in the range of 200 to 250 mV. Note also that the errors in non-aqueous solvents are likely to improve since the solvation contribution to the solution-phase reduction free energies may be smaller.

We have found that alternative approaches such as the calculation of relative reduction potentials are generally more accurate by virtue of systematic error cancellation. By selecting an appropriate reference, one can further construct an isodesmic reaction to afford further error cancellation in the gas-phase electronic structure calculations.[78] Konezny *et al.*[249] (see also ref. 250) have also recently discussed ways to reduce systematic uncertainties in DFT predictions of reduction potentials using the Born–Haber thermochemical cycle (see Scheme 2 in the present article), and they have concluded that one can calculate reduction potentials that are as accurate as those from cyclic voltammetry even with a "modest" level of DFT, in particular B3LYP/6-311G(d) combined with the continuum solvation model of Jaguar.[189–191] To do so, one needs to calculate the reduction potential relative to an internal reference redox couple such as the ferricenium/ferrocene redox couple calculated at the same level of theory rather than relative to the SHE.[249] The authors[249] also note that experimental reduction potentials are typically measured against some reference redox couple and then converted to an equivalent value *versus* a standard electrode, but this conversion may be fraught with difficulties associated with the standard reference electrodes such as the presence of liquid junction potentials and the issues of reproducibility due to electrode surface chemistry.

4. Protocols based on explicit-solvent models

In this section we review theoretical protocols that treat solvent molecules explicitly. These methods expand the scope

of computational studies to permit examination of solvent structure and reorganization.

4.1. Theoretical background

Usually, the nuclear motion is treated classically,[251] although procedures for quantizing vibrational energies in some kinds of simulations are available.[252–254] The potential energy function that governs nuclear motion (in molecular dynamics simulations) or that generates the ensemble average (in Monte Carlo simulations) may come from quantum mechanical (QM) electronic structure calculations (*e.g.*, through the Car–Parrinello method[5,255] or the X-Pol method[154] to propagate the dynamics), from molecular mechanics (MM),[256] or from combined QM/MM methods.[13,20–22,257,258] The MM and QM/MM approaches can be useful for the study of reduction potentials in large or complex systems that are impractical for full electronic structure calculations, *e.g.* because they may require extensive statistical mechanical sampling of configurations in order to obtain a meaningful ensemble average.

Liquid-phase free energies may be computed from simulations by statistical perturbation theory or thermodynamic integration based on an ensemble of configurations generated from the MD trajectory or by using MC procedures.[259–263] When explicit-solvent simulations are employed, careful attention must be paid to energetic effects associated with various technical aspects of the calculations, such as the size of the unit cell if periodic boundary conditions are employed or the size of the treated system if stochastic boundary conditions are employed, and the possible use of Ewald summation to compute electrostatic interactions. For example, Hummer *et al.*[264] and Ayala and Sprik[265] concluded that computed solvation free energies require a finite-size correction that scales as the inverse third power of the effective length of the simulation cell.

Selected computational techniques that utilize explicit-solvent modeling and relevant concepts will be discussed next. For further discussion of the use of explicit-solvent simulations to compute reduction potentials, we refer readers to the relevant primary literature.[261,266–274] The free energy problem in regard to MC and MD simulations is reviewed elsewhere.[262,275]

Standard liquid-phase computer simulations usually utilize either a canonical ensemble, also called an *NVT* ensemble,[276,277] in which the number of particles (N), volume (V) and temperature (T) are conserved, or an isothermal–isobaric ensemble, also called an *NPT* ensemble, in which the pressure (P) rather than the volume is fixed.[278–280] In the text below we will consider canonical *NVT* ensembles, and we will also discuss grand canonical ensembles when N is a variable.[276,281–284] In addition, when we talk about free energies, we do not distinguish here between Gibbs free energy (G) and Helmholtz free energy (A) for simplicity. In fact, the difference between ΔG and ΔA for reactions in solution under ambient conditions is expected to be negligible because the volume change is small for such reactions.

In the context of explicit-solvent simulations, the free energy G_X for the solute in the oxidation state X (X = O or R) depends on the solute's activity (a_X), while the quantity a_X depends on the number of solvent molecules included in a simulation box. For example, in the case of 1 M aqueous solution we would need approximately 56 water molecules per solute molecule (because the density of water is $\sim$1 kg L^{-1} at 298 K and 1 bar, and the molecular weight is 0.018 kg mol^{-1}). However, the number of solvent molecules that determines the size of a simulation box in actual simulations is not tied to the standard-state concentration (1 M) because the standard state is an ideal 1 M solution and so it must be modeled at a low enough concentration that solute–solute interactions are negligible. Lowering the concentration increases the number of solvent molecules per solute molecule over the number calculated above.

4.2. Potential of mean force

In this section we will show a connection between explicit-solvent and implicit-solvent models through the concept of potential of mean force.

The free energy of an individual solute species X in the system of solute plus solvent can be expressed as[87,285]

$$G(\mathrm{X}) = -\beta^{-1} \ln\left[\int \mathrm{d}\mathbf{R} \mathrm{e}^{-\beta W(\mathbf{R})}\right] + C \qquad (33)$$

where $W(\mathbf{R})$ is

$$W(\mathbf{R}) = -\beta^{-1} \ln\left[\int \mathrm{d}\mathbf{P}\,\mathrm{d}\mathbf{r}\,\mathrm{d}\mathbf{p} \mathrm{e}^{-\beta H(\mathbf{P},\mathbf{r},\mathbf{p})}\right] + C' \qquad (34)$$

In eqn (33) and (34), β is equal to $1/k_B T$ (k_B is Boltzmann's constant), C and C' are geometry-independent constants defined by the choice of zero energy and standard state, H is the classical Hamiltonian, the vector $\mathbf{R}$ denote n internal coordinates of the solute molecule X containing N atoms (where $n = 3N - 6$), the vector $\mathbf{P}$ denotes the conjugate momenta of $\mathbf{R}$, and $\mathbf{r}$ and $\mathbf{p}$ denote the remaining coordinates and conjugate momenta of the entire solute–solvent system.[87] The quantity $W(\mathbf{R})$ is the potential of mean force,[276,286–289] *i.e.* the average force (averaged over $\mathbf{r}$, $\mathbf{p}$, and $\mathbf{P}$) acting on the solute molecule X at the fixed configuration $\mathbf{R} = \{R_1,\ldots,R_n\}$ in the thermally equilibrated ensemble. The function $W(\mathbf{R})$ can be considered as the solution-phase analogue of a gas-phase potential energy surface (PES) and it is sometimes called the free energy surface (FES).[87,290,291]

The potential of mean force is an effective free energy potential that depends on state variables such as concentrations, temperature, and pressure.[277] In the case when solvent effects are modeled implicitly using dielectric continuum models (see Section 3), and the solution is infinitely dilute, the potential of mean force $W(\mathbf{R})$ can be simply approximated by the $3N - 6$ surface (with a convenient choice for the zero of energy) as[290,292]

$$W(\mathbf{R}) = V(\mathbf{R}) + \Delta G_S^*(\mathbf{R}) \qquad (35)$$

where the first term on the right-hand side is the gas-phase PES of the solute molecule X, and the second term is the 1 M fixed-concentration free energy of solvation into an ideal solution (see Section 3). The equation is based on the assumption that the solute geometry as well as the rotational–vibrational free

energy component are the same in both phases (appropriate corrections[87] can be introduced if desired).

When solvent effects are modeled explicitly by Monte Carlo or molecular dynamics simulation, the potential of mean force $W(\mathbf{R})$ can be evaluated, for example, with the use of umbrella sampling techniques;[293,294] see the literature[295] for recent applications. In general, the potential of mean force can be obtained from simulations in two ways.[275] First, the coordinate $\mathbf{R}$ can be considered as an additional variable in the simulation, thereby producing a direct estimate of $W(\mathbf{R})$. Second, one can perform separate simulations at different fixed values of $\mathbf{R}$, compute the forces due to the surroundings, and then integrate the force functions numerically.[275]

In many cases, solving the free energy problem through MC or MD simulations requires determining a free energy difference between two well-defined states rather than absolute free energies for individual states, and the calculation of relative free energy can be performed using the thermodynamic integration approach or the perturbation free energy method,[275,296] which two approaches will be outlined next, or other techniques described in detail elsewhere.[275,297]

4.3. Thermodynamic integration

As explained in Section 2.3, if one uses the electron convention, the reduction potential of the half-reaction (1) in solution can be computed from the free energy of the reaction expressed as

$$\Delta_r G = G_R - G_O \tag{36}$$

where G_R and G_O are free energies of the reduced (R) and the oxidized (O) species in solution, respectively. The electron is treated as a gas-phase particle, and the free energy of the free electron is assumed to be zero (Table 1). The free energy change $\Delta_r G$ depends in general on the activities a_O and a_R. If the free energies G_O and G_R are derived from two independent MC or MD computations with the same size of a simulation box in each (by keeping the number of solvent molecules and the solvent's density unchanged), then we can assume that $a_O = a_R$ (provided that the corresponding activity coefficients are also the same). In this case, we have $\Delta_r G$ equal to $\Delta_r G^o$ where $\Delta_r G^o$ is the standard-state free energy of the half-reaction.

The solute–solvent system containing the solute in the oxidation state X has the total potential energy $U_X(\mathbf{x})$ where the vector $\mathbf{x}$ denote Cartesian coordinates of all atoms in the system. By using the thermodynamic integration approach to calculate $\Delta_r G^o$,[275,298] one can introduce a hypothetical hybrid system with the total potential energy $U(\eta,\mathbf{x})$ defined as a function of $U_R(\mathbf{x})$ and $U_O(\mathbf{x})$ where η is a coupling parameter that varies from $\eta = 0$ for the oxidized state to $\eta = 1$ for the reduced state. The free energy $\Delta_r G^o$ can then be evaluated by integrating over η as

$$\Delta_r G^o = \int_0^1 d\eta \frac{\partial G(\eta)}{\partial \eta} \tag{37}$$

with the free energy of the new system, $G(\eta)$, defined as

$$G(\eta) = -\beta^{-1} \ln Z(\eta) + C_{NVT} \tag{38}$$

where β is equal to $1/k_B T$, C_{NVT} is a geometry-independent constant for a given canonical (NVT) ensemble, and $Z(\eta)$ is the configurational part of the total canonical partition function, Q_{NVT}. The function $Z(\eta)$ is defined as

$$Z(\eta) = \sum_k e^{-\beta U(\eta, \mathbf{x}_k)} \tag{39}$$

where the index k runs over all instantaneous solute–solvent configurations $\mathbf{x}_k$ (snapshots) derived, for example, from MC simulations.

The function $G(\eta)$ has the meaning of the potential of mean force with respect to the coordinate η.[275] The derivative $\partial G/\partial \eta$ can be recast as

$$\frac{\partial G(\eta)}{\partial \eta} = \frac{1}{Z(\eta)} \sum_k \frac{\partial U(\eta, \mathbf{x}_k)}{\partial \eta} e^{-\beta U(\eta, \mathbf{x}_k)} = \left\langle \frac{\partial U(\eta, \mathbf{x})}{\partial \eta} \right\rangle_\eta \tag{40}$$

where the derivative $\partial U/\partial \eta$ is taken as an ensemble average at fixed η. Therefore, we have

$$\Delta_r G^o = \int_0^1 d\eta \left\langle \frac{\partial U(\eta, \mathbf{x})}{\partial \eta} \right\rangle_\eta \tag{41}$$

Eqn (41) shows the essence of the thermodynamic integration method[275] originating from Kirkwood's work on liquid state theory.[299] The methodology of thermodynamic integration in the context of MC or MD simulations includes a series of independent simulations at discrete values of η, Boltzmann averaging of $\partial U/\partial \eta$ at each η, and then numerical integration over η.[275]

The most frequently used form for $U(\eta,\mathbf{x})$ is a linear dependence on η as[275]

$$U(\eta,\mathbf{x}) = U_O(\mathbf{x}) + \eta[U_R(\mathbf{x}) - U_O(\mathbf{x})] \tag{42}$$

Recall that $U_O(\mathbf{x})$ and $U_R(\mathbf{x})$ denote the total potential energy of the solute–solvent system at the solute–solvent configuration $\mathbf{x}$ with the solute in the oxidation state O ($\eta = 0$) and R ($\eta = 1$), respectively. With the use of eqn (42), $\partial U/\partial \eta$ can be expressed as

$$\frac{\partial U(\eta, \mathbf{x})}{\partial \eta} = U_R(\mathbf{x}) - U_O(\mathbf{x}) = \Delta U(\mathbf{x}) \tag{43}$$

where $\Delta U(\mathbf{x})$ is the vertical energy gap (VEG) as an analogue of the vertical excitation energy controlled by the Franck–Condon principle.[300] Note that, although the quantity $\Delta U(\mathbf{x})$ does not depend on the coupling parameter η, the resulting ensemble average used in eqn (41) must be taken over the distribution $Z(\eta)$ that depends on η as

$$\langle \Delta U \rangle_\eta = \frac{1}{Z(\eta)} \sum_k \Delta U(\mathbf{x}_k) e^{-\beta U(\eta, \mathbf{x}_k)} \tag{44}$$

In addition, one can assume the linear response regime for $\langle \Delta U \rangle_\eta$ with respect to η as

$$\langle \Delta U \rangle_\eta = \langle \Delta U \rangle_O + \eta(\langle \Delta U \rangle_R - \langle \Delta U \rangle_O) \tag{45}$$

where $\langle \Delta U \rangle_X$ (X = O or R) is the VEG averaged over thermal fluctuations of the solvent as

$$\langle \Delta U \rangle_X = \frac{1}{Z_X} \sum_k \Delta U(\mathbf{x}_k) e^{-\beta U_X(\mathbf{x}_k)} \quad (46)$$

The configurational partition functions Z_O and Z_R are obtained as

$$Z_X = \sum_k e^{-\beta U_X(\mathbf{x}_k)} \quad (47)$$

where the index k runs over all instantaneous solute–solvent configurations $\mathbf{x}_k$ containing the solute in the oxidation state X (X = O or R). By integrating $\langle \Delta U \rangle_\eta$ over η, we arrive at the following expression for the free energy difference:

$$\Delta_r G^o = \tfrac{1}{2}(\langle \Delta U \rangle_O + \langle \Delta U \rangle_R) \quad (48)$$

In practice, the quantities $\langle \Delta U \rangle_O$ and $\langle \Delta U \rangle_R$ are obtained by averaging the corresponding VEGs over equilibrium trajectories derived independently for each oxidation state. Eqn (48) was found to be a good approximation for many half-reactions,[272] and it has been recently used, for example, by Wang and van Voorhis[301] in the context of their QM/MM MD simulation. However, for certain half-reactions (*e.g.*, proton-coupled electron-transfer reactions) the solvent response is often nonlinear, and, in practice, $U(\eta,\mathbf{x})$ needs to be calculated at several intermediate values of η (in addition to η = 0 and 1).[272]

4.4. Free energy perturbation method

In the free energy perturbation method,[302,303] the free energy change for the half-reaction (1) can be computed as[275]

$$\Delta_r G^o = -\beta^{-1} \ln \langle e^{-\beta \Delta U} \rangle_O \quad (49)$$

where the expression in brackets is defined as

$$\langle e^{-\beta \Delta U} \rangle_O = \frac{1}{Z_O} \sum_k e^{-\beta \Delta U(\mathbf{x}_k)} e^{-\beta U_O(\mathbf{x}_k)} \quad (50)$$

where the distribution Z_O is given by eqn (47) at X = O, and the remaining quantities are defined above. Alternatively, one can cast the free energy difference as

$$\Delta_r G^o = \beta^{-1} \ln \langle e^{\beta \Delta U} \rangle_R \quad (51)$$

obtained using the distribution Z_R. The hysteresis between results obtained from the forward integration [eqn (49)] and the backward integration [eqn (51)] is expected to be small when the final state (R) is geometrically close to the initial state (O) so that one state can be regarded as a perturbation of the other.[275] This is not the case when relaxation effects upon the reduction O → R (for example, in aqueous solutions) are large enough to lead to very different equilibrium configurations. In this case, configurations sampled in an equilibrium MD run for O do not represent well the configurational space for R and *vice versa*. However, one can obtain a fairly accurate estimate for the free energy difference simply by averaging the energies calculated using eqn (49) and (51).[304] A relation of eqn (49) and (51) to eqn (48) has been proved.[305] Other "tricks," such as "double wide sampling," are also employed to make the calculations more efficient.[306]

4.5. Grand canonical approach

In this section we discuss the grand canonical ensemble[276,281–284] formalism which is also used sometimes in the literature[305,307] in particular, in connection to Car–Parrinello[5] molecular dynamics (CPMD) simulations of redox reactions. Unlike a canonical *NVT* ensemble, in a grand canonical ensemble the number of particles (N) is allowed to fluctuate by exchanging the particles with a reservoir while keeping the ensemble's macroscopic variables μ, V, and T conserved, where μ is the chemical potential.[276] The equilibrium partition function of the μVT ensemble can be defined as[276]

$$\Xi_{\mu VT} = \sum_N z^N Q_{NVT} \quad (52)$$

where Q_{NVT} is the partition function of a canonical ensemble, and the quantity z is the so-called absolute activity related to the chemical potential (μ) of the grand canonical ensemble as

$$z = e^{\beta \mu} \quad (53)$$

where β is equal to $1/k_B T$.

The grand canonical formalism is employed for MD simulations by coupling the MD system to a generic electron reservoir which allows the number of electrons to vary during a single MD simulation at a given value of the electronic chemical potential treated as a thermodynamic control parameter, while the other particles in the system are treated by canonical ensembles.[305] The generic electron reservoir plays a role of a fictitious electrode. The grand canonical MD approach is based on the grand canonical partition function of the electronic system in the limit of zero temperature (thereby ignoring electronic excitations).[308]

In the case of the half-reaction (1), the grand canonical partition function of eqn (52) is expressed as[305]

$$\Xi_{\mu_e VT} = e^{\beta \mu_e N_e^O} Q_O + e^{\beta \mu_e N_e^R} Q_R \quad (54)$$

where μ_e is the electronic chemical potential, N_e^O is the number of electrons in the solute–solvent system containing the solute in the oxidized state, N_e^R is the number of electrons in the system containing the solute in the reduced state, Q_O and Q_R are canonical partition functions for the systems O and R, respectively. The number of electrons (N_e) in the system changes from N_e^O to N_e^R. The electronic chemical potential can then be expressed as

$$\mu_e = -\frac{1}{\beta n_e} \ln \frac{\xi}{n_e - \xi} + \frac{1}{n_e} \Delta_r G^o \quad (55)$$

where n_e is equal to $N_e^R - N_e^O$ [according to eqn (1)], and $\Delta_r G^o$ is the free energy change for eqn (1) related to Q_O and Q_R as

$$\Delta_r G^o = -\frac{1}{\beta} \ln \frac{Q_R}{Q_O} \quad (56)$$

In eqn (55), ξ is the fractional charge calculated relative to R as

$$\xi = N_e^R - \bar{N}_e \quad (57)$$

where $\bar{N}_e$ is the average number of electrons in the grand canonical ensemble calculated as[276]

$$\bar{N}_e = \frac{1}{\beta}\left(\frac{\partial \Xi_{\mu_e VT}}{\partial \mu_e}\right)_{V,T} \quad (58)$$

According to eqn (55), the free energy $\Delta_r G^o$ is equal to $n_e\mu_e$ in the case of $\xi = n_e/2$, which in the context of MD simulations means a situation when the system spends equal amounts of time in both oxidized and reduced states.[305] Therefore, the quantity $\Delta_r G^o$ can be obtained by varying μ_e as an external parameter in the simulation. By expressing the fractional charge ξ in eqn (55) as $\xi(\mu_e)$, one can find the optimum value of μ_e when ξ equals $n_e/2$. How to do it in practice is described elsewhere.[268] The approach is called numerical titration because the sigma-shaped function $\xi(\mu_e)$ resembles a titration curve.[305]

The effective PES used in practical computations using the numerical titration method depends on μ_e as a mixing parameter, and it is constructed as

$$U(\mu_e,\mathbf{x}) = \min[U_O(\mathbf{x}) + n_e\mu_e,\ U_R(\mathbf{x})] \quad (59)$$

where $U_O(\mathbf{x})$ and $U_R(\mathbf{x})$ are the adiabatic potential energy surfaces for each oxidation state. The composite surface $U(\mu_e,\mathbf{x})$ consists of the lowest branches of two intersecting surfaces, and the parameter μ_e simply shifts one surface relative to the other.[305] The method was implemented for CPMD simulations with inclusion of analytical nuclear gradients.[307] To some extent, the numerical titration approach based on eqn (59) is similar to the thermodynamic integration method outlined in Section 4.3. However, in the latter case the hybrid PES is constructed through a linear coupling of $U_O(\mathbf{x})$ and $U_R(\mathbf{x})$ [see eqn (42)] rather than by mixing [see eqn (59)].

The numerical titration method based on the grand canonical ensemble is not limited by the linear response approximation [see eqn (48)] and it is completely general.[305] There is a similarity between this scheme and the surface hopping method of Nikitin[309] and Tully[310] for studying excited-state dynamics. Since vertical ionization potentials are positive, the reduced species can be understood as a molecular system in the ground electronic state while the oxidized species can be the same system in the excited electronic state. However, the dynamics in the numerical titration case is strictly adiabatic.[268]

4.6. Connection to the Marcus theory of electron transfer

The microscopic interpretation of the free energy functions for electron-transfer and proton-transfer reactions in solution is frequently discussed[308,311,312] using the language and concepts of the Marcus theory of weak-overlap electron transfer.[313–317] We note, however, that Marcus theory strictly applies only to a subset of charge transfer reactions.[315,318–320] Here we recall the basic ideas of Marcus theory relevant to prediction of the free energy of the half-reaction (1), $\Delta_r G^o$.

In Marcus theory, the free energy curves (actually they are potentials of mean force – see below) $G_R(q)$ and $G_O(q)$ are represented by intersecting diabatic free energy curves as functions of an appropriate reaction coordinate q as shown in Scheme 3, and these curves are assumed to be quadratic with respect to q, with equal curvature.[308,311] The quadratic nature of the free energy curves results from assuming that the solvent responds linearly to the changes in the solute. The reaction coordinate q nominally describes solvent polarization,[313] although it is not directly related to the polarization of the first solvation shell.[311] In the original theory,[313,316] it refers to the bulk electrostatics, but in extensions,[314] the reaction coordinate can also describe the inner sphere of ligands on the redox center. The solvent polarization coordinate q can be related to the fractional amount of charge transferred as the reaction proceeds. The quantity $G_X(q)$ has the meaning of the potential of mean force with respect to q taken as an ensemble average over all remaining degrees of freedom in the solute–solvent system. The electron transfer between O and R can then be treated as a transition between the reactant and product states, with progress measured by the average change of the solvent.[311,313]

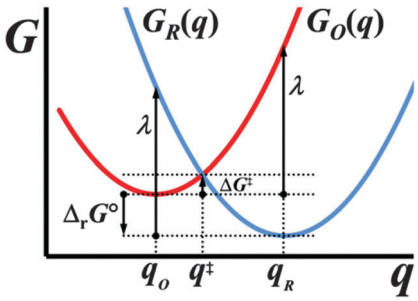

$$\lambda = G_R(q_O) - G_R(q_R) = G_O(q_R) - G_O(q_O)$$

$$\Delta_r G^\circ = G_R(q_R) - G_O(q_O)$$

$$\Delta G^\ddagger = (\Delta_r G + \lambda)^2 / (4\lambda)$$

Scheme 3 The charge transfer between the oxidized (O) and reduced (R) species in terms of Marcus theory. The curves describe the free energies of O and R as functions of the solvent polarization coordinate q. The values of q_O and q_R refer to the corresponding equilibrium positions, and $q^\ddagger$ refers to the transition state. The quantities λ, $\Delta_r G^\circ$, and $\Delta G^\ddagger$ are the solvent reorganization free energy, the free energy of the O + e^- = R reaction, and the activation free energy, respectively.

Using Scheme 3, and neglecting the work required to bring the reactants to a suitable electron transfer distance and to separate the reactants and products,[317] one can relate the free energy of the half-reaction (1), $\Delta_r G^o$, to the solute's vertical energy gap ΔG and the solvent's reorganization free energy λ as follows

$$\Delta_r G^o = \Delta G(q_R) + \lambda \quad (60)$$

where $\Delta G(q_R)$ is $G_R - G_O$ calculated at $q = q_R$. The value of $\Delta G(q_X)$ is the vertical energy gap of the solute–solvent system containing the solute in the oxidation state X (X = O or R) averaged over the distribution Z_X given by eqn (47). Similarly we can write

$$\Delta_r G^o = \Delta G(q_O) - \lambda \quad (61)$$

where $\Delta G(q_O)$ is $G_R - G_O$ calculated at $q = q_O$. By combining these equations, we arrive at

$$\Delta_r G^o = \tfrac{1}{2}[\Delta G(q_O) + \Delta G(q_R)] \quad (62)$$

where eqn (62) is the same as eqn (48), provided that $\Delta G(q_X) \equiv \langle \Delta U \rangle_X$ (see Section 4.3).

In the practical adaptation of Marcus theory to computer simulations, the reaction coordinate q should describe the equilibrium states O and R and the transition (nonequilibrium) state (see Scheme 3), and it must be formally defined as a function of the microscopic configuration **x** (where **x** refers to the coordinates of all atoms in the solute–solvent system).[321] Thus, this can be the solvent polarization function in terms of the solvent electrostatic potential, some geometric coordinate, or the vertical energy gap itself (used, for example, by King and Warshel[311]).[321] If the assumptions of Marcus theory were to hold for the chosen reaction coordinate, the two free energy functions (Scheme 3) could be approximated by only two parameters, namely, the solvent reorganization free energy λ and the thermodynamic driving force $\Delta_r G^o$.[321]

Based on computer simulations utilizing the free energy perturbation method (see Section 4.4), King and Warshel[311] investigated how closely the computed free energy functions for electron transfer reactions follow the parabolic form of Marcus theory, and they found that Marcus's approximation (using the linear response regime) could provide a valid description of the solvent's role in electron transfer processes over a wide range of conditions.[311] Sprik and co-workers[322] studied the $Ru^{3+}|Ru^{2+}$ half-reaction in water and noted that the particular system was almost ideal for the Marcus theory assumption that the surfaces must be quadratic with respect to a reaction coordinate q, with similar curvatures. These authors[322] also discussed how to proceed when the conditions for Marcus theory are not satisfied. For example, the $Ag^{2+}|Ag^{+}$ system in water exhibits moderately nonlinear deviations from Marcus behavior due to a change in the coordination number of Ag depending on its oxidation state.[322]

4.7. Accuracy of explicit-solvent models

Explicit-solvent simulations can be expensive[267] because they require a large number of solvent molecules to converge the electrostatics and because extensive configurational sampling is required. For example, in MD simulations in aqueous solution, the simulation must be carried out over a much longer time scale than the dipole relaxation time of water (which is about 10 ps at room temperature[323,324]). Nevertheless, the hope (not necessarily realized) is that they are more accurate for some kinds of processes.

In principle, explicit-solvent models would allow for a better treatment of first-solvation-shell electrostatics and polarization effects. In practice though, this potential advantage is often mitigated by other approximations made in explicit-solvent treatments. For example, calculations based on nonpolarizable mechanics cannot treat solvent polarization except perhaps indirectly by choice of parameters. Explicit-solvent simulations are often restricted to less accurate quantum mechanical models for the solute than are employed in implicit models; for example, explicit-solvent models are often carried out with local density functionals that are less accurate than the best available quantum mechanical models used for implicit-solvent calculations. In particular, Sprik *et al.*[325] have found that the electronic states of redox species in aqueous solution can mix with the valence and conduction band edges of water. The authors[325] have noted that the commonly used density functionals based on the generalized gradient approximation can exaggerate the mixing with the water valence band leading to a systematic underestimation of their redox potentials and to spurious nonlinearity in the solvent reorganization. The authors[325] also note that the predicted mixing of the electronic states of redox species with the unoccupied states of water may be real. The latter effect should thus be missing in *implicit* water models, though explicit-solvent models have been less broadly validated than implicit-solvent ones in general.

5. Protocols based on LFERs and other models

Alternative approaches that have been explored include linear free energy relationships (LFERs) that correlate reduction potentials with other computed or experimental observables. LFER methods can be useful for fast predictions of reduction potentials with moderate accuracy. Typically, such methods involve the calculation or measurement of one or more likely to be relevant properties, especially ionization energies or electron affinities in the gas phase, which are then regressed on solution-phase reduction potentials in order to develop a predictive equation. Here we will briefly discuss several selected protocols, and we refer the reader to primary sources[1,326–340] for details.

Winget *et al.*[1] tested several linear regression models for predicting the oxidation potentials of substituted anilines in aqueous solution using various descriptors such as experimental ionization potentials, pK_a values, and Hammett constants. Hicks *et al.*[328] found a good linear correlation between experimental reduction potentials for 29 monosubstituted chalcones in acetonitrile and their gas-phase electron affinities computed by DFT.

Shamsipur *et al.*[330] performed a quantitative structure–property relationship analysis of experimental electrochemical properties of 33 anthraquinone derivatives in acetonitrile using quantum-chemical, topological, constitutional (such as molecular weights), and chemical (such as $\log P$ values) descriptors. Moens *et al.*[332,333,335] studied a correlation between redox potentials and ionization potentials, electron affinities, electrophilicity or chemical hardness. Davis and Fry[337] have shown that experimental and computed redox potentials of polycyclic aromatic hydrocarbons are highly correlated over a large number of systems.

Cwiertny *et al.*[338] developed quantitative structure–activity relationships for alkyl polyhalide reductive dehalogenation by granular iron using gas-phase homolytic carbon–halogen bond dissociation energies and liquid-phase one-electron reduction potentials computed by a quantum chemistry composite method (G3MP2) for a series of 24 alkyl polyhalides.[338]

More recently Phillips *et al.*[339] have developed a linear model that relates the experimental one-electron reduction potentials

of several nitroaromatic compounds to their experimental or computed electron affinities.

Lynch *et al.*[340] have developed a method for predicting the ground-state reduction potentials based on the correlation of computed energy differences between the initial S_0 and one-electron-reduced D_0 species with experimental reduction potentials for 74 compounds of six different classes in acetonitrile.

Francke and Little[341] found a linear correlation between calculated effective ionization potentials and experimental oxidation potentials of phenanthro[9,10-*d*]imidazole derivatives.

6. Applications

In this section we discuss recent applications of various computational protocols for predicting liquid-phase reduction potentials and other electrochemical properties for a variety of chemical systems; these are representative examples as the full literature is too extensive for complete coverage in a feature article. The applied protocols are based on implicit- and explicit-solvent models as well as on LFERs and other models as described in the previous sections. In order to help readers find specific applications, the studies discussed in this section are organized based on the chemistry rather than on the method used. First, we will provide a survey of these studies and then we will discuss several selected topics in more detail.

6.1. Survey

6.1.1. Inorganic chemistry. We begin the survey with inorganic compounds. Recent computations of standard reduction potentials include studies of aqueous metal ions,[268,301,304,305,308,321,322,342–345] inorganic clusters containing sulfur and iron in different oxidation states,[346,347] systems of various complexity with the Pt_2X_2 (X = chalcogenide) cores,[348] and the MFe_2S_4 clusters (M = Mn, Fe, Co, Ni, Cu, Zn, and Mo) in water by testing four different exchange–correlation functionals (B3LYP, BP86, TPSS, and TPSSh) and the COSMO implicit-solvent model.[349]

Houk and co-workers[350,351] computed the standard redox potentials of 36 nitrogen oxides and related species in water using a complete basis set extrapolation method (CBS-QB3) for gas-phase free energies and the PCM implicit-solvent model for solvation free energies with use of the Born–Haber thermochemical cycle (Scheme 2). Studies on organic nitroxide radical species can also be found in the literature.[55,215,222,352] Density functional calculations of the reduction potentials of iron-containing nitrosyl complexes have been recently reported by Emel'yanova *et al.*[353,354]

The standard reduction potentials (in CH_2Cl_2 solution), proton affinities, and transition-state structures for prototypical H-atom transfer reactions were predicted for a novel class of heterobimetallic CuPd and CuPt bis(μ-oxo) complexes.[355] The influence of the size of the heteroatom X on the redox potentials of hetero-polytungstates $[XW_{12}O_{40}]^{q-}$ (X = B, Al, Ga, Si, Ge, P, As) in water was investigated by density functional theory using the dielectric continuum approximation.[356] See also a recent DFT study of the redox properties of W,O-containing Keggin compounds by Aparicio *et al.*[357] Structure, properties and reactivity of various polyoxometalates have been recently reviewed from a theoretical perspective by Lopez *et al.*[358] A theoretical study of high-valent oxoruthenium Keggin-type species has been conducted by Liu *et al.*[359] Many such polyoxometalates are known as efficient and robust oxygenation catalysts.[359] Ruthenium-based oxides with rutile structure were investigated in regard to their properties in electrocatalytic ethene oxidation in acid media, and DFT calculations were employed to study the energetics of key reaction steps.[360]

The accuracy of various exchange–correlation functionals for predicting the redox potentials of certain transition metal compounds have been addressed by Ceder and co-workers.[361] In particular, they have studied Li_xMO_2 (M = Co, Ni), Li_xTiS_2; Li_xMPO_4 (M = Mn, Fe, Co, Ni), $Li_xMn_2O_4$, and $Li_xTi_2O_4$ that can be important as Li-ion intercalation battery materials.[361]

Ding *et al.*[362] carried out a combined experimental and theoretical (DFT atomistic) study of the effects of carbon and nitrogen-doped carbon coating on the electrochemical performance of $Li_4Ti_5O_{12}$ (LTO) which is a promising anode material in lithium ion battery applications. The study revealed a strong binding between the graphene coating layer and the Ti-terminated LTO surface, which could significantly reduce the chemical activity of LTO surfaces and improve the electric conductivity of the electrode/electrolyte interface.[362] Also motivated by an interest in better understanding the behavior of possible battery electrolytes, Bryantsev *et al.*[363] employed DFT and coupled-cluster calculations together with continuum solvation for neutral molecules and mixed cluster/continuum solvation for single ions to study the electrochemical behavior of lithium nitrite in acetonitrile.

Mueller *et al.*[364] carried out large-scale DFT calculations of electrochemical and structural properties of tavorite-structured oxyphosphates, fluorophosphates, oxysulfates, and fluorosulfates as potential cathode materials in lithium-ion batteries. Tavorite-like compounds have the general formula $AM(TO_4)X$ where A is an alkaline or alkaline-earth element, M is another metal (*e.g.*, Al, Ti, V, or Fe), T is a p-block element, and X is O, OH, or F.[364]

Chaplin *et al.*[365] have recently carried out DFT implicit-solvent calculations on boron–carbon clusters with up to 34 carbon atoms per one boron atom to investigate possible mechanisms that would explain anodic wear of boron-doped diamond film electrodes.[365] The redox energetics of boron hydrides B_nH_n (n = 6–13) and the $B_{12}X_{12}$ compounds (X = F, Cl, OH, and CH_3) in water has also been investigated recently using density functional theory and implicit-solvent models.[366] Measured and calculated oxidation potentials of 31 icosahedral carborane anions have been reported by Wahab *et al.*[367]

Steele *et al.*[368] have recently predicted the standard reduction potentials for several actinide(VI)/actinide(V) redox couples in water in close agreement with available experimental data. In particular, they have investigated the $[AO_2(H_2O)_n]^{2+/+}$ systems (where A = U, Np, and Pu, and n = 4–6) using the M06[125] and M06-L[369] exchange–correlation functionals.[368] The M06 exchange–correlation functional has been found to be competitive with high level *ab initio* methods in the recent study of the water exchange

mechanism of the $[UO_2(H_2O)_5]^{2+}$ ion and the redox potentials of the AO_2^{2+} aqua complexes (A = U, Np and Pu).[370]

Shamov and Schreckenbach[371,372] have reviewed various theoretical approaches to predicting the chemistry of the actinide elements, for instance, the aqueous actinide(VI)/actinide(V) redox potentials. In particular, they have noted that implicit-solvent models can be reliable as long as the first coordination sphere of the metal is treated explicitly, and there is no advantage for the (potentially costly) explicit treatment of the second coordination sphere.[372]

Structure–reactivity relationships in inorganic electrochemistry have been discussed in a recent review by Schultz,[373] with emphasis on transition metal electron-transfer reactions. The author[373] considered several examples to illustrate how relations between structure and electron transfer reactivity underlie many important electrochemical applications and provide fundamental insight into chemical and biological processes. In particular, the author investigates the influence of sulfur *versus* oxygen donation on molybdenum-centered electron transfer, the role of spin crossover in electrochemical reactions in which electron transfer is coupled to a change in the spin state of a metal atom, and the case of concomitant multi-electron transfer and metal–metal bond cleavage in binuclear, ligand-bridged complexes.[373]

Hwang *et al.*[374] studied the oxygen reduction reaction in polymer electrolyte membrane fuel cells and showed how some of the bond interaction strength trends governing a volcano plot could be explained by d-band fillings and heat of alloy formation.

6.1.2. Organic chemistry. Electrochemical computation studies of organic compounds (here excluding metalorganic and organometallic species) involve anilines and phenols,[3] chlorinated aliphatic and aromatic environmental contaminants[4,375,376] hexakis (alkylsulfonyl) benzenes,[377] nitroaromatics[378–383] and other heteroaromatics.[384–388] Some of the studies cited above were reviewed by the four of us elsewhere[78] and have been partly discussed in Section 3 in the present paper.

There have been several studies on substituted indoles[389,390] and imidazoles,[391,392] pyridine and pyridine derivatives,[140,220] phenazine,[393] nucleotide bases,[394–396] and amino acids including tyrosine and tryptophan.[274] There were also computational electrochemical studies of polycyclic aromatic hydrocarbons,[397–400] dihydroxyanthracene and thioxanthens derivatives.[401,402] A DFT implicit-solvent calculation of the standard redox potential of anthraquinone-1-carboxylic acid and anthraquinone-2-sulfonic acid in water was reported.[403,404]

There have been numerous studies on flavins and related compounds,[261,273,405–409] and quinones and their derivatives.[3,140,214,217,218,220,221,223,272,410–413] For example, Zare *et al.*[221] studied the pH dependent oxidation of *o*-chloranil using both cyclic voltammetry and theoretical calculations, the latter were carried out using G3 energies and C-PCM solvation energies. The theoretical results are in excellent agreement with experiment, and they show that the competition between the alternative two-electron–one-proton and two-electron–two-proton processes is pH dependent. The same authors have used similar methodology to study the oxidation mechanisms of Rutin (also known as vitamin P),[217] 3,4-dihydroxyphenylacetic acid (DOPAC),[220] and hematoxylin,[223] demonstrating excellent agreement between theory and experiment in all cases, and highlighting the crucial role played by solvation effects and pH in determining the oxidation mechanism. A similar approach has been applied to studying the electrode potential and thermodynamic parameters of L-3,4-dihydroxyphenylalanine (L-DOPA) oxidized in aqueous solution.[414]

Barrows *et al.*[415] studied the factors controlling regioselectivity in the reduction of polynitroaromatics in aqueous solution using a semiempirical implicit-solvent model and showed the importance of proper treatment of solvation effects in order to correctly predict the preference for the reduction of one nitro group over the others.

A study of the electrochemical one-electron oxidation of low-generation polyamidoamine-type dendrimers with a 1,4-phenylene-diamine core was conducted by using cyclic voltammetry and density functional theory.[416]

Combined QM/MM studies of the electron-transfer reactions involving carbon tetrachloride in aqueous solution were carried out by Valiev *et al.*[417] In particular, they studied the reductive dechlorination of CCl_4 by a concerted electron transfer-bond breaking mechanism using either density functional theory or coupled cluster theory [CCSD(T)] for the QM part. Their predicted activation barriers and reduction potentials were found to be consistent with available experimental data.[417] Bylaska *et al.*[418] carried out *ab initio* quantum-mechanical studies of the thermodynamics of reductive dechlorination, reductive β-elimination, dehydrochlorination, and nucleophilic substitution by OH^- of 1,2,3-trichloropropane in the gas phase and in water.

Huang *et al.*[419] have employed experimental voltammetry, surface-enhanced Raman spectroscopy, and density functional theory to elucidate the mechanism of benzyl chloride reduction at silver cathodes, and they have found that the exceptional electrocatalytic properties of silver cathodes in such reactions could be related to the electrophilicity of the silver cathode surface toward organic halides.[419]

Gennaro, Coote, and co-workers have employed cyclic voltammetry and high-level *ab initio* molecular orbital theory calculations on a series of alkyl halides and their radicals to discriminate between inner-sphere electron transfer (ISET) and outer-sphere electron transfer (OSET) in atom transfer radical polymerization (ATRP)[216] and single-electron transfer living radical polymerization (SET-LRP).[420] In the former work, the authors used Marcus theory to predict OSET reaction barriers for halogen atom transfer, based on the computational redox potentials for the alkyl radicals and alkyl halides, and experimental values of the other parameters. These were compared with experimental barriers the halogen atom transfer process to show that an OSET process was energetically unfeasible. Subsequent work examined the reductive cleavage process relevant to SET-LRP directly using both cyclic voltammetry and multireference calculations, finding that dissociative electron transfer proceeds exclusively in a stepwise rather than concerted manner.

Wang and Yu[421] carried out a computation of the redox potentials of about 100 organic radicals in different solvents

using various density functionals and the PCM implicit-solvent model. Redox potentials for a series of carbamates in methanol were predicted with the use of DFT and PCM by Haya *et al.*[422] A computational study of the electrochemistry of several organic radicals derived from hydroxyurea and its methylated analogues was conducted by Vrček *et al.*[423]

Electrochemical properties such as electrochemical bandgaps were investigated in a combined experimental and theoretical (DFT) study of monoytterbium endohedral metallofullerenes, Yb@C_{2n} (n = 40, 41, 42), in 1,2-dichlorobenzene.[424]

Effects of *N*-substituents on redox, optical, and electronic properties of alkyl and alkylaryl naphthalene bisimides used for field-effect transistors fabrication were investigated in another combined experimental and DFT study.[425]

Paukku and Hill[426] have carried out a theoretical study of the one-electron redox potentials of several DNA bases, base pairs, and stacks using the M06-2X[125] exchange–correlation functional and found the computed potentials in good agreement with the experimental ones.[426] Recently, as part of a broader study of SOMO–HOMO orbital conversion, Gryn'ova *et al.*[352,427] used G3(MP2,CC)(+) calculations to study the one-electron gas-phase oxidation of deprotonated N-centered nucleic acid radicals, formed as a result of oxidative damage *via* hydrogen atom abstraction. They demonstrated that under these conditions the phosphate, rather than the nucleic acid radical, undergoes preferential oxidation to yield triplet species. When the phosphate is protonated, "normal" oxidation of the nucleic acid radical occurs instead to yield a closed shell product. In contrast, corresponding C-centered sugar-derived radicals oxidize to closed shell products irrespective of the phosphate protonation state. DFT studies of the extent of hole delocalization in one-electron oxidized adenine and guanine base stacks have been carried out by Kumar and Sevilla.[428] Several exchange–correlation functionals have been tested for prediction of the gas-phase adiabatic ionization potentials and the aqueous standard reduction potentials of 51 nitrogen-rich heterocyclic compounds by Sviatenko *et al.*[429]

Silva and Ramos have tested the performance of 18 different exchange–correlation functionals in calculations of the energetics of a number of organic acid/base and redox reactions, using MP2/CBS and CCSD(T)/aug-cc-pVTZ energies as benchmark.[430] Electrochemical properties of homogentisic acid in water and water–acetonitrile mixtures have been studied by DFT and C-PCM.[431]

Keith and Carter[432] computed the reduction potentials and other properties of pyridinium cations and pyridinyl radicals in acetonitrile using density functional theory (B3LYP) and an implicit-solvent model (C-PCM) in order to gain insights into pyridinium-based photoelectrocatalytic reduction of CO_2. Based on the computed energetics, the authors have concluded that (contrary to previous assumptions) the homogeneous pyridinyl radicals in solution cannot be considered active catalysts for CO_2 reduction, and the electrode surface may play a critical (yet unknown) role in this process.[432] A more recent study on the mechanism of CO_2 reduction by pyridine has been published by Lim *et al.*[433]

Liu *et al.*[434] have carried out a DFT study of the oxidation of phenolates by the $[Cu_2O_2(N,N'\text{-di-}tert\text{-butylethylenediamine})_2]^{2+}$ complex and suggested a mechanism of the phenolate oxidation in agreement with experimental observations. Ghosh *et al.*[435] have applied a first-principle protocol to calculating the ionization and redox potentials of phenol and phenolate in water using coupled cluster theory and the EFP method. Chua *et al.*[436] investigated the reduction pathways of trinitrotoluene by cyclic voltammetry and DFT.

Effects of polar and nonpolar ligands as well as monovalent cations on the one-electron reduction potential of the thiyl radical $CH_3S^{\bullet}$ and the CH_3SSCH_3 disulfide have been investigated using density functional theory and implicit-solvent models and discussed in terms of the vertical electron affinity and reorganization energy, and molecular orbital theory.[437] Effects of substituents on the preferred modes of one-electron reductive cleavage of N–Cl and N–Br bonds in the X–NRR′ (X = Cl and Br) molecules have also been studied recently.[438]

Varejao *et al.*[439] found a good correlation between calculated and experimental reduction potentials of rubrolides, but only when they carried out averaging of over multiple conformations.

6.1.3. Biochemistry. Free energy calculations on disulfide bridge reduction in proteins were carried out by David and Enescu using the hybrid QM/MM approach in which the QM region was treated at the B3LYP/6-311+G(d,p) level of theory.[440] In particular, they elucidated the role of the protein environment in the reduction of four disulfide bridges in lysozyme by tris(2-carboxyethyl)phosphine. See also a combined theoretical and spectroscopic study on the two-electron reduction of aryl disulfide bonds conducted with an ultimate goal to design a simple molecular system intended to act as a memory storage bank.[441]

Density functional calculations of the standard reduction potentials of methylcobalamin and adenosylcobalamin cofactors in various media (in combination with a PCM implicit-solvent model) have been recently reported.[442]

Formaneck *et al.*[443] developed a new QM/MM approach for computing accurate redox potentials in enzymes based on the free energy perturbation technique and applied it to studying the first reduction potential of the flavin adenine dinucleotide cofactor in cholesterol oxidase.[443]

Hybrid QM/MM calculations on the first redox step of the catalytic cycle of bovine glutathione peroxidase GPX1 have been recently carried out using the ONIOM methodology.[444]

Blomberg and Siegbahn[445] investigated the catalytic mechanism of reduction of NO to N_2O in the bacterial enzyme nitric oxide reductase using the B3LYP exchange–correlation functional and an implicit-solvent model (the Poisson–Boltzmann solver of Jaguar) applied to a molecular model system of the binuclear (Fe–Fe) center of the protein. The authors[445] suggest a catalytic reduction mechanism that involves a formation of stable *cis*-hyponitrite, and it is shown that from this intermediate one N–O bond can be cleaved without the transfer of a proton or an electron into the binuclear active site, in agreement with experimental observations.[445] See also another study[446] by Blomberg and Siegbahn on the reduction of NO in

cytochrome *c* dependent nitric oxide reductase. Quantum chemical calculations of active-site models of nitrous oxide reductase have also been carried out by Ertem *et al.*[447] to elucidate the N–O bond cleavage mechanisms mediated by the supported tetranuclear Cu_4S core found in the enzymatic active site.

Roy *et al.*[448] calculated DFT SCRF redox potentials for small models of dinuclear iron hydrogenase enzymes in acetonitrile and found an average error of 0.12 V with one exchange–correlation potential but much larger errors ($\sim$0.8 V) with another. They found that the redox potentials correlated with the spectrochemical series for the ligands and with the extent of ligand-to-metal electron transfer.

Surawatanawong and Hall[449] calculated reduction potentials for species derived from a tetranuclear iron complex model of hydrogenase to elucidate the routes to hydrogen production.

The QM/MM minimum free energy path (QM/MM-MFEP) method was developed and applied to calculate the redox free energies of lumichrome and riboflavin in solution.[450] The authors demonstrated that the method could be an efficient approach to free energy simulations of complex electron transfer reactions.[450]

Several other enzymatic redox reactions have also been studied recently using the tools of computational electrochemistry, in particular for the following enzymes: photosystem II,[270,451–453] ribonuclease reductase,[454,455] rubredoxin,[456] green fluorescent protein,[457,458] adenosine-5′-phosphosulfate reductase,[459] methyltransferases,[460] monoamine oxidase B,[461] and methionine synthase.[462] Billiet *et al.*[463] have studied the thermodynamics of thiol sulfenylation in the sulfenic acid-forming protein human Prx.

Redox calculations of ground and excited states of Ru(II) polypyridyl complexes were used to explain DNA-photocleavage.[464] Another theoretical study on Ru(II) polypyridyl complexes using various density functionals have been reported.[465]

Additional studies that involve the electrochemistry of metal-organic compounds are discussed later in the paper.

6.1.4. Special topics. Recent computational studies of the energetics of redox reactions also involve special topics such as anticancer agents and medicinal chemistry,[466,467] complexes with non-innocent ligands,[468] energetic materials,[469] molecular organic semiconductors[470] and organic light-emitting diodes,[471] photovoltaic and conducting polymers,[472–474] charge transport in molecular electronic junctions,[475] organic cathode materials,[476] rhodanine dyes[477–479] and redox mediators[222] for dye-sensitized solar cells, water oxidation catalysts[480–494] and electrocatalytic oxidation and reduction on metal surfaces.[495–498]

Wagner *et al.*[499] discuss the potential impact of electrochemical energy systems on the future of the automobile by comparing lithium ion battery and hydrogen fuel cell systems used in automotive applications in terms of their overall efficacy and operating costs. The authors have concluded that both Li ion battery electric vehicles and fuel cell vehicles warrant continued strong development investment.[499]

Various theoretical models for calculation of the electrochemical phase diagram for the oxidation and reduction of water over the Pt(111) surface have been applied and discussed by Rossmeisl *et al.*[500] Applications of DFT methods to modeling electrochemical processes at the Pt(111)–water interface and the rutile TiO_2(110)–water interface have been also reviewed recently by Cheng and Sprik.[297] They have noted that systematic underestimation of the LUMO–HOMO bandgap using the generalized gradient approximation (GGA) (for example, BLYP[225,226]) may be a potentially dangerous source of error in the modeling of electrocatalytic processes using DFT-based (Car–Parrinello) molecular dynamics.[297,325] Note that the GGA exchange–correlation functionals remain most frequently used in the context of CPMD simulations due to their relatively low computational costs.

Shiratori and Nobusada[501] proposed a new finite-temperature density functional approach to electrochemical reactions. Solvent effects are treated by an extended self-consistent reaction field model that accounts for nonequilibrium solvation, and an exchange–correlation functional with a long-range correction is employed.[501]

Koper[502] has reviewed the thermodynamic theory of multi-electron transfer reactions and its implications for electrocatalysis. In particular, its application to hydrogen evolution and oxidation, oxygen evolution and reduction, and carbon dioxide reduction has been discussed.[502]

Calle-Vallejo and Koper[503] have recently reviewed the progress of first-principles computational electrochemistry and noted that more accurate exchange–correlation functionals are needed for a better description of explicit-solvent effects, surface–adsorbate interactions, and other interactions such as van der Waals forces.[503] It has been also noted[495] that most DFT methods do not predict the correct adsorption site of CO on Pt, which is a serious problem because the oxidation of CO on Pt is a prototype problem in electrochemistry. However, we note here that the M06-L[369] exchange–correlation functional can overcome this problem.[504]

The current state of computational electrochemistry has been discussed by Bieniasz.[505] A comprehensive review on one-electron and two-electron transfers in electrochemistry and homogeneous solution reactions has been recently published by Evans.[506] Schneider *et al.*[507] provided a tutorial on experimental and theoretical approaches to CO_2 reduction at metal centers. In the next sections we will discuss several selected topics in more detail.

6.2. Transition metals

In this section we will first discuss DFT studies of aqueous transition metal ions and then continue the discussion to cover primarily metalorganic coordination complexes. For applications of DFT to transition metals and transition metal chemistry in general we refer the reader to the recent review.[508]

6.2.1. Aqueous transition metal ions. Uudsemaa and Tamm[342] employed density functional theory in combination with the COSMO implicit-solvent model to predict the standard reduction potentials of the M^{3+}/M^{2+} redox couples in water for several fourth-period transition metals M (in particular Sc, Ti, V, Cr, Mn, Fe, Co, Ni, and Cu), resulting in the average absolute error of 0.29 V against experimental data. The calculations were

performed using the Born–Haber thermochemical cycle relating the reduction potential in solution to the adiabatic gas-phase ionization potential. The latter was computed using the BP98[225,509] exchange–correlation functional and basis sets of triple-zeta quality and then augmented with a gas-phase thermal correction estimated using experimental reference data.[342] Solvation effects in the first and the second hydration shell were treated explicitly by adding up to 18 explicit water molecules to the $M^{3+/2+}$ ion while the rest of the solvent was treated using the dielectric continuum approximation.[342] See also a study on the hydration of copper(II) by Bryantsev *et al.*[510]

In our recent study (by three of us),[345] we have predicted the standard reduction potential of the $Ru^{3+}|Ru^{2+}$ couple in aqueous solution (E^o) in excellent agreement (within 0.05 V) with experiment[48] by using the SMD solvation model[82] and new Minnesota exchange–correlation functionals, M11[135] and M11-L.[136] To represent the first and second hydration shell surrounded by continuum solvent we added up to 18 water molecules explicitly. The Gibbs free energy of the Ru^{2+} and Ru^{3+} cations in aqueous solution were computed by eqn (20) using Boltzmann averaging over multiple low-energy molecular conformations and spin states for each species, thereby explicitly accounting for the entropy associated with including multiple alternative structures used to describe the two hydration shells of Ru^{2+} and Ru^{3+}.[345] Note that such an approach is more sophisticated than a traditional approach based on thermochemical cycles using only global minimum gas-phase optimized structures (see Section 3.2 and Scheme 2). The latter approach neglects the additional entropy contributions that would come from considering additional conformations. The predicted Pourbaix diagram of the aqueous $Ru^{2+/3+}$ cations was found in close quantitative agreement with the experimental measurements[511,512] of $E(Ru^{3+}|Ru^{2+})$ as a function of pH.[345]

In an earlier study (by three of us),[343] we obtained the value of $E^o(Ru^{3+}|Ru^{2+})$ (relative to the SHE) in the range between 0.6 and +1.0 V by testing 37 exchange–correlation functionals (excluding the newer M11, M11-L, or any other Minnesota exchange–correlation functional) combined with the SM6 implicit-solvent model[79] based on the generalized Born approximation.

The standard reduction potentials of selected Group 8 octahedral complexes in water such as $[M(H_2O)_6]^{2+/3+}$, $[M(NH_3)_6]^{2+/3+}$, $[M(CN)_6]^{4-/3-}$, and $[MCl_6]^{4-/3-}$ (M = Fe, Os, Ru) have been recently calculated using density functional theory and the COSMO-RS implicit-solvent model, and it has shown that an addition of explicit water molecules to model the second solvation shell (in addition to the six ligands in the first solvation shell) may not be necessary with COSMO-RS.[513]

Srnec *et al.*[514] investigated the role of spin–orbit coupling on the reduction potentials of octahedral Ru(II/III) and Os(II/III) complexes and they concluded that a proper treatment of spin–orbit coupling could be necessary to avoid systematic errors of $\sim$300 mV in the calculated reduction potentials.[514]

Wang and Voorhis[301] calculated the standard reduction potentials for nine octahedrally coordinated transition metal complexes in water, namely, for $[Ti(H_2O)_6]^{3+}$, $[V(H_2O)_6]^{3+}$, $[Cr(H_2O)_6]^{3+}$, $[Mn(H_2O)_6]^{3+}$, $[Fe(H_2O)_6]^{3+}$, $[Fe(CN)_6]^{3+}$, $[Co(H_2O)_6]^{3+}$, $[Co(NH_3)_6]^{3+}$, and $[Cu(H_2O)_6]^{3+}$. The authors[301] used both implicit-solvent and explicit-solvent models. In particular, they used the COSMO implicit-solvent model in combination with B3LYP and triple-zeta quality basis sets, and the model was shown to consistently overestimate the computed standard reduction potentials by over 1.6 V relative to available experimental data.[301] They attributed such a large error to the presence of solvent structure effects in the second solvation shell (such as hydrogen bonding) unaccounted for by a pure implicit-solvent model. By using the QM/MM explicit-solvent model, they achieved a much better agreement with experiment (within 0.3 V on average).[301] The QM/MM simulation cell included six water molecules in the QM region along with the transition metal ion, and the rest of the solvent was represented by about 1720 explicit water molecules treated classically using the Simple Point Charge Extended or SPC/E[515] force field. The QM/MM reduction potentials were calculated from the corresponding reaction free energies $\Delta_r G^o$ estimated in the linear response approximation [see eqn (48) in the present work].

Zeng *et al.*[516] have investigated the redox potentials of aqueous $Fe^{2+/3+}$ and $Ru^{2+/3+}$ ions using the fractional electron approach to the QM/MM simulation of electron transfer process, with the fractional number of electrons being treated as a thermodynamic integration parameter.[516]

Sprik and co-workers carried out DFT-based (Car–Parrinello[5]) molecular dynamics (CPMD) studies of a number of redox reactions in water, involving $Ag^{2+/1+}$,[268,304] $Cu^{2+/1+}$,[268,517] $Ru^{3+/2+}$,[308,321,518] $MnO_4^{2-/1-}$ and $RuO_4^{2-/1-}$,[305] $Ru(CN)_6^{4-/3-}$, $RuCl_6^{4-/3-}$, $(NH_3)_5PyRu^{3+/2+}$, and $(NH_3)_6Ru^{3+/2+}$.[322] Some of these studies are based on a grand canonical ensemble modification of CPMD (see Section 4.5) for treating exchange of electrons between electroactive species and an electron reservoir. The latter plays the role of a fictitious electrode. This method can be understood as a direct theoretical model of voltammetric experiments.[343] The redox half-reaction takes place when the electroactive species reaches a crossing between the free energy surfaces of the two redox states at some value of the chemical potential, and this value of the electronic chemical potential serves as an estimate of the free energy of the half-reaction under study.[343] Note that in the case of half-reactions the computed redox potentials cannot be directly compared to the experimental values tabulated relative to the SHE (or other reference electrodes).[305] To do so, one would need to know the conversion constant between the reference electrode and the fictitious electrode used in the grand canonical simulation. Energy levels and redox properties of aqueous $Mn^{2+/3+}$ ions were investigated using photoemission spectroscopy and DFT-based MD simulations by Moens *et al.*[519]

Due to computational costs, the CPMD simulations can afford only a very limited number of explicit solvent molecules. For example, the grand canonical CPMD simulation of a half-reaction with $Ru^{3+/2+}$,[308,321] employed 32 water molecules using a GGA exchange–correlation functional (BLYP[225,226]) in combination with a plane wave basis set and a pseudo-potential constructed according to the Troullier–Martins[520] scheme. When the small cell dimensions are used to keep the MD simulations

affordable the computed free energies may dependent on the system size because the interaction between the ion, its periodic box images, and the compensating background charge becomes large. The finite-size effects may be different for different reactions, and the issue of the effects will remain unresolved unless larger systems are simulated, *e.g.* with the help of QM/MM methods.[305]

6.2.2. Metalorganic compounds. Electrochemical computational studies of transition metal metalorganic compounds have appeared focused on cobalt,[295,521–524] copper,[525–530] iron,[86,250,531–538] manganese,[539,540] nickel,[541,542] and other transition metals.[250,543–545]

In addition, Galstyan and Knapp[219] performed DFT calculations of 58 standard redox potentials for 48 different mononuclear transition metal complexes involving iron, manganese, and nickel and organic and inorganic ligands of various complexity in acetonitrile, dimethylformamide, and water using the Born–Haber thermochemical cycle and an implicit-solvent model.

More recently Hughes and Friesner[546] have performed an extensive computation of the standard reduction potentials for 95 octahedrally coordinated fourth-row transition metal ions binding a diverse set of organic and inorganic ligands in water and nonaqueous solvents. The authors[546] used the B3LYP[225,226] exchange–correlation functional, relativistic effective core potentials, and basis sets of triple-zeta quality along with the Poisson–Boltzmann solver[189–191] as an implicit-solvent model. They noted a significant error (around 2 eV) introduced by single reference B3LYP for predicting the energetics of simple multireference systems in their data set such as mononuclear transition metal complexes.[546] The mean unsigned error in predicting the standard redox potentials over the whole test set was about 0.4 V, which could be further reduced to 0.12 V by using an additional seven-parameter model that was designed to make up for systematic errors in B3LYP's HOMO/LUMO energetics and spin splitting.[546]

A computational density functional study of polypyrrolic macrocycles containing actinyl ions and 3d transition metal ions has been carried out by Berard *et al.*[547]

Matsui *et al.*[548] have proposed an improved scheme for computation of the redox potentials of transition metal complexes based on generalized Born theory. The tested systems include $M(CO)_5(pyCN)$ (M = Cr, Mo, W), $M(mnt)_2$ (M = Ni, Pd, Pt), and $M(bpy)_3$ (M = Fe, Ru, Os) in water and organic solvents (where pyCN = 4-cyanopyridine, mnt = maleonitrile-dithiolate, and bpy = 2,2′-bipyridine).[548]

Haines *et al.*[549] have been conducted a combined cyclic voltammetry and DFT study of electrochemistry and electronic structures of over 30 tungsten–alkylidyne compounds and found out that the redox potential of such compounds is correlated linearly with the d_{xy} orbital energy, thereby providing a valuable computational descriptor for the potential.[549]

DFT calculations have been employed in a recent study of the spectroscopic properties and electrochemistry of mixed ligand complexes of copper(I) halide with PPh3 and naphthylazo-imidazole.[550]

DFT calculations of two newly synthesized metalorganic Ru(II)Pt(II) dimers that exhibit hydrogen-evolving catalytic activities in photochemical water splitting have shown a link between the H_2-evolving activity and the LUMO energy level of the Ru(II)Pt(II) molecular complexes.[551]

Hammes-Schiffer and co-workers[552] have studied a proton-coupled electron transfer reaction in an aqueous osmium complex comprised of the $[Os(bpy)_2(4\text{-aminomethyl-pyridine})(H_2O)]^{2+/3+}$ (bpy = 2,2′-bipyridine) unit bonded *via* hydrogen bonding to $CH_3CH_2COO^-$ in both the reduced and oxidized states. The authors[552] have employed an implicit-solvent model and the B3LYP exchange–correlation functional to estimate the rate constant of such a reaction as well as the solvent reorganization energy.

Solis and Hammes-Schiffer[553] have performed a DFT analysis of mechanistic pathways for hydrogen evolution catalyzed by the two cobalt complexes with supporting diglyoxime ligands in acetonitrile, $Co(dmgBF_2)_2$ (dmg = dimethylglyoxime) and $Co(dpgBF_2)_2$ (dpg = diphenylglyoxime). Using the Born–Haber cycle and an implicit-solvent model (C-PCM), the authors[553] have predicted the reduction potentials, pK_a values, reaction free energies, solvent reorganization energies, and electron transfer free energy barriers for several proton-coupled electron transfer reactions that involve these complexes. Lei *et al.*[554] have considered analogous cobalt, and also manganese, corrole complexes, achieving good agreement with experiment for both proton reduction and water oxidation.

The redox chemistry of homoleptic tris(2,2′-bipyridine)metal complexes, in particular, $[Cr(^tbpy)_3]^{n+}$ (n = 0–3) has been investigated in a combined X-ray absorption spectroscopic and DFT study.[555] Another combined spectroscopic and DFT study has been focused on the photochemical reduction of carbon dioxide catalyzed by a ruthenium-substituted polyoxometalate.[556]

The effect of the solvent on the redox potential of tetraethyl ammonium hexacyano-manganate(III) has been investigated by DFT implicit-solvent calculations in acetonitrile, dimethyl sulfoxide, and methanol using the Born–Haber thermochemical cycle.[557]

Mosconi *et al.*[558] have studied the cobalt electrolyte–dye interactions in dye-sensitized solar cells (DSSCs) using an experimental approach combined with density functional theory molecular dynamics simulations. In particular, they have studied the nature of the interactions between cobalt redox mediators and TiO_2 surfaces sensitized by ruthenium and organic dyes, and their impact on the performance of the corresponding DSSCs.[558]

The standard reduction potentials of several cobalt complexes with pyrazole and pyridine ligands in acetonitrile have been calculated based on the Born–Haber thermochemical cycle using the B3LYP exchange–correlation functional and the IEFPCM implicit-solvent model in the study of redox reaction mechanisms with non-triiodide mediators (such as these compounds) in dye-sensitized solar cells.[559] Another recent work involves a DFT study of the structure and redox behavior of iron oxophlorin and the role of electron transfer in the heme degradation process.[560]

A combined experimental and theoretical (DFT) approach has been carried out to study the redox properties of two dinuclear Ru(II) complexes containing the planar dpt-ph-dpt

bridging ligand where dpt-ph-dpt denotes 1″,4″-bis(2,4-dipyrid-2′-yl-1,3,5-triazin-6-yl) benzene.[561]

Redox potential calculations for the set of 21 iron-containing complexes in acetonitrile have been carried using density functional theory and the PCM implicit-solvent model.[562] Castro and Bühl examined the specific case of one-electron reduction potentials for several oxoiron(IV)porphyrin complexes, noting the sensitivity of their results to functional, solvation model, and whether or not a counterion was included at the open axial position trans to the oxo group.[563] In another interesting case of a complex involving coordinated iron and scandium, Swart found that the redox behavior of the compound involved the non-innocence of the scandium ion.[564]

There have been a number of electrochemical computation studies of metalloproteins. For example, Noodleman and co-workers[565] discussed the DFT calculations of molecular structures, spin states, redox energetics and reaction pathways for several metalloenzymes including Fe- and Mn-containing superoxide dismutase, Cu-containing galactose oxidase, Zn-containing glyoxalase I, and iron-oxo enzymes such as methane monooxygenase and ribonucleotide reductase. The experimental and computational data on the properties and energetics of iron–sulfur proteins from simple clusters to nitrogenase were reviewed earlier.[566] Van den Bosch *et al.*[567] examined the influence of residue changes on the reduction potentials of copper atoms in azurin mutants using free energy perturbation MD simulations, with errors of up to 10 k_BT attributed to the slow relaxation of internal hydrogen bond networks in response to changes in atomic charges.

Si and Li[568] elucidated the influence of ligand interaction and solvation effects on the reduction potential of the type I copper centers in five redox active proteins by studying active site model molecules with a heterogeneous conductor-like polarizable continuum model and B3LYP.

More recently, Jackson *et al.*[569] have studied the active-site structures of the oxidized and reduced forms of manganese-substituted iron superoxide dismutase [Mn(Fe)SOD] using spectroscopic absorption and circular dichroism techniques supported by QM/MM computations on complete protein models of Mn(Fe)SOD in both the oxidized and reduced states. The reduction midpoint potential of Mn(Fe)SOD that corresponds to a proton-coupled electron transfer reaction has been computed by separating the electron transfer and proton transfer steps,[569] by following (with some modifications) a protocol developed by Noodleman and co-workers[570] in earlier studies of the redox potentials of manganese and iron superoxide dismutases based on DFT and electrostatic calculations.

6.3. Proton-coupled electron transfer and Pourbaix diagrams

Many important energy conversion processes involve oxidation–reduction reactions in which both electrons and protons are transferred. Broad reviews of such reactions have been given by Meyer and co-workers.[571,572] Thermodynamics of the hydride transfer reactions in water and organic solvents has also been of interest.[573]

Consider the following half-reaction that involves a proton transfer:

$$\mathrm{OH} + \mathrm{H}^+ + \mathrm{e}^- \leftrightarrow \mathrm{RH} \quad (63)$$

where OH and RH refer to protonated forms of an oxidized (O) or reduced (R) reagent in solution (either charged or neutral), H^+ is a proton in solution, and e^- is an electron in the gas phase. The reduction potential at arbitrary activities (a) of OH, RH, and H^+ can be expressed using the Nernst equation as

$$E(\mathrm{OH}|\mathrm{RH}) = E^{\mathrm{o}}(\mathrm{OH}|\mathrm{RH}) + 0.059\log\frac{a_{\mathrm{OH}}}{a_{\mathrm{RH}}} - 0.059\mathrm{pH} \quad (64)$$

where the reduction potential E and the standard reduction potential E^{o} are given in volts (they can be either absolute or relative to the reference, *e.g.* SHE), and $\mathrm{pH} = -\log a_{\mathrm{H}^+}$. The activities of OH and RH can be expressed through the corresponding pK_a values as

$$a_{\mathrm{XH}} = a_{\mathrm{X}}10^{\mathrm{p}K_a(\mathrm{XH}) \,-\, \mathrm{pH}} \quad (65)$$

where X is O or R, and the value pK_a(XH) corresponds to the following reaction

$$\mathrm{XH} \leftrightarrow \mathrm{X} + \mathrm{H}^+ \quad (66)$$

Thus, the reduction potential depends on pH as a parameter. Reduction potential–pH diagrams are sometimes called Pourbaix diagrams,[571,572] and they have been a subject of numerous theoretical studies (see recent works[345,481–484] and references therein).

Scheme 4 (part a) shows a Pourbaix diagram for the case when $0 < \mathrm{p}K_a(\mathrm{OH}) < \mathrm{p}K_a(\mathrm{RH})$. If pH = 0 and $a_{\mathrm{OH}} = a_{\mathrm{RH}} = 1$ (*i.e.*, at the standard-state bulk concentrations of H^+, OH, and RH), the potential E is equal to E^{o}. If $\mathrm{pH} < \mathrm{p}K_a(\mathrm{OH})$ then $a_{\mathrm{O}} < a_{\mathrm{OH}} = 1$ and $a_{\mathrm{R}} < a_{\mathrm{RH}} = 1$. If $\mathrm{p}K_a(\mathrm{OH}) \le \mathrm{pH} < \mathrm{p}K_a(\mathrm{RH})$ then $a_{\mathrm{OH}} \le a_{\mathrm{O}} = 1$ where a_{OH} is expressed through a_{O} by eqn (65). If $\mathrm{p}K_a(\mathrm{RH}) \le \mathrm{pH}$ then $a_{\mathrm{RH}} \le a_{\mathrm{R}} = 1$ where a_{RH} is expressed by eqn (65) through a_{R}. One can obtain a Pourbaix diagram for the case $0 < \mathrm{p}K_a(\mathrm{RH}) < \mathrm{p}K_a(\mathrm{OH})$ in a similar way (see Scheme 4, part b).

In the case when OH or RH can be protonated, the Pourbaix diagram includes additional features related to the second pK_a. For transition metal complexes when multiple oxidation states with stabilization of higher states by metal oxo formation are possible, pH-dependent proton-coupled electron transfer behavior becomes complex.[572] For example, oxidation of [*cis*-$\mathrm{Ru^{II}(bpy)_2(H_2O)_2}]^{2+}$ (bpy = 2,2′-bipyridine) involves four oxidation states and four different pK_a's from pH = 1 to 9.[572] Another example is the complex $[\mathrm{Ru^{II}(tpa)(H_2O)_2}]^{2+}$ [tpa = tris(2-pyridylmethyl)amine] that can produce five oxidation states with different pK_a's.[345,574]

Scheme 5 shows the Pourbaix diagram predicted for a ruthenium-based water oxidation catalyst, the Ru(db) complex, in a recent study (by three of us)[345] compared to experimental data.[489] We used the SMD solvation model[82] and new Minnesota exchange–correlation functionals, M11[135] and M11-L.[136] Our choice of M11 and M11-L was motivated by the fact that these new exchange–correlation functionals employ dual-range local exchange (M11-L) or range-separated-hybrid meta-generalized gradient approximation exchange (M11), and they demonstrate

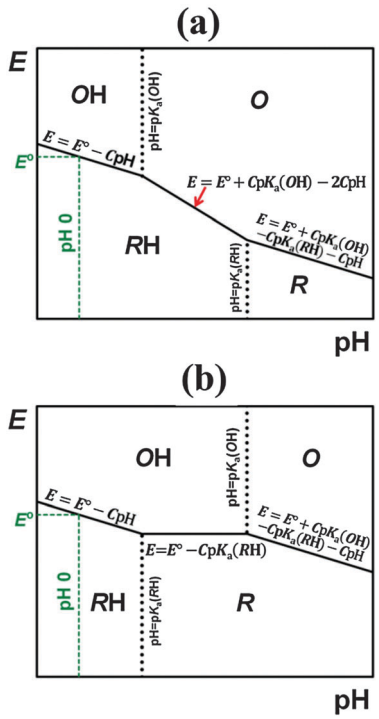

Scheme 4 A schematic Pourbaix diagram where OH and RH are protonated forms of the oxidized and reduced species, respectively, with the corresponding pK_a values, $0 < pK_a(OH) < pK_a(RH)$ (part a) and $0 < pK_a(RH) < pK_a(OH)$ (part b). The quantity C is a constant equal to ≈ 0.059 volts per log unit. See the text for more details.

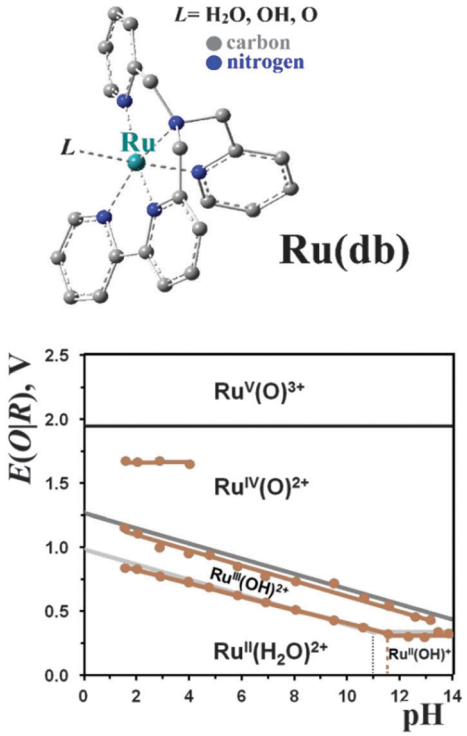

Scheme 5 Predicted and observed Pourbaix diagram of the Ru(db) complex [db = *N*,*N*-bis(2-pyridinylmethyl)-2,2′-bipyridine-6-methanamine] based on theoretical data from our previous work[345] (gray lines) and on experimental data of Radaram *et al.*[489] measured by UV/Vis spectrophotometric titration (brown dots and lines), respectively. The reduction potential E is defined relative to the SHE. Vertical lines show the corresponding pK_a value (both theoretical and experimental).

improved accuracy in comparison with many popular (but less sophisticated) functionals against a broad database of energetic chemical properties.[135,136] This advance in methodology allows for sufficiently reliable results in comparison with experiment. Indeed, for this particular complex (Scheme 5), we can predict the main features of an experimental Pourbaix diagram qualitatively and quantitatively (within a mean unsigned error of about 0.1 V for E^o).

6.4. Water oxidation catalysts

It is recognized that efficient conversion of solar radiation into chemical fuels is important for making the energy economy less dependent on fossil fuels, and one of the key reactions involved in the conversion of solar energy is the oxidation of water to O_2 with the use of catalysts containing transition metals.[345,575–577] The development of efficient schemes for the oxygenation of hydrocarbons with water as both the oxygen source and the solvent by using supported metal compounds as catalysts has been found to be relevant and important as well.[345,574]

Water splitting to molecular hydrogen and oxygen ($2H_2O \rightarrow 2H_2 + O_2$) consists of two half-reactions. The first reaction involves the generation of oxygen (water oxidation) as $H_2O \rightarrow \frac{1}{2}O_2 + 2H^+ + 2e^-$ with the oxidation potential (relative to the SHE in volts) $E = 1.23 - 0.059$ pH, and the second reaction involves proton reduction as $H^+ + e^- \rightarrow \frac{1}{2}H_2$ with the reduction potential $E = -0.059$ pH.[492] The water oxidation step requires strongly oxidizing conditions (*e.g.*, using Ce^{IV} as a sacrificial oxidant) and it is generally considered to be the bottleneck of the whole water-splitting reaction because of the complex nature of O–O bond making or breaking processes that may involve multiple proton-coupled electron transfers.[492,575,577]

There has been a dramatic surge of activity in the search for novel transition metal molecular complexes (*e.g.*, containing Ru, Ir, Co, Fe, Cu, or Mn) able to catalyze effectively the oxidation of water to molecular oxygen (see, for example, ref. 345, 492 and 577–586 and references therein). Computer-aided search for novel water oxidation catalysts involves elucidation of the mechanisms of catalytically activated water–oxidation reactions and the key factors that control such reactions,[485] with one goal being to increase the catalysts' efficacy. This search also includes studying the mechanisms of ligand dissociation and oxidative decomposition as major deactivation pathways for such catalysts, with intent to improve the catalysts' durability.[492]

Many recent studies[480–485,487,489,492,587–590] have explored ruthenium-based water oxidation catalysts, based on the favorable oxidation potentials associated with proton-coupled-electron-transfer processes that take coordinated water molecules to electrophilic metal-oxo species. However, the search for cheaper materials based on more earth-abundant metals has been under way as well. For example, the mechanistic details of water splitting by a supported iron catalyst have been investigated recently by using DFT and multireference second-order perturbation theory.[491]

The same comparison of levels was undertaken by Vigara *et al.*[590] who found that the CASPT2 level afforded agreement with experiment to within 110 mV for an oxidation that did *not* involve proton transfer. By contrast, predictions from M06-L were found to be somewhat sensitive to basis set, with the largest basis sets leading to underestimations of reduction potentials on the order of 300 mV. More recent work suggests that M06-L may systematically underestimate some higher oxidation potentials of ruthenium-based water splitting catalysts; however, good results have been obtained with the more recent M11-L functional.[345,591] The degree to which this observation may affect computations involving metal centers other than ruthenium has not yet been fully explored, although results from one of our laboratories suggests that the same improved performance of M11-L compared to M06-L applies to copper-based catalysts as well.[592]

Another recent work with earth-abundant metals involves a DFT study of the complete water oxidation and oxygen evolution reaction cycle based on a Mn^{III}–Mn^{V} dimer model catalyst.[488] Studies of the water oxidation catalysts based on abundant first row transition metals have been recently reviewed by Singh and Spiccia.[593] The present status of DFT studies on water oxidation in photosystem II (including studies of proton release pathways and mechanisms for O–O bond formation and O_2 release) has been discussed by Siegbahn.[581] One hallmark of Siegbahn's work on redox catalysis in general is a reliance on the B3LYP functional, often with a somewhat reduced percentage of Hartree–Fock exchange (*e.g.*, 15%), to predict reduction potentials; Siegbahn has emphasized that the computation of the energetic change for an entire catalytic cycle, and its comparison to experiment, is a more rigorous test of the utility of a given functional than comparison of errors for individual redox steps, where systematic errors can accumulate to a larger error for the full cycle.[581]

Water oxidation on pure and doped hematite (α-Fe_2O_3) (0001) surfaces has been studied by periodic DFT calculations (studied dopants include Ti, Mn, Co, and Ni, as well as Si and F).[490] In addition, Man *et al.*[594] have recently employed first principles periodic DFT calculations to elucidate the mechanism for electrocatalytic oxygen evolution on oxide surfaces for a number of oxides including rutile, perovskite, spinel, rock salt, and bixbyite. A density functional investigation of the activity of cobalt oxides for the electrochemical oxidation of water has been carried out by Bajdich *et al.*[595]

When water splitting is used to generate protons, it may be their reduction to dihydrogen gas that generates a solar fuel. In one recent study of the electrochemical details associated with *that* process, Sundstrom *et al.*[596] explored the mechanism of proton reduction for a molybdenum-based catalyst. Comparing B3LYP, BP86, and ωB97, they found that only BP86 gave good agreement with measured reduction potentials. It was not assessed whether this observation might be assigned to the local character of the BP86 functional *versus* the hybrid character of the other two, but it is interesting to note that BP86 has also been found to predict bond-dissociation enthalpies for cobalt–carbon bond homolysis in better agreement with experiment than, say, B3LYP;[522,597] the Co–C bond homolysis by its nature reduces cobalt by one electron so the reduction potential plays a role in the net bond strength.

7. Concluding remarks

We have discussed various approaches for the prediction of liquid-phase reduction potentials and related properties based on implicit-solvent and explicit-solvent models and on linear free energy relationships, together with recent studies applying these computational protocols to various classes of chemical systems in aqueous and nonaqueous solutions. We have emphasized the challenges associated with the use of such protocols for applications to real systems (see, for example, Sections 3.6 and 4.7). We have also addressed issues pertaining to the thermochemical convention for the electron and the proton as well as to the absolute reference potential of the standard hydrogen electrode.

We believe that the future of computational electrochemistry lies in incorporating more complexity and less ideality into the modeling of real systems including, for example, the presence of side reactions, capacitance, unwanted oxidation or reduction of solvent, poisoning of electrodes, coupling electrochemical events to photon absorption, overpotentials, and kinetic effects in addition to static voltages. One reason (among many) for the increased interest in electrochemistry now and in the near future is the increasing demand for better batteries and fuel cells, and a key challenge for theory is to help design better ones, not just to understand existing ones.

Acknowledgements

We gratefully acknowledge support from the Australian Research Council Centre of Excellence for Electromaterials Science and the generous allocation of computing time on the National Facility of the National Computational Infrastructure (JH, MLC). MLC also acknowledges an ARC Future Fellowship. This work was supported in part by the U.S. Army Research Laboratory under grant no. W911NF09-100377 and by the U.S. Department of Energy, Office of Basic Energy Sciences, under SciDAC grant no. DE-SC0008666 (AVM, CJC, DGT).

Notes and references

1 P. Winget, E. J. Weber, C. J. Cramer and D. G. Truhlar, *Phys. Chem. Chem. Phys.*, 2000, **2**, 1231–1239.
2 J. Llano and L. A. Eriksson, *J. Chem. Phys.*, 2002, **117**, 10193–10206.
3 P. Winget, C. J. Cramer and D. G. Truhlar, *Theor. Chem. Acc.*, 2004, **112**, 217–227.
4 A. Lewis, J. A. Bumpus, D. G. Truhlar and C. J. Cramer, *J. Chem. Educ.*, 2004, **81**, 596–604. Erratum, *J. Chem. Educ.*, 2007, 84, 934.
5 R. Car and M. Parrinello, *Phys. Rev. Lett.*, 1985, **55**, 2471–2474.
6 I. S. Y. Wang and M. Karplus, *J. Am. Chem. Soc.*, 1973, **95**, 8160–8164.

7 D. J. Malcolme-Lawes, *J. Chem. Soc., Faraday Trans. 2*, 1975, **71**, 1183–1199.
8 C. Leforestier, *J. Chem. Phys.*, 1978, **68**, 4406–4410.
9 D. G. Truhlar, J. W. Duff, N. C. Blais, J. C. Tully and B. C. Garrett, *J. Chem. Phys.*, 1982, **77**, 764–776.
10 D. A. Gibson, I. V. Ionova and E. A. Carter, *Chem. Phys. Lett.*, 1995, **240**, 261–267.
11 M. J. Field, P. A. Bash and M. Karplus, *J. Comput. Chem.*, 1990, **11**, 700–733.
12 F. Maseras and K. Morokuma, *J. Comput. Chem.*, 1995, **16**, 1170–1179.
13 J. Gao, *Rev. Comput. Chem.*, 1996, **7**, 119–185.
14 K. Merz, In *Combined Quantum Mechanical and Molecular Mechanical Methods*, ACS Symp. Ser., 1998, vol. 712, pp. 2–15.
15 N. A. Burton, M. J. Harrison, J. C. Hart, I. H. Hillier and D. W. Sheppard, *Faraday Discuss.*, 1998, **110**, 463–475.
16 T. Vreven and K. Morokuma, *J. Chem. Phys.*, 1999, **111**, 8799–8803.
17 S. Dapprich, I. Komaromi, K. S. Byun, K. Morokuma and M. J. Frisch, *THEOCHEM*, 1999, **461**, 1–21.
18 T. Vreven and K. Morokuma, *J. Comput. Chem.*, 2000, **21**, 1419–1432.
19 P. Sherwood, in *Modern methods and algorithms of quantum chemistry*, ed. J. Grotendorst, John von Neumann Institute for Computing, Jülich, 2000, pp. 285–305.
20 J. Gao and D. G. Truhlar, *Annu. Rev. Phys. Chem.*, 2002, **53**, 467–505.
21 H. Lin and D. G. Truhlar, *Theor. Chem. Acc.*, 2007, **117**, 185–199.
22 H. M. Senn and W. Thiel, *Angew. Chem., Int. Ed.*, 2009, **48**, 1198–1229.
23 B. Wang and D. G. Truhlar, *J. Chem. Theory Comput.*, 2010, **6**, 359–369.
24 L. W. Chung, H. Hirao, X. Li and K. Morokuma, *Comput. Mol. Biosci.*, 2012, **2**, 327–350.
25 A. Heyden, H. Lin and D. G. Truhlar, *J. Phys. Chem. B*, 2007, **111**, 2231–2241.
26 A. Heyden and D. G. Truhlar, *J. Chem. Theory Comput.*, 2008, **4**, 217–221.
27 R. Delgado-Buscalioni, K. Kremer and M. Praprotnik, *J. Chem. Phys.*, 2008, **128**, 114110.
28 R. E. Bulo, B. Ensing, J. Sikkema and L. Visscher, *J. Chem. Theory Comput.*, 2009, **5**, 2212–2221.
29 S. Poblete, M. Praprotnik, K. Kremer and L. Delle Site, *J. Chem. Phys.*, 2010, **132**, 114101.
30 A. B. Poma and L. Delle Site, *Phys. Rev. Lett.*, 2010, **104**, 250201.
31 S. O. Nielsen, R. E. Bulo, P. B. Moore and B. Ensing, *Phys. Chem. Chem. Phys.*, 2010, **12**, 12401–12414.
32 S. O. Nielsen, P. B. Moore and B. Ensing, *Phys. Rev. Lett.*, 2010, **105**, 237802.
33 M. Bockmann, D. Marx, C. Peter, L. D. Site, K. Kremer and N. L. Doltsinis, *Phys. Chem. Chem. Phys.*, 2011, **13**, 7604–7621.
34 S. Pezeshki and H. Lin, *J. Chem. Theory Comput.*, 2011, **7**, 3625–3634.
35 N. Takenaka, Y. Kitamura, Y. Koyano and M. Nagaoka, *Chem. Phys. Lett.*, 2012, **524**, 56–61.
36 S. Fritsch, S. Poblete, C. Junghans, G. Ciccotti, L. Delle Site and K. Kremer, *Phys. Rev. Lett.*, 2012, **108**, 170602.
37 H. Wang, C. Schutte and L. Delle Site, *J. Chem. Theory Comput.*, 2012, **8**, 2878–2887.
38 R. Potestio, S. Fritsch, P. Espanol, R. Delgado-Buscalioni, K. Kremer, R. Everaers and D. Donadio, *Phys. Rev. Lett.*, 2013, **110**, 108301.
39 A. Ben-Naim, *Statistical Thermodynamics for Chemists and Biochemists*, Plenum Press, New York, 1992, p. 697.
40 R. S. Berry, S. A. Rice and J. Ross, *Physical Chemistry*, 2nd edn Oxford University Press, New York, 2000, p. 749.
41 C. G. Zoski, *Handbook of Electrochemistry*, Elsevier, Amsterdam, 2007, p. 892.
42 T. Biegler and R. Woods, *J. Chem. Educ.*, 1973, **50**, 604.
43 H. Reiss and A. Heller, *J. Phys. Chem.*, 1985, **89**, 4207–4213.
44 S. Trasatti, *Pure Appl. Chem.*, 1986, **58**, 955–966.
45 R. W. Ramette, *J. Chem. Educ.*, 1987, **64**, 885.
46 W. A. Donald and E. R. Williams, *Pure Appl. Chem.*, 2011, **83**, 2129–2151.
47 V. V. Pavlishchuk and A. W. Addison, *Inorg. Chim. Acta*, 2000, **298**, 97–102.
48 P. Vanýsek, in *CRC Handbook of Chemistry and Physics, 2012–2013*, ed. W. M. Haynes, CRC, Boca Raton, FL, 93rd edn, 2013, pp. 5-80/89.
49 J. W. Diggle and A. J. Parker, *Aust. J. Chem.*, 1974, **27**, 1617.
50 A. J. Bard and L. R. Faulkner, *Electrochemical Methods: Fundamentals and Applications*, John Wiley & Sons, Inc., New York, 2nd edn, 2001, p. 839.
51 W. C. Schumb, M. S. Sherrill and S. B. Sweetser, *J. Am. Chem. Soc.*, 1937, **59**, 2360–2365.
52 F. Scholz, in *Electroanalytical Methods: Guide to Experiments and Applications*ed. F. Scholz, Springer, Berlin, 2nd edn, 2010, vol. 210, pp. 11–32.
53 J. J. Warren, T. A. Tronic and J. M. Mayer, *Chem. Rev.*, 2010, **110**, 6961–7001.
54 Y. Kato, Y. Shimizu, L. Yijing, K. Unoura, H. Utsumi and T. Ogata, *Electrochim. Acta*, 1995, **40**, 2799–2802.
55 J. L. Hodgson, M. Namazian, S. E. Bottle and M. L. Coote, *J. Phys. Chem. A*, 2007, **111**, 13595–13605.
56 S. Trasatti, *Electrochim. Acta*, 1990, **35**, 269–271.
57 K. R. Siefermann, Y. Liu, E. Lugovoy, O. Link, M. Faubel, U. Buck, B. Winter and B. Abel, *Nat. Chem.*, 2010, **2**, 274–279.
58 W. A. Donald, M. Demireva, R. D. Leib, M. J. Aiken and E. R. Williams, *J. Am. Chem. Soc.*, 2010, **132**, 4633–4640.
59 C. P. Kelly, C. J. Cramer and D. G. Truhlar, *J. Phys. Chem. B*, 2006, **110**, 16066–16081.
60 W. R. Fawcett, *Langmuir*, 2008, **24**, 9868–9875.
61 W. A. Donald, R. D. Leib, J. T. O'Brien and E. R. Williams, *Chem. – Eur. J.*, 2009, **15**, 5926–5934.
62 W. A. Donald, R. D. Leib, M. Demireva, J. T. O'Brien, J. S. Prell and E. R. Williams, *J. Am. Chem. Soc.*, 2009, **131**, 13328–13337.
63 S. G. Lias and J. E. Bartmess, Gas-Phase Ion Thermochemistry, *NIST Chemistry WebBook*, NIST Standard Reference Database Number 69, U.S. Secretary of Commerce, Gaithersburg, MD, 2011, http://webbook.nist.gov/chemistry, accessed July 15, 2013.

64 J. E. Bartmess, *J. Phys. Chem.*, 1994, **98**, 6420–6424. Erratum, *J. Phys. Chem.*, 1995, 99, 6755.
65 K. M. Ervin, *Chem. Rev.*, 2001, **101**, 391–444.
66 S. Trasatti, *Electrochim. Acta*, 1987, **32**, 843–850.
67 P. Hünenberger and M. Reif, *Single-Ion Solvation: Experimental and Theoretical Approaches to Elusive Thermodynamic Quantities*, RSC Publishing, Cambridge, 2011, p. 690.
68 J. E. B. Randles, *Phys. Chem. Liq.*, 1977, **7**, 107–179.
69 J. R. Farrell and P. McTigue, *J. Electroanal. Chem.*, 1982, **139**, 37–56.
70 V. P. Sokhan and D. J. Tildesley, *Mol. Phys.*, 1997, **92**, 625–640.
71 S. M. Kathmann, I. F. Kuo and C. J. Mundy, *J. Am. Chem. Soc.*, 2008, **130**, 16556–16561.
72 L. I. Krishtalik, *Electrochim. Acta*, 2008, **53**, 3722–3733.
73 M. D. Tissandier, K. A. Cowen, W. Y. Feng, E. Gundlach, M. H. Cohen, A. D. Earhart, J. V. Coe and T. R. Tuttle, *J. Phys. Chem. A*, 1998, **102**, 7787–7794.
74 C. P. Kelly, C. J. Cramer and D. G. Truhlar, *J. Phys. Chem. B*, 2007, **111**, 408–422.
75 D. M. Camaioni and C. A. Schwerdtfeger, *J. Phys. Chem. A*, 2005, **109**, 10795–10797.
76 A. A. Isse and A. Gennaro, *J. Phys. Chem. B*, 2010, **114**, 7894–7899.
77 W. A. Donald, R. D. Leib, J. T. O'Brien, M. F. Bush and E. R. Williams, *J. Am. Chem. Soc.*, 2008, **130**, 3371–3381.
78 J. Ho, M. L. Coote, C. J. Cramer and D. G. Truhlar, in *Organic Electrochemistry*, ed. O. Hammerich and B. Speiser, 5th edn, CRC Press, Boca Raton, FL, 2015, ISBN: 978-1-42-008401-6, in press.
79 C. P. Kelly, C. J. Cramer and D. G. Truhlar, *J. Chem. Theory Comput.*, 2005, **1**, 1133–1152.
80 J. R. Pliego Jr. and J. M. Riveros, *Chem. – Eur. J.*, 2002, **8**, 1945–1953.
81 D. J. Henry, M. B. Sullivan and L. Radom, *J. Chem. Phys.*, 2003, **118**, 4849–4860.
82 A. V. Marenich, C. J. Cramer and D. G. Truhlar, *J. Phys. Chem. B*, 2009, **113**, 6378–6396.
83 *Standard Potentials in Aqueous Solution*, ed. A. J. Bard, R. Parsons and J. Jordan, IUPAC, Marcel Dekker, New York, 1985, p. 835.
84 J. Lind, X. Shen, T. E. Eriksen and G. Merenyi, *J. Am. Chem. Soc.*, 1990, **112**, 479–482.
85 T. N. Das and P. Neta, *J. Phys. Chem. A*, 1998, **102**, 7081–7085.
86 M. Namazian, C. Y. Lin and M. L. Coote, *J. Chem. Theory Comput.*, 2010, **6**, 2721–2725.
87 R. F. Ribeiro, A. V. Marenich, C. J. Cramer and D. G. Truhlar, *J. Phys. Chem. B*, 2011, **115**, 14556–14562.
88 I. M. Alecu, J. J. Zheng, Y. Zhao and D. G. Truhlar, *J. Chem. Theory Comput.*, 2010, **6**, 2872–2887.
89 C. Y. Lin, E. I. Izgorodina and M. L. Coote, *J. Phys. Chem. A*, 2008, **112**, 1956–1964.
90 B. A. Ellingson, V. A. Lynch, S. L. Mielke and D. G. Truhlar, *J. Chem. Phys.*, 2006, **125**, 084305.
91 J. Zheng, T. Yu, E. Papajak, I. M. Alecu, S. L. Mielke and D. G. Truhlar, *Phys. Chem. Chem. Phys.*, 2011, **13**, 10885–10907.
92 J. J. Zheng and D. G. Truhlar, *J. Chem. Theory Comput.*, 2013, **9**, 1356–1367.
93 T. Helgaker, P. Jorgensen and J. Olsen, *Molecular Electronic-Structure Theory*, Wiley, Chichester, 2000, p. 938.
94 J. Noga, S. Kedzuch, J. Simunek and S. Ten-No, *J. Chem. Phys.*, 2008, **128**, 174103.
95 G. Knizia, T. B. Adler and H. J. Werner, *J. Chem. Phys.*, 2009, **130**, 054104.
96 T. B. Adler and H. J. Werner, *J. Chem. Phys.*, 2009, **130**, 241101.
97 S. Ten-no, *Theor. Chem. Acc.*, 2012, **131**, 1070–1080.
98 (*a*) K. A. Peterson, T. B. Adler and H. J. Werner, *J. Chem. Phys.*, 2008, **128**, 084102; (*b*) H. Stoll, *Chem. Phys. Lett.*, 1992, **191**, 548–552; (*c*) J. Friedrich and J. Hänchen, *J. Chem. Theory Comput.*, 2013, **9**, 5381–5394; (*d*) J. Friedrich, H. Yu, H. R. Leverentz, P. Bai, J. I. Siepmann and D. G. Truhlar, *J. Phys. Chem. Lett.*, 2014, **5**, 666–670.
99 P. Pulay and S. Saebo, *Theor. Chim. Acta*, 1986, **69**, 357–368.
100 C. Krause and H. J. Werner, *Phys. Chem. Chem. Phys.*, 2012, **14**, 7591–7604.
101 G. A. Petersson, A. Bennett, T. G. Tensfeldt, M. A. Allaham, W. A. Shirley and J. Mantzaris, *J. Chem. Phys.*, 1988, **89**, 2193–2218.
102 F. B. Brown and D. G. Truhlar, *Chem. Phys. Lett.*, 1985, **117**, 307–313.
103 M. S. Gordon and D. G. Truhlar, *J. Am. Chem. Soc.*, 1986, **108**, 5412–5419.
104 L. A. Curtiss, K. Raghavachari, P. C. Redfern and J. A. Pople, *J. Chem. Phys.*, 2000, **112**, 1125–1132.
105 L. A. Curtiss, P. C. Redfern, K. Raghavachari and J. A. Pople, *J. Chem. Phys.*, 2001, **114**, 108–117.
106 L. A. Curtiss, P. C. Redfern and K. Raghavachari, *J. Chem. Phys.*, 2007, **126**, 084108.
107 L. A. Curtiss, K. Raghavachari, P. C. Redfern, V. Rassolov and J. A. Pople, *J. Chem. Phys.*, 1998, **109**, 7764–7776.
108 L. A. Curtiss, P. C. Redfern, K. Raghavachari, V. Rassolov and J. A. Pople, *J. Chem. Phys.*, 1999, **110**, 4703.
109 P. L. Fast, J. C. Corchado, M. L. Sánchez and D. G. Truhlar, *J. Phys. Chem. A*, 1999, **103**, 5129–5136.
110 P. L. Fast, M. L. Sánchez, J. C. Corchado and D. G. Truhlar, *J. Chem. Phys.*, 1999, **110**, 11679–11681.
111 P. L. Fast, M. a. L. Sánchez and D. G. Truhlar, *Chem. Phys. Lett.*, 1999, **306**, 407–410.
112 C. M. Tratz, P. L. Fast and D. G. Truhlar, *PhysChemComm*, 1999, **2**, 70–79.
113 P. L. Fast and D. G. Truhlar, *J. Phys. Chem. A*, 2000, **104**, 6111–6116.
114 B. J. Lynch and D. G. Truhlar, *J. Phys. Chem. A*, 2003, **107**, 3898–3906.
115 Y. Zhao, B. J. Lynch and D. G. Truhlar, *J. Phys. Chem. A*, 2004, **108**, 4786–4791.
116 B. J. Lynch and D. G. Truhlar, *ACS Symp. Ser.*, 2007, **958**, 153–167.
117 J. A. Montgomery, M. J. Frisch, J. W. Ochterski and G. A. Petersson, *J. Chem. Phys.*, 1999, **110**, 2822.
118 N. J. DeYonker, T. R. Cundari and A. K. Wilson, *J. Chem. Phys.*, 2006, **124**, 114104.

119 N. J. DeYonker, T. G. Williams, A. E. Imel, T. R. Cundari and A. K. Wilson, *J. Chem. Phys.*, 2009, **131**, 024106.
120 B. J. Lynch, Y. Zhao and D. G. Truhlar, *J. Phys. Chem. A*, 2005, **109**, 1643–1649.
121 W. Kohn, A. D. Becke and R. G. Parr, *J. Phys. Chem.*, 1996, **100**, 12974–12980.
122 J. Baker, M. Muir, J. Andzelm and A. Scheiner, in *Chemical Applications of Density-Functional Theory*, ACS Symp. Ser., 1996, vol. 629, pp. 342–367.
123 E. I. Izgorodina, M. L. Coote and L. Radom, *J. Phys. Chem. A*, 2005, **109**, 7558–7566.
124 E. I. Izgorodina, D. R. Brittain, J. L. Hodgson, E. H. Krenske, C. Y. Lin, M. Namazian and M. L. Coote, *J. Phys. Chem. A*, 2007, **111**, 10754–10768.
125 Y. Zhao and D. G. Truhlar, *Theor. Chem. Acc.*, 2008, **120**, 215–241.
126 J. Ho and M. L. Coote, *Theor. Chem. Acc.*, 2010, **125**, 3–21.
127 L. Goerigk and S. Grimme, *Phys. Chem. Chem. Phys.*, 2011, **13**, 6670–6688.
128 R. Peverati and D. G. Truhlar, *Philos. Trans. R. Soc., A*, 2014, **372**, 20120476.
129 Y. Zhao, N. E. Schultz and D. G. Truhlar, *J. Chem. Theory Comput.*, 2006, **2**, 364–382.
130 Y. Zhao and D. G. Truhlar, *J. Phys. Chem. A*, 2008, **112**, 1095–1099.
131 Y. Zhao and D. G. Truhlar, *J. Chem. Theory Comput.*, 2011, **7**, 669–676.
132 R. Peverati, Y. Zhao and D. G. Truhlar, *J. Phys. Chem. Lett.*, 2011, **2**, 1991–1997.
133 R. Peverati and D. G. Truhlar, *J. Chem. Theory Comput.*, 2011, **7**, 3983–3994.
134 R. Peverati and D. G. Truhlar, *J. Chem. Phys.*, 2011, **135**, 191102.
135 R. Peverati and D. G. Truhlar, *J. Phys. Chem. Lett.*, 2011, **2**, 2810–2817.
136 R. Peverati and D. G. Truhlar, *J. Phys. Chem. Lett.*, 2012, **3**, 117–124.
137 B. J. Lynch and D. G. Truhlar, *Theor. Chem. Acc.*, 2004, **111**, 335–344.
138 E. L. Coitiño, D. G. Truhlar and K. Morokuma, *Chem. Phys. Lett.*, 1996, **259**, 159–164.
139 S. Humbel, S. Sieber and K. Morokuma, *J. Chem. Phys.*, 1996, **105**, 1959–1967.
140 M. Namazian and M. L. Coote, *J. Phys. Chem. A*, 2007, **111**, 7227–7232.
141 S. Lobachevsky, C. H. Schiesser, C. Y. Lin and M. L. Coote, *J. Phys. Chem. A*, 2008, **112**, 13622–13627.
142 C. Y. Lin and M. L. Coote, *Aust. J. Chem.*, 2009, **62**, 1479.
143 C. Y. Lin, E. I. Izgorodina and M. L. Coote, *Macromolecules*, 2010, **43**, 553–560.
144 P. N. Day, J. H. Jensen, M. S. Gordon, S. P. Webb, W. J. Stevens, M. Krauss, D. Garmer, H. Basch and D. Cohen, *J. Chem. Phys.*, 1996, **105**, 1968.
145 M. S. Gordon, J. M. Mullin, S. R. Pruitt, L. B. Roskop, L. V. Slipchenko and J. A. Boatz, *J. Phys. Chem. B*, 2009, **113**, 9646–9663.
146 M. S. Gordon, M. A. Freitag, P. Bandyopadhyay, J. H. Jensen, V. Kairys and W. J. Stevens, *J. Phys. Chem. A*, 2001, **105**, 293–307.
147 M. S. Gordon, L. Slipchenko, H. Li and J. H. Jensen, *Annu. Rep. Comput. Chem.*, 2007, **3**, 177–193.
148 J. Jensen and H. Li, in *Computational Inorganic and Bioinorganic Chemistry*, ed. E. I. Solomon, R. A. Scott and R. B. King, John Wiley & Sons, Chichester, 2009, pp. 109–122.
149 K. Kitaura, E. Ikeo, T. Asada, T. Nakano and M. Uebayasi, *Chem. Phys. Lett.*, 1999, **313**, 701–706.
150 D. G. Fedorov and K. Kitaura, *J. Chem. Phys.*, 2004, **120**, 6832–6840.
151 D. G. Fedorov and K. Kitaura, *J. Phys. Chem. A*, 2007, **111**, 6904–6914.
152 D. G. Fedorov, T. Nagata and K. Kitaura, *Phys. Chem. Chem. Phys.*, 2012, **14**, 7562–7577.
153 W. Xie, L. Song, D. G. Truhlar and J. Gao, *J. Chem. Phys.*, 2008, **128**, 234108.
154 W. Xie, M. Orozco, D. G. Truhlar and J. Gao, *J. Chem. Theory Comput.*, 2009, **5**, 459–467.
155 E. E. Dahlke and D. G. Truhlar, *J. Chem. Theory Comput.*, 2007, **3**, 46–53.
156 E. E. Dahlke and D. G. Truhlar, *J. Chem. Theory Comput.*, 2007, **3**, 1342–1348.
157 A. S. Mahadevi, A. P. Rahalkar, S. R. Gadre and G. N. Sastry, *J. Chem. Phys.*, 2010, **133**, 164308.
158 N. J. Mayhall and K. Raghavachari, *J. Chem. Theory Comput.*, 2011, **7**, 1336–1343.
159 J. O. B. Tempkin, H. R. Leverentz, B. Wang and D. G. Truhlar, *J. Phys. Chem. Lett.*, 2011, **2**, 2141–2144.
160 N. J. Mayhall and K. Raghavachari, *J. Chem. Theory Comput.*, 2012, **8**, 2669–2675.
161 R. M. Richard and J. M. Herbert, *J. Chem. Phys.*, 2012, **137**, 064113.
162 S. Wen, K. Nanda, Y. Huang and G. J. Beran, *Phys. Chem. Chem. Phys.*, 2012, **14**, 7578–7590.
163 M. Isegawa, B. Wang and D. G. Truhlar, *J. Chem. Theory Comput.*, 2013, **9**, 1381–1393.
164 W. Li, S. Li and Y. Jiang, *J. Phys. Chem. A*, 2007, **111**, 2193–2199.
165 E. Suarez, N. Diaz and D. Suarez, *J. Chem. Theory Comput.*, 2009, **5**, 1667–1679.
166 H. A. Le, H. J. Tan, J. F. Ouyang and R. P. A. Bettens, *J. Chem. Theory Comput.*, 2012, **8**, 469–478.
167 G. J. Beran and S. Hirata, *Phys. Chem. Chem. Phys.*, 2012, **14**, 7559–7561.
168 M. J. Frisch, G. W. Trucks, H. B. Schlegel, G. E. Scuseria, M. A. Robb, J. R. Cheeseman, G. Scalmani, V. Barone, B. Mennucci, G. A. Petersson, H. Nakatsuji, M. L. Caricato, X. Li, H. P. Hratchian, A. F. Izmaylov, J. Bloino, G. Zheng, J. L. Sonnenberg, M. Hada, M. Ehara, K. Toyota, R. Fukuda, J. Hasegawa, M. Ishida, T. Nakajima, Y. Honda, O. Kitao, H. Nakai, T. Vreven, J. A. Montgomery Jr., J. E. Peralta, F. Ogliaro, M. Bearpark, J. J. Heyd, E. Brothers, K. N. Kudin, V. N. Staroverov, R. Kobayashi, J. Normand, K. Raghavachari, A. Rendell, J. C. Burant, S. S. Iyengar,

J. Tomasi, M. Cossi, N. Rega, J. M. Millam, M. Klene, J. E. Knox, J. B. Cross, V. Bakken, C. Adamo, J. Jaramillo, R. Gomperts, R. E. Stratmann, O. Yazyev, A. J. Austin, R. Cammi, C. Pomelli, J. W. Ochterski, R. L. Martin, K. Morokuma, V. G. Zakrzewski, G. A. Voth, P. Salvador, J. J. Dannenberg, S. Dapprich, A. D. Daniels, Ö. Farkas, J. B. Foresman, J. V. Ortiz, J. Cioslowski and D. J. Fox, *Gaussian 09, Revisions A02-C01*, Gaussian Inc., Wallingford, CT, 2009.

169 L. Onsager, *J. Am. Chem. Soc.*, 1936, **58**, 1486–1493.

170 C. J. Cramer and D. G. Truhlar, in *Solvent Effects and Chemical Reactivity*, ed. O. Tapia and J. Bertrán, Kluwer, Dordrecht, 1996, pp. 1–80.

171 R. K. Wangsness, *Electromagnetic Fields*, Wiley, New York, 1979, p. 645.

172 J. Tomasi, B. Mennucci and R. Cammi, *Chem. Rev.*, 2005, **105**, 2999–3093.

173 C. J. Cramer and D. G. Truhlar, *Chem. Rev.*, 1999, **99**, 2161–2200.

174 M. Born, *Z. Phys.*, 1920, **1**, 45–48.

175 W. M. Latimer, K. S. Pitzer and C. M. Slansky, *J. Chem. Phys.*, 1939, **7**, 108.

176 G. J. Hoijtink, E. de Boer, P. H. van der Meij and W. P. Weijland, *Recl. Trav. Chim. Pays-Bas*, 1956, **75**, 487–503.

177 F. Peradejordi, *Cah. Phys.*, 1963, **17**, 393–447.

178 S. C. Tucker and D. G. Truhlar, *Chem. Phys. Lett.*, 1989, **157**, 164–170.

179 W. C. Still, A. Tempczyk, R. C. Hawley and T. Hendrickson, *J. Am. Chem. Soc.*, 1990, **112**, 6127–6129.

180 C. J. Cramer and D. G. Truhlar, *J. Am. Chem. Soc.*, 1991, **113**, 8305–8311.

181 C. Curutchet, C. J. Cramer, D. G. Truhlar, M. F. Ruiz-Lopez, D. Rinaldi, M. Orozco and F. J. Luque, *J. Comput. Chem.*, 2003, **24**, 284–297.

182 T. H. Zhu, J. B. Li, G. D. Hawkins, C. J. Cramer and D. G. Truhlar, *J. Chem. Phys.*, 1998, **109**, 9117–9133.

183 J. L. Rivail and D. Rinaldi, *Chem. Phys.*, 1976, **18**, 233–242.

184 J. L. Rivail and D. Rinaldi, in *Computational chemistry: reviews of current trends*, ed. J. Leszczynski, World Scientific, Singapore, 1996, vol. 1, pp. 139–174.

185 S. Miertuš, E. Scrocco and J. Tomasi, *Chem. Phys.*, 1981, **55**, 117–129.

186 V. Barone and M. Cossi, *J. Phys. Chem. A*, 1998, **102**, 1995–2001.

187 M. Cossi, N. Rega, G. Scalmani and V. Barone, *J. Comput. Chem.*, 2003, **24**, 669–681.

188 E. Cances, B. Mennucci and J. Tomasi, *J. Chem. Phys.*, 1997, **107**, 3032–3041.

189 D. J. Tannor, B. Marten, R. Murphy, R. A. Friesner, D. Sitkoff, A. Nicholls, M. Ringnalda, W. A. Goddard and B. Honig, *J. Am. Chem. Soc.*, 1994, **116**, 11875–11882.

190 B. Marten, K. Kim, C. Cortis, R. A. Friesner, R. B. Murphy, M. N. Ringnalda, D. Sitkoff and B. Honig, *J. Phys. Chem.*, 1996, **100**, 11775–11788.

191 X. Jaguar, *Version 8.0*, Schrödinger, LLC, New York, NY, 2013.

192 A. Klamt and G. Schuurmann, *J. Chem. Soc., Perkin Trans. 2*, 1993, 799–805.

193 A. Klamt, V. Jonas, T. Burger and J. C. W. Lohrenz, *J. Phys. Chem. A*, 1998, **102**, 5074–5085.

194 F. J. Luque, M. Bachs and M. Orozco, *J. Comput. Chem.*, 1994, **15**, 847–857.

195 M. Bachs, F. J. Luque and M. Orozco, *J. Comput. Chem.*, 1994, **15**, 446–454.

196 A. V. Marenich, R. M. Olson, C. P. Kelly, C. J. Cramer and D. G. Truhlar, *J. Chem. Theory Comput.*, 2007, **3**, 2011–2033.

197 A. V. Marenich, C. J. Cramer and D. G. Truhlar, *J. Chem. Theory Comput.*, 2009, **5**, 2447–2464.

198 A. V. Marenich, C. J. Cramer and D. G. Truhlar, *J. Chem. Theory Comput.*, 2013, **9**, 609–620.

199 D. Bashford and D. A. Case, *Annu. Rev. Phys. Chem.*, 2000, **51**, 129–152.

200 A. Onufriev, D. A. Case and D. Bashford, *J. Comput. Chem.*, 2002, **23**, 1297–1304.

201 A. W. Lange and J. M. Herbert, *J. Chem. Theory Comput.*, 2012, **8**, 1999–2011.

202 M. Orozco and F. J. Luque, *Chem. Rev.*, 2000, **100**, 4187–4226.

203 C. J. Cramer and D. G. Truhlar, *Acc. Chem. Res.*, 2008, **41**, 760–768.

204 C. J. Cramer and D. G. Truhlar, *Acc. Chem. Res.*, 2009, **42**, 493–497.

205 A. V. Marenich, C. J. Cramer and D. G. Truhlar, *J. Chem. Theory Comput.*, 2008, **4**, 877–887.

206 B. S. Brunschwig, S. Ehrenson and N. Sutin, *J. Phys. Chem. A*, 1986, **90**, 3657–3668.

207 B. Jayaram, R. Fine, K. Sharp and B. Honig, *J. Phys. Chem.*, 1989, **93**, 4320–4327.

208 Y. Marcus, *J. Chem. Soc., Faraday Trans.*, 1991, **87**, 2995–2999.

209 S. W. Rick and B. J. Berne, *J. Am. Chem. Soc.*, 1994, **116**, 3949–3954.

210 A. A. Kornyshev and G. Sutmann, in *Electron and Ion Transfer in Condensed Media*, ed. A. A. Kornyshev, M. Tosi and J. Ulstrup, World Scientific, Singapore, 1997, pp. 73–97.

211 K. S. Alongi and G. C. Shields, *Annu. Rep. Comput. Chem.*, 2010, **6**, 113–138.

212 Y. Fu, L. Liu, H. Z. Yu, Y. M. Wang and Q. X. Guo, *J. Am. Chem. Soc.*, 2005, **127**, 7227–7234.

213 M. Schmidt Am Busch and E. W. Knapp, *J. Am. Chem. Soc.*, 2005, **127**, 15730–15737.

214 M. Namazian, S. Siahrostami, M. R. Noorbala and M. L. Coote, *THEOCHEM*, 2006, **759**, 245–247.

215 J. P. Blinco, J. L. Hodgson, B. J. Morrow, J. R. Walker, G. D. Will, M. L. Coote and S. E. Bottle, *J. Org. Chem.*, 2008, **73**, 6763–6771.

216 C. Y. Lin, M. L. Coote, A. Gennaro and K. Matyjaszewski, *J. Am. Chem. Soc.*, 2008, **130**, 12762–12774.

217 M. Namazian, H. R. Zare and M. L. Coote, *Biophys. Chem.*, 2008, **132**, 64–68.

218 M. Namazian, S. Siahrostami and M. L. Coote, *J. Fluorine Chem.*, 2008, **129**, 222–225.

219 A. Galstyan and E. W. Knapp, *J. Comput. Chem.*, 2009, **30**, 203–211.

220 H. R. Zare, M. Namazian and M. L. Coote, *Electrochim. Acta*, 2009, **54**, 5353–5357.
221 H. R. Zare, M. Eslami, M. Namazian and M. L. Coote, *J. Phys. Chem. B*, 2009, **113**, 8080–8085.
222 G. Gryn'ova, J. M. Barakat, J. P. Blinco, S. E. Bottle and M. L. Coote, *Chem. – Eur. J.*, 2012, **18**, 7582–7593.
223 M. Namazian, H. R. Zare and M. L. Coote, *Aust. J. Chem.*, 2012, **65**, 486–489.
224 M. H. Baik and R. A. Friesner, *J. Phys. Chem. A*, 2002, **106**, 7407–7412.
225 A. D. Becke, *Phys. Rev. A: At., Mol., Opt. Phys.*, 1988, **38**, 3098–3100.
226 C. T. Lee, W. T. Yang and R. G. Parr, *Phys. Rev. B: Condens. Matter Mater. Phys.*, 1988, **37**, 785–789.
227 L. Sviatenko, O. Isayev, L. Gorb, F. Hill and J. Leszczynski, *J. Comput. Chem.*, 2011, **32**, 2195–2203.
228 G. te Velde, F. M. Bickelhaupt, E. J. Baerends, C. Fonseca Guerra, S. J. A. van Gisbergen, J. G. Snijders and T. Ziegler, *J. Comput. Chem.*, 2001, **22**, 931–967.
229 H.-J. Werner, P. J. Knowles, G. Knizia, F. R. Manby, M. Schütz, P. Celani, T. Korona, R. Lindh, A. Mitrushenkov, G. Rauhut, K. R. Shamasundar, T. B. Adler, R. D. Amos, A. Bernhardsson, A. Berning, D. L. Cooper, M. J. O. Deegan, A. J. Dobbyn, F. Eckert, E. Goll, C. Hampel, A. Hesselmann, G. Hetzer, T. Hrenar, G. Jansen, C. Köppl, Y. Liu, A. W. Lloyd, R. A. Mata, A. J. May, S. J. McNicholas, W. Meyer, M. E. Mura, A. Nicklass, D. P. O'Neill, P. Palmieri, K. Pflüger, R. Pitzer, M. Reiher, T. Shiozaki, H. Stoll, A. J. Stone, R. Tarroni, T. Thorsteinsson, M. Wang and A. Wolf, *MOLPRO, version 2012.1, A package of ab initio* programs, Cardiff University, Cardiff, UK, http://www.molpro.net, 2012.
230 H.-J. Werner, P. J. Knowles, G. Knizia, F. R. Manby and M. Schütz, *Comput. Mol. Biosci.*, 2012, **2**, 242–253.
231 D. Meisel and G. Czapski, *J. Phys. Chem.*, 1975, **79**, 1503–1509.
232 Y. A. Ilan, G. Czapski and D. Meisel, *Biochim. Biophys. Acta*, 1976, **430**, 209–224.
233 C. Creutz, *Inorg. Chem.*, 1981, **20**, 4449–4452.
234 N. H. Williams and J. K. Yandell, *Aust. J. Chem.*, 1982, **35**, 1133–1144.
235 M. Kimura and Y. Kaneko, *J. Chem. Soc., Dalton Trans.*, 1984, **3**, 341–343.
236 P. S. Surdhar and D. A. Armstrong, *J. Phys. Chem.*, 1986, **90**, 5915–5917.
237 G. Merenyi, J. Lind and X. Shen, *J. Phys. Chem.*, 1988, **92**, 134–137.
238 M. Jonsson, J. Lind, T. E. Eriksen and G. Merenyi, *J. Am. Chem. Soc.*, 1994, **116**, 1423–1427.
239 M. Jonsson, D. D. M. Wayner and J. Lusztyk, *J. Phys. Chem.*, 1996, **100**, 17539–17543.
240 D. A. Armstrong, Q. Sun and R. H. Schuler, *J. Phys. Chem. A*, 1996, **100**, 9892–9899.
241 R. Zhao, J. Lind, G. Merenyi and T. E. Eriksen, *J. Am. Chem. Soc.*, 1998, **120**, 2811–2816.
242 R. Zhao, J. Lind, G. Merenyi and T. E. Eriksen, *J. Phys. Chem. A*, 1999, **103**, 71–74.
243 R. Zhao, J. Lind, G. Merenyi, M. Jonsson and T. E. Eriksen, *J. Phys. Chem. A*, 2000, **104**, 8524–8526.
244 G. Merenyi, J. Lind and S. Goldstein, *J. Phys. Chem. A*, 2002, **106**, 11127–11129.
245 A. Israeli, M. Patt, M. Oron, A. Samuni, R. Kohen and S. Goldstein, *Free Radical Biol. Med.*, 2005, **38**, 317–324.
246 J. Lind and G. Merenyi, *J. Phys. Chem. A*, 2006, **110**, 192–197.
247 S. Goldstein, A. Samuni, K. Hideg and G. Merenyi, *J. Phys. Chem. A*, 2006, **110**, 3679–3685.
248 J. J. Guerard and J. S. Arey, *J. Chem. Theory Comput.*, 2013, **9**, 5046–5058.
249 S. J. Konezny, M. D. Doherty, O. R. Luca, R. H. Crabtree, G. L. Soloveichik and V. S. Batista, *J. Phys. Chem. C*, 2012, **116**, 6349–6356.
250 L. E. Roy, E. Jakubikova, M. G. Guthrie and E. R. Batista, *J. Phys. Chem. A*, 2009, **113**, 6745–6750.
251 R. V. Stanton, J. L. Miller and P. A. Kollman, in *Modern Methods for Multidimentional Dynamics Computations in Chemistry*, ed. D. L. Thompson, World Scientific, Singapore, 1998, pp. 355–383.
252 U. W. Schmitt and G. A. Voth, *J. Chem. Phys.*, 1999, **111**, 9361–9381.
253 M. Garcia-Viloca, C. Alhambra, D. G. Truhlar and J. Gao, *J. Chem. Phys.*, 2001, **114**, 9953.
254 N. Boekelheide, R. Salomon-Ferrer and T. F. Miller 3rd, *Proc. Natl. Acad. Sci. U. S. A.*, 2011, **108**, 16159–16163.
255 D. Marx, J. Hutter, *Ab initio Molecular Dynamics: Basic Theory and Advanced Methods*, Cambridge University Press, Cambridge, 2012, p. 577.
256 A. D. Mackerell, Jr., *J. Comput. Chem.*, 2004, **25**, 1584–1604.
257 B. M. Rode and T. S. Hofer, *Pure Appl. Chem.*, 2006, **78**, 525–539.
258 B. M. Rode, T. S. Hofer, B. R. Randolf, C. F. Schwenk, D. Xenides and V. Vchirawongkwin, *Theor. Chem. Acc.*, 2006, **115**, 77–85.
259 M. H. Olsson, G. Hong and A. Warshel, *J. Am. Chem. Soc.*, 2003, **125**, 5025–5039.
260 J. Blumberger, Y. Tateyama and M. Sprik, *Comput. Phys. Commun.*, 2005, **169**, 256–261.
261 S. Bhattacharyya, M. T. Stankovich, D. G. Truhlar and J. Gao, *J. Phys. Chem. A*, 2007, **111**, 5729–5742.
262 *Free Energy Calculations: Theory and Applications in Chemistry and Biology*, ed. C. Chipot and A. Pohorille, Springer, Berlin, 2007, p. 517.
263 B. M. Sattelle and M. J. Sutcliffe, *J. Phys. Chem. A*, 2008, **112**, 13053–13057.
264 G. Hummer, L. R. Pratt and A. E. Garcia, *J. Chem. Phys.*, 1997, **107**, 9275–9277.
265 R. Ayala and M. Sprik, *J. Phys. Chem. B*, 2008, **112**, 257–269.
266 C. A. Reynolds, P. M. King and W. G. Richards, *J. Chem. Soc., Chem. Commun.*, 1988, 1434–1436.
267 K. S. Raymond, A. K. Grafton and R. A. Wheeler, *J. Phys. Chem. B*, 1997, **101**, 623–631.
268 J. Blumberger, L. Bernasconi, I. Tavernelli, R. Vuilleumier and M. Sprik, *J. Am. Chem. Soc.*, 2004, **126**, 3928–3938.

269 A. Pandey and S. N. Datta, *J. Phys. Chem. B*, 2005, **109**, 9066–9072.
270 N. Mehta and S. N. Datta, *J. Phys. Chem. B*, 2007, **111**, 7210–7217.
271 J. Blumberger, *Phys. Chem. Chem. Phys.*, 2008, **10**, 5651–5667.
272 J. Cheng, M. Sulpizi and M. Sprik, *J. Chem. Phys.*, 2009, **131**, 154504.
273 J. C. Rauschnot, C. Yang, V. Yang and S. Bhattacharyya, *J. Phys. Chem. B*, 2009, **113**, 8149–8157.
274 F. Costanzo, M. Sulpizi, R. G. Della Valle and M. Sprik, *J. Chem. Phys.*, 2011, **134**, 244508.
275 D. L. Beveridge and F. M. DiCapua, *Annu. Rev. Biophys. Biophys. Chem.*, 1989, **18**, 431–492.
276 D. A. McQuarrie, *Statistical Mechanics*, University Science Books, Sausalito, CA, 2000, p. 641.
277 T. Schlick, *Molecular Modeling and Simulation: An Interdisciplinary Guide*, Springer-Verlag, New York, 2002, p. 634.
278 J. C. Owicki and H. A. Scheraga, *J. Phys. Chem.*, 1978, **82**, 1257–1264.
279 P. Cristinziano, F. Lelj, P. Amodeo and V. Barone, *Chem. Phys. Lett.*, 1987, **140**, 401–405.
280 J. Aqvist, P. Wennerstrom, M. Nervall, S. Bjelic and B. O. Brandsdal, *Chem. Phys. Lett.*, 2004, **384**, 288–294.
281 D. F. Coker and R. O. Watts, *Chem. Phys. Lett.*, 1981, **78**, 333–336.
282 J. Ji and B. M. Pettitt, in *Computer Simulation of Biomolecular Systems: Theoretical And Experimental Applications*, ed. W. F. van Gunsteren, P. K. Weiner and A. J. Wilkinson, ESCOM, Leiden, 1993, vol. 2, pp. 67–81.
283 G. C. Lynch and B. M. Pettitt, *J. Chem. Phys.*, 1997, **107**, 8594–8610.
284 H. Eslami and F. Muller-Plathe, *J. Comput. Chem.*, 2007, **28**, 1763–1773.
285 G. K. Schenter, B. C. Garrett and D. G. Truhlar, *J. Chem. Phys.*, 2003, **119**, 5828–5833.
286 J. G. Kirkwood and J. C. Poirier, *J. Phys. Chem.*, 1954, **58**, 591–596.
287 B. M. Pettitt and M. Karplus, *Chem. Phys. Lett.*, 1985, **121**, 194–201.
288 D. E. Smith and L. X. Dang, *J. Chem. Phys.*, 1994, **100**, 3757–3766.
289 B. Roux, *Comput. Phys. Commun.*, 1995, **91**, 275–282.
290 Y. Kim, J. R. Mohrig and D. G. Truhlar, *J. Am. Chem. Soc.*, 2010, **132**, 11071–11082.
291 S. J. Klippenstein, V. S. Pande and D. G. Truhlar, *J. Am. Chem. Soc.*, 2014, **136**, 528–546.
292 Y. Y. Chuang, C. J. Cramer and D. G. Truhlar, *Int. J. Quantum Chem.*, 1998, **70**, 887–896.
293 G. M. Torrie and J. P. Valleau, *J. Comput. Phys.*, 1977, **23**, 187–199.
294 D. Chandler, *Introduction to Modern Statistical Mechanics*, Oxford University Press, New York, 1987, p. 288.
295 K. Leung, I. M. Nielsen, N. Sai, C. Medforth and J. A. Shelnutt, *J. Phys. Chem. A*, 2010, **114**, 10174–10184.
296 T. Simonson, in *Computational Biochemistry and Biophysics*, ed. O. M. Becker, A. D. MacKerell, Jr., B. Roux and M. Watanabe, Dekker, New York, 2001, pp. 169–197.
297 J. Cheng and M. Sprik, *Phys. Chem. Chem. Phys.*, 2012, **14**, 11245–11267.
298 E. Darve, in *Free Energy Calculations*, ed. C. Chipot and A. Pohorille, Springer, Berlin, 2007, pp. 119–170.
299 J. G. Kirkwood, *J. Chem. Phys.*, 1935, **3**, 300–313.
300 W. F. Libby, *J. Phys. Chem.*, 1952, **56**, 863–868.
301 L. P. Wang and T. Van Voorhis, *J. Chem. Theory Comput.*, 2012, **8**, 610–617.
302 R. W. Zwanzig, *J. Chem. Phys.*, 1954, **22**, 1420.
303 C. Chipot and and A. Pohorille, in *Free Energy Calculations: Theory and Applications in Chemistry and Biology*, ed. C. Chipot and A. Pohorille, Springer, Berlin, 2007, pp. 33–75.
304 J. Blumberger, I. Tavernelli, M. L. Klein and M. Sprik, *J. Chem. Phys.*, 2006, **124**, 64507.
305 Y. Tateyama, J. Blumberger, M. Sprik and I. Tavernelli, *J. Chem. Phys.*, 2005, **122**, 234505.
306 W. L. Jorgensen and C. Ravimohan, *J. Chem. Phys.*, 1985, **83**, 3050–3054.
307 I. Tavernelli, R. Vuilleumier and M. Sprik, *Phys. Rev. Lett.*, 2002, **88**, 213002.
308 J. Blumberger and M. Sprik, *J. Phys. Chem. B*, 2005, **109**, 6793–6804.
309 E. E. Nikitin, in *Chemische Elementarprozesse*, ed. H. Hartmann, J. Heidberg, H. Heydtmann and G. H. Kohlmaier, Springer, Verlag, Berlin, 1968, pp. 43–77.
310 J. C. Tully, *J. Chem. Phys.*, 2012, **137**, 22A301.
311 G. King and A. Warshel, *J. Chem. Phys.*, 1990, **93**, 8682–8692.
312 C. Drechsel-Grau and M. Sprik, *J. Chem. Phys.*, 2012, **136**, 034506.
313 R. A. Marcus, *J. Chem. Phys.*, 1956, **24**, 966–978.
314 R. A. Marcus, *Discuss. Faraday Soc.*, 1960, **29**, 21–31.
315 R. A. Marcus, *J. Phys. Chem.*, 1963, **67**, 853–857.
316 R. A. Marcus, *Angew. Chem., Int. Ed. Engl.*, 1993, **32**, 1111–1121.
317 R. A. Marcus, in *Physical Chemistry*, ed. R. S. Berry, S. A. Rice and J. Ross, Oxford University Press, New York, 2000, pp. 945–948.
318 A. M. Kuznetsov, in *Electron and Ion Transfer in Condensed Media*, ed. A. A. Kornyshev, M. Tosi and J. Ulstrup, World Scientific, Singapore, 1997, pp. 165–185.
319 V. May and O. Kühn, *Charge and Energy Transfer Dynamics in Molecular Systems*, Wiley-VCH, Berlin, 2nd edn, 2004, p. 490.
320 J. Pu, J. Gao and D. G. Truhlar, *Chem. Rev.*, 2006, **106**, 3140–3169.
321 J. Blumberger and M. Sprik, *Theor. Chem. Acc.*, 2006, **115**, 113–126.
322 J. VandeVondele, R. Ayala, M. Sulpizi and M. Sprik, *J. Electroanal. Chem.*, 2007, **607**, 113–120.
323 M. Neumann, *J. Chem. Phys.*, 1985, **82**, 5663–5672.
324 Z. Kurtovic, M. Marchi and D. Chandler, *Mol. Phys.*, 1993, **78**, 1155–1165.
325 C. Adriaanse, J. Cheng, V. Chau, M. Sulpizi, J. VandeVondele and M. Sprik, *J. Phys. Chem. Lett.*, 2012, **3**, 3411–3415.

326 J. J. Wolfe, J. D. Wright, C. A. Reynolds and A. C. Saunders, *Anticancer Drug Des.*, 1994, **9**, 85–102.
327 J. Y. Alston and A. J. Fry, *Electrochim. Acta*, 2004, **49**, 455–459.
328 L. D. Hicks, A. J. Fry and V. C. Kurzweil, *Electrochim. Acta*, 2004, **50**, 1039–1047.
329 A. Bottoni, B. Cosimelli, E. Scavetta, D. Spinelli, R. Spisani, M. Stenta and D. Tonelli, *Mol. Phys.*, 2006, **104**, 2961–2982.
330 M. Shamsipur, A. Siroueinejad, B. Hemmateenejad, A. Abbaspour, H. Sharghi, K. Alizadeh and S. Arshadi, *J. Electroanal. Chem.*, 2007, **600**, 345–358.
331 C. E. Crespo-Hernandez, D. M. Close, L. Gorb and J. Leszczynski, *J. Phys. Chem. B*, 2007, **111**, 5386–5395.
332 J. Moens, P. Geerlings and G. Roos, *Chem. – Eur. J.*, 2007, **13**, 8174–8184.
333 J. Moens, G. Roos, P. Jaque, F. De Proft and P. Geerlings, *Chem. – Eur. J.*, 2007, **13**, 9331–9343.
334 J. Cody, S. Mandal, L. Yang and C. J. Fahrni, *J. Am. Chem. Soc.*, 2008, **130**, 13023–13032.
335 J. Moens, P. Jaque, F. De Proft and P. Geerlings, *J. Phys. Chem. A*, 2008, **112**, 6023–6031.
336 A. L. Speelman and J. G. Gillmore, *J. Phys. Chem. A*, 2008, **112**, 5684–5690.
337 A. P. Davis and A. J. Fry, *J. Phys. Chem. A*, 2010, **114**, 12299–12304.
338 D. M. Cwiertny, W. A. Arnold, T. Kohn, L. A. Rodenburg and A. L. Roberts, *Environ. Sci. Technol.*, 2010, **44**, 7928–7936.
339 K. L. Phillips, S. I. Sandler and P. C. Chiu, *J. Comput. Chem.*, 2011, **32**, 226–239.
340 E. J. Lynch, A. L. Speelman, B. A. Curry, C. S. Murillo and J. G. Gillmore, *J. Org. Chem.*, 2012, **77**, 6423–6430.
341 R. Francke and R. D. Little, *J. Am. Chem. Soc.*, 2014, **136**, 427–435.
342 M. Uudsemaa and T. Tamm, *J. Phys. Chem. A*, 2003, **107**, 9997–10003.
343 P. Jaque, A. V. Marenich, C. J. Cramer and D. G. Truhlar, *J. Phys. Chem. C*, 2007, **111**, 5783–5799.
344 Y. Zhao and D. G. Truhlar, *Rev. Mineral. Geochem.*, 2010, **71**, 19–37.
345 A. V. Marenich, A. Majumdar, M. Lenz, C. J. Cramer and D. G. Truhlar, *Angew. Chem., Int. Ed.*, 2012, **51**, 12810–12814.
346 J. M. Mouesca, J. L. Chen, L. Noodleman, D. Bashford and D. A. Case, *J. Am. Chem. Soc.*, 1994, **116**, 11898–11914.
347 R. A. Torres, T. Lovell, L. Noodleman and D. A. Case, *J. Am. Chem. Soc.*, 2003, **125**, 1923–1936.
348 R. Mas-Balleste, M. Capdevila, P. Gonzalez-Duarte, M. Hamidi, A. Lledos, C. Megret and D. de Montauzon, *Dalton Trans.*, 2004, 706–712.
349 K. P. Jensen, *J. Inorg. Biochem.*, 2008, **102**, 87–100.
350 M. D. Bartberger, W. Liu, E. Ford, K. M. Miranda, C. Switzer, J. M. Fukuto, P. J. Farmer, D. A. Wink and K. N. Houk, *Proc. Natl. Acad. Sci. U. S. A.*, 2002, **99**, 10958–10963.
351 A. S. Dutton, J. M. Fukuto and K. N. Houk, *Inorg. Chem.*, 2005, **44**, 4024–4028.
352 G. Gryn'ova, D. L. Marshall, S. J. Blanksby and M. L. Coote, *Nat. Chem.*, 2013, **5**, 474–481.
353 N. S. Emel'yanova, A. F. Shestakov and N. A. Sanina, *Int. J. Quantum Chem.*, 2013, **113**, 740–744.
354 N. Emel'yanova, N. Sanina, A. Krivenko, R. Manzhos, K. Bozhenko and S. Aldoshin, *Theor. Chem. Acc.*, 2013, **132**, 1316–1323.
355 J. T. York, A. Llobet, C. J. Cramer and W. B. Tolman, *J. Am. Chem. Soc.*, 2007, **129**, 7990–7999.
356 I. M. Mbomekalle, X. Lopez, J. M. Poblet, F. Secheresse, B. Keita and L. Nadjo, *Inorg. Chem.*, 2010, **49**, 7001–7006.
357 P. A. Aparicio, J. M. Poblet and X. López, *Eur. J. Inorg. Chem.*, 2013, 1910–1916.
358 X. Lopez, J. J. Carbo, C. Bo and J. M. Poblet, *Chem. Soc. Rev.*, 2012, **41**, 7537–7571.
359 C. G. Liu, W. Guan, L. K. Yan and Z. M. Su, *Dalton Trans.*, 2011, **40**, 2967–2974.
360 J. S. Jirkovsky, M. Busch, E. Ahlberg, I. Panas and P. Krtil, *J. Am. Chem. Soc.*, 2011, **133**, 5882–5892.
361 V. L. Chevrier, S. P. Ong, R. Armiento, M. K. Y. Chan and G. Ceder, *Phys. Rev. B: Condens. Matter Mater. Phys.*, 2010, **82**, 075122.
362 Z. Ding, L. Zhao, L. Suo, Y. Jiao, S. Meng, Y. S. Hu, Z. Wang and L. Chen, *Phys. Chem. Chem. Phys.*, 2011, **13**, 15127–15133.
363 V. S. Bryantsev, J. Uddin, V. Giordani, W. Walker, G. V. Chase and D. Addison, *J. Am. Chem. Soc.*, 2014, **136**, 3087–3096.
364 T. Mueller, G. Hautier, A. Jain and G. Ceder, *Chem. Mater.*, 2011, **23**, 3854–3862.
365 B. P. Chaplin, D. K. Hubler and J. Farrell, *Electrochim. Acta*, 2013, **89**, 122–131.
366 T. B. Lee and M. L. McKee, *Inorg. Chem.*, 2012, **51**, 4205–4214.
367 A. Wahab, B. Stepp, C. Douvris, M. Valasek, J. Stursa, J. Klima, M. C. Piqueras, R. Crespo, J. Ludvik and J. Michl, *Inorg. Chem.*, 2012, **51**, 5128–5137.
368 H. M. Steele, D. Guillaumont and P. Moisy, *J. Phys. Chem. A*, 2013, **117**, 4500–4505.
369 Y. Zhao and D. G. Truhlar, *J. Chem. Phys.*, 2006, **125**, 194101.
370 J. P. Austin, N. A. Burton, I. H. Hillier, M. Sundararajan and M. A. Vincent, *Phys. Chem. Chem. Phys.*, 2009, **11**, 1143–1145.
371 G. A. Shamov and G. Schreckenbach, *J. Am. Chem. Soc.*, 2008, **130**, 13735–13744.
372 G. Schreckenbach and G. A. Shamov, *Acc. Chem. Res.*, 2010, **43**, 19–29.
373 F. A. Schultz, *J. Solid State Electrochem.*, 2011, **15**, 1833–1843.
374 S. J. Hwang, S. K. Kim, J. G. Lee, S. C. Lee, J. H. Jang, P. Kim, T. H. Lim, Y. E. Sung and S. J. Yoo, *J. Am. Chem. Soc.*, 2012, **134**, 19508–19511.
375 E. V. Patterson, C. J. Cramer and D. G. Truhlar, *J. Am. Chem. Soc.*, 2001, **123**, 2025–2031.
376 W. A. Arnold, P. Winget and C. J. Cramer, *Environ. Sci. Technol.*, 2002, **36**, 3536–3541.
377 B. Fabre, P. Hapiot and J. Simonet, *J. Phys. Chem. A*, 2002, **106**, 5422–5428.
378 G. Camurri, P. Ferrarini, R. Giovanardi, R. Benassi and C. Fontanesi, *J. Electroanal. Chem.*, 2005, **585**, 181–190.

379 T. B. Hofstetter, A. Neumann, W. A. Arnold, A. E. Hartenbach, J. Bolotin, C. J. Cramer and R. P. Schwarzenbach, *Environ. Sci. Technol.*, 2008, **42**, 1997–2003.

380 A. E. Hartenbach, T. B. Hofstetter, M. Aeschbacher, M. Sander, D. Kim, T. J. Strathmann, W. A. Arnold, C. J. Cramer and R. P. Schwarzenbach, *Environ. Sci. Technol.*, 2008, **42**, 8352–8359.

381 P. B. Merkel, P. Luo, J. P. Dinnocenzo and S. Farid, *J. Org. Chem.*, 2009, **74**, 5163–5173.

382 R. I. Zubatyuk, L. Gorb, O. V. Shishkin, M. Qasim and J. Leszczynski, *J. Comput. Chem.*, 2010, **31**, 144–150.

383 H. Mohammad-Shiri, M. Ghaemi, S. Riahi and A. Akbari-Sehat, *Int. J. Electrochem. Sci.*, 2011, **6**, 317–336.

384 P. Kaszynski, *J. Phys. Chem. A*, 2001, **105**, 7626–7633.

385 S. Riahi, A. B. Moghaddam, A. Hooshmand, P. Norouzi, M. R. Ganjali, R. Z. Dorabei and K. Bagherzadeh, *Anal. Lett.*, 2007, **40**, 2574–2588.

386 T. Tugsuz, *J. Phys. Chem. B*, 2010, **114**, 17092–17101.

387 P. A. Dub and R. Poli, *J. Am. Chem. Soc.*, 2010, **132**, 13799–13812.

388 T. Liu, C. Du, Z. Yu, L. Han and D. Zhang, *J. Phys. Chem. B*, 2013, **117**, 2081–2087.

389 L. J. Kettle, S. P. Bates and A. R. Mount, *Phys. Chem. Chem. Phys.*, 2000, **2**, 195–201.

390 J. B. Henry and A. R. Mount, *J. Phys. Chem. A*, 2009, **113**, 13023–13028.

391 J. Scheers, P. Johansson, P. Szczecinski, W. Wieczorek, M. Armand and P. Jacobsson, *J. Power Sources*, 2010, **195**, 6081–6087.

392 T. Tugsuz, *Int. J. Quantum Chem.*, 2013, **113**, 715–722.

393 J. J. Chen, W. Chen, H. He, D. B. Li, W. W. Li, L. Xiong and H. Q. Yu, *Environ. Sci. Technol.*, 2013, **47**, 1033–1039.

394 M. H. Baik, J. S. Silverman, I. V. Yang, P. A. Ropp, V. A. Szalai, W. T. Yang and H. H. Thorp, *J. Phys. Chem. B*, 2001, **105**, 6437–6444.

395 B. T. Psciuk, R. L. Lord, B. H. Munk and H. B. Schlegel, *J. Chem. Theory Comput.*, 2012, **8**, 5107–5123.

396 B. T. Psciuk and H. B. Schlegel, *J. Phys. Chem. B*, 2013, **117**, 9518–9531.

397 M. Harada, I. Watanabe and H. Watarai, *Chem. Phys. Lett.*, 1999, **301**, 270–274.

398 L. D. Betowski, M. Enlow, L. Riddick and D. H. Aue, *J. Phys. Chem. A*, 2006, **110**, 12927–12946.

399 C. Bruno, R. Benassi, A. Passalacqua, F. Paolucci, C. Fontanesi, M. Marcaccio, E. A. Jackson and L. T. Scott, *J. Phys. Chem. B*, 2009, **113**, 1954–1962.

400 D. D. Mendez-Hernandez, P. Tarakeshwar, D. Gust, T. A. Moore, A. L. Moore and V. Mujica, *J. Mol. Model.*, 2013, **19**, 2845–2848.

401 S. Riahi, P. Norouzi, A. Bayandori Moghaddam, M. R. Ganjali, G. R. Karimipour and H. Sharghi, *Chem. Phys.*, 2007, **337**, 33–38.

402 P. Winget, *Chem. Phys.*, 2010, **378**, 118–119.

403 S. Riahi, S. Eynollahi and M. R. Ganjali, *Int. J. Electrochem. Sci.*, 2009, **4**, 1128–1137.

404 S. Riahi, S. Eynollahi and M. R. Ganjali, *Int. J. Electrochem. Sci.*, 2009, **4**, 1309–1318.

405 A. A. Freitas, K. Shimizu, L. G. Dias and F. H. Quina, *J. Braz. Chem. Soc.*, 2007, **18**, 1537–1546.

406 M. A. North, S. Bhattacharyya and D. G. Truhlar, *J. Phys. Chem. B*, 2010, **114**, 14907–14915.

407 R. M. Mueller, M. A. North, C. Yang, S. Hati and S. Bhattacharyya, *J. Phys. Chem. B*, 2011, **115**, 3632–3641.

408 S. Chen, M. S. Hossain and F. W. Foss Jr., *Org. Lett.*, 2012, **14**, 2806–2809.

409 M. Kılıç and B. Ensing, *J. Chem. Theory Comput.*, 2013, **9**, 3889–3899.

410 C. A. Reynolds, *Int. J. Quantum Chem.*, 1995, **56**, 677–687.

411 J. R. Johnsson Wass, E. Ahlberg, I. Panas and D. J. Schiffrin, *J. Phys. Chem. A*, 2006, **110**, 2005–2020.

412 K. Alizadeh and M. Shamsipur, *THEOCHEM*, 2008, **862**, 39–43.

413 A. H. Pakiari, S. Siahrostami and A. Mohajeri, *THEOCHEM*, 2008, **870**, 10–14.

414 M. Eslami, H. R. Zare and M. Namazian, *J. Phys. Chem. B*, 2012, **116**, 12552–12557.

415 S. E. Barrows, C. J. Cramer, D. G. Truhlar, M. S. Elovitz and E. J. Weber, *Environ. Sci. Technol.*, 1996, **30**, 3028–3038.

416 O. Hammerich, T. Hansen, A. Thorvildsen and J. B. Christensen, *ChemPhysChem*, 2009, **10**, 1805–1824.

417 M. Valiev, E. J. Bylaska, M. Dupuis and P. G. Tratnyek, *J. Phys. Chem. A*, 2008, **112**, 2713–2720.

418 E. J. Bylaska, K. R. Glaesemann, A. R. Felmy, M. Vasiliu, D. A. Dixon and P. G. Tratnyek, *J. Phys. Chem. A*, 2010, **114**, 12269–12282.

419 Y. F. Huang, D. Y. Wu, A. Wang, B. Ren, S. Rondinini, Z. Q. Tian and C. Amatore, *J. Am. Chem. Soc.*, 2010, **132**, 17199–17210.

420 A. A. Isse, A. Gennaro, C. Y. Lin, J. L. Hodgson, M. L. Coote and T. Guliashvili, *J. Am. Chem. Soc.*, 2011, **133**, 6254–6264.

421 H. J. Wang and C. J. Yu, *Res. Chem. Intermed.*, 2010, **36**, 1003–1019.

422 L. Haya, F. J. Sayago, A. M. Mainar, C. Cativiela and J. S. Urieta, *Phys. Chem. Chem. Phys.*, 2011, **13**, 17696–17703.

423 I. V. Vrček, D. Šakić, V. Vrček, H. Zipse and M. Biruš, *Org. Biomol. Chem.*, 2012, **10**, 1196–1206.

424 X. Lu, Z. Slanina, T. Akasaka, T. Tsuchiya, N. Mizorogi and S. Nagase, *J. Am. Chem. Soc.*, 2010, **132**, 5896–5905.

425 P. Gawrys, D. Djurado, J. Rimarcik, A. Kornet, D. Boudinet, J. M. Verilhac, V. Lukes, I. Wielgus, M. Zagorska and A. Pron, *J. Phys. Chem. B*, 2010, **114**, 1803–1809.

426 Y. Paukku and G. Hill, *J. Phys. Chem. A*, 2011, **115**, 4804–4810.

427 G. Gryn'ova and M. L. Coote, *J. Am. Chem. Soc.*, 2013, **135**, 15392–15403.

428 A. Kumar and M. D. Sevilla, *J. Phys. Chem. B*, 2011, **115**, 4990–5000.

429 L. K. Sviatenko, L. Gorb, F. C. Hill and J. Leszczynski, *J. Comput. Chem.*, 2013, **34**, 1094–1100.

430 P. J. Silva and M. J. Ramos, *Comput. Theor. Chem.*, 2011, **966**, 120–126.

431 M. Eslami, M. Namazian and H. R. Zare, *J. Phys. Chem. B*, 2013, **117**, 2757–2763.

432 J. A. Keith and E. A. Carter, *J. Am. Chem. Soc.*, 2012, **134**, 7580–7583.
433 C. H. Lim, A. M. Holder and C. B. Musgrave, *J. Am. Chem. Soc.*, 2013, **135**, 142–154.
434 Y. F. Liu, J. G. Yu, P. E. M. Siegbahn and M. R. A. Blomberg, *Chem. – Eur. J.*, 2013, **19**, 1942–1954.
435 D. Ghosh, A. Roy, R. Seidel, B. Winter, S. Bradforth and A. I. Krylov, *J. Phys. Chem. B*, 2012, **116**, 7269–7280.
436 C. K. Chua, M. Pumera and L. Rulisek, *J. Phys. Chem. C*, 2012, **116**, 4243–4251.
437 G. Roos, F. De Proft and P. Geerlings, *Chem. – Eur. J.*, 2013, **19**, 5050–5060.
438 R. J. O'Reilly, A. Karton and L. Radom, *J. Phys. Chem. A*, 2013, **117**, 460–472.
439 J. O. S. Varejao, L. C. A. Barbosa, C. R. A. Maltha, M. R. Lage, M. Lanznaster, J. W. M. Carneiro and G. Forlani, *Electrochim. Acta*, 2014, **120**, 334–343.
440 C. David and M. Enescu, *J. Phys. Chem. B*, 2010, **114**, 3020–3027.
441 A. C. Benniston, B. D. Allen, A. Harriman, I. Llarena, J. P. Rostron and B. Stewart, *New J. Chem.*, 2009, **33**, 417–427.
442 M. Kumar, W. Galezowski and P. M. Kozlowski, *Int. J. Quantum Chem.*, 2013, **113**, 479–488.
443 M. S. Formaneck, G. Li, X. Zhang and Q. Cui, *J. Theor. Comput. Chem.*, 2002, **1**, 53–67.
444 J. Kona and W. M. F. Fabian, *J. Chem. Theory Comput.*, 2011, **7**, 2610–2616.
445 M. R. Blomberg and P. E. Siegbahn, *Biochemistry*, 2012, **51**, 5173–5186.
446 M. R. Blomberg and P. E. Siegbahn, *Biochim. Biophys. Acta*, 2013, **1827**, 826–833.
447 M. Z. Ertem, C. J. Cramer, F. Himo and P. E. Siegbahn, *JBIC, J. Biol. Inorg. Chem.*, 2012, **17**, 687–698.
448 L. E. Roy, E. R. Batista and P. J. Hay, *Inorg. Chem.*, 2008, **47**, 9228–9237.
449 P. Surawatanawong and M. B. Hall, *Inorg. Chem.*, 2010, **49**, 5737–5747.
450 X. Zeng, H. Hu, X. Hu and W. Yang, *J. Chem. Phys.*, 2009, **130**, 164111.
451 N. Mehta and S. N. Datta, *J. Chem. Sci.*, 2007, **119**, 501–508.
452 N. Mehta and S. N. Datta, *Indian J. Phys.*, 2007, **81**, 851–869.
453 N. Mehta and S. N. Datta, *THEOCHEM*, 2008, **870**, 15–22.
454 W. G. Han and L. Noodleman, *Dalton Trans.*, 2009, 6045–6057.
455 W. G. Han, D. A. Giammona, D. Bashford and L. Noodleman, *Inorg. Chem.*, 2010, **49**, 7266–7281.
456 A. P. Gamiz-Hernandez, A. S. Galstyan and E. W. Knapp, *J. Chem. Theory Comput.*, 2009, **5**, 2898–2908.
457 K. B. Bravaya, M. G. Khrenova, B. L. Grigorenko, A. V. Nemukhin and A. I. Krylov, *J. Phys. Chem. B*, 2011, **115**, 8296–8303.
458 K. M. Solntsev, D. Ghosh, A. Amador, M. Josowicz and A. I. Krylov, *J. Phys. Chem. Lett.*, 2011, **2**, 2593–2597.
459 D. P. Bhave, W. G. Han, S. Pazicni, J. E. Penner-Hahn, K. S. Carroll and L. Noodleman, *Inorg. Chem.*, 2011, **50**, 6610–6625.
460 M. Kumar, H. Hirao and P. M. Kozlowski, *JBIC, J. Biol. Inorg. Chem.*, 2012, **17**, 1107–1121.
461 R. Borstnar, M. Repic, S. C. L. Kamerlin, R. Vianello and J. Mavri, *J. Chem. Theory Comput.*, 2012, **8**, 3864–3870.
462 M. Kumar and P. M. Kozlowski, *J. Inorg. Biochem.*, 2013, **126**, 26–34.
463 L. Billiet, P. Geerlings, J. Messens and G. Roos, *Free Radical Biol. Med.*, 2012, **52**, 1473–1485.
464 L. C. Xu, S. Shi, J. Li, S. Y. Liao, K. C. Zheng and L. N. Ji, *Dalton Trans.*, 2008, 291–301.
465 T. F. Miao, S. Li, Q. Chen, N. L. Wang and K. C. Zheng, *Inorg. Chim. Acta*, 2013, **407**, 37–40.
466 I. Chiorescu, D. V. Deubel, V. B. Arion and B. K. Keppler, *J. Chem. Theory Comput.*, 2008, **4**, 499–506.
467 N. J. Galant, H. Wang, D. R. Lee, Z. Mucsi, D. H. Setiadi, B. Viskolcz and I. G. Csizmadia, *J. Phys. Chem. A*, 2009, **113**, 9138–9149.
468 S. Zalis, R. F. Winter and W. Kaim, *Coord. Chem. Rev.*, 2010, **254**, 1383–1396.
469 M. Uchimiya, L. Gorb, O. Isayev, M. M. Qasim and J. Leszczynski, *Environ. Pollut.*, 2010, **158**, 3048–3053.
470 P. I. Djurovich, E. I. Mayo, S. R. Forrest and M. E. Thompson, *Org. Electron.*, 2009, **10**, 515–520.
471 P. Winget and J. L. Bredas, *J. Phys. Chem. C*, 2011, **115**, 10823–10835.
472 C. Bruno, F. Paolucci, M. Marcaccio, R. Benassi, C. Fontanesi, A. Mucci, F. Parenti, L. Preti, L. Schenetti and D. Vanossi, *J. Phys. Chem. B*, 2010, **114**, 8585–8592.
473 M. B. Camarada, P. Jaque, F. R. Diaz and M. A. del Valle, *J. Polym. Sci., Part B: Polym. Phys.*, 2011, **49**, 1723–1733.
474 B. N. Norris, S. P. Zhang, C. M. Campbell, J. T. Auletta, P. Calvo-Marzal, G. R. Hutchison and T. Y. Meyer, *Macromolecules*, 2013, **46**, 1384–1392.
475 S. Y. Sayed, J. A. Fereiro, H. Yan, R. L. McCreery and A. J. Bergren, *Proc. Natl. Acad. Sci. U. S. A.*, 2012, **109**, 11498–11503.
476 C. Karlsson, E. Jämstorp, M. Strømme and M. Sjödin, *J. Phys. Chem. C*, 2012, **116**, 3793–3801.
477 T. Marinado, D. P. Hagberg, M. Hedlund, T. Edvinsson, E. M. Johansson, G. Boschloo, H. Rensmo, T. Brinck, L. Sun and A. Hagfeldt, *Phys. Chem. Chem. Phys.*, 2009, **11**, 133–141.
478 M. Matsui, T. Shiota, Y. Kubota, K. Funabiki, J. Y. Jin, T. Yoshida, S. Higashijima and H. Miura, *Tetrahedron*, 2012, **68**, 4286–4291.
479 F. B. Anne, N. Galland and D. Jacquemin, *Int. J. Quantum Chem.*, 2012, **112**, 3763–3768.
480 X. F. Yang and M. H. Baik, *J. Am. Chem. Soc.*, 2004, **126**, 13222–13223.
481 F. Liu, J. J. Concepcion, J. W. Jurss, T. Cardolaccia, J. L. Templeton and T. J. Meyer, *Inorg. Chem.*, 2008, **47**, 1727–1752.
482 I. Romero, M. Rodriguez, C. Sens, J. Mola, M. Rao Kollipara, L. Francas, E. Mas-Marza, L. Escriche and A. Llobet, *Inorg. Chem.*, 2008, **47**, 1824–1834.

483 M. K. Tsai, J. Rochford, D. E. Polyansky, T. Wada, K. Tanaka, E. Fujita and J. T. Muckerman, *Inorg. Chem.*, 2009, **48**, 4372–4383.

484 F. Bozoglian, S. Romain, M. Z. Ertem, T. K. Todorova, C. Sens, J. Mola, M. Rodriguez, I. Romero, J. Benet-Buchholz, X. Fontrodona, C. J. Cramer, L. Gagliardi and A. Llobet, *J. Am. Chem. Soc.*, 2009, **131**, 15176–15187.

485 X. Sala, M. Z. Ertem, L. Vigara, T. K. Todorova, W. Z. Chen, R. C. Rocha, F. Aquilante, C. J. Cramer, L. Gagliardi and A. Llobet, *Angew. Chem., Int. Ed.*, 2010, **49**, 7745–7747.

486 L. P. Wang, Q. Wu and T. Van Voorhis, *Inorg. Chem.*, 2010, **49**, 4543–4553.

487 S. Ghosh and M. H. Baik, *Inorg. Chem.*, 2011, **50**, 5946–5957.

488 M. Busch, E. Ahlberg and I. Panas, *Phys. Chem. Chem. Phys.*, 2011, **13**, 15069–15076.

489 B. Radaram, J. A. Ivie, W. M. Singh, R. M. Grudzien, J. H. Reibenspies, C. E. Webster and X. Zhao, *Inorg. Chem.*, 2011, **50**, 10564–10571.

490 P. Liao, J. A. Keith and E. A. Carter, *J. Am. Chem. Soc.*, 2012, **134**, 13296–13309.

491 M. Z. Ertem, L. Gagliardi and C. J. Cramer, *Chem. Sci.*, 2012, **3**, 1293–1299.

492 L. Duan, C. M. Araujo, M. S. Ahlquist and L. Sun, *Proc. Natl. Acad. Sci. U. S. A.*, 2012, **109**, 15584–15588.

493 N. Kaveevivitchai, L. Kohler, R. Zong, M. El Ojaimi, N. Mehta and R. P. Thummel, *Inorg. Chem.*, 2013, **52**, 10615–10622.

494 X. Li and P. E. Siegbahn, *J. Am. Chem. Soc.*, 2013, **135**, 13804–13813.

495 M. T. M. Koper, *Faraday Discuss.*, 2008, **140**, 11–24.

496 W. Gao, J. A. Keith, J. Anton and T. Jacob, *J. Am. Chem. Soc.*, 2010, **132**, 18377–18385.

497 J. A. Keith and T. Jacob, *Angew. Chem., Int. Ed.*, 2010, **49**, 9521–9525.

498 A. B. Anderson, *Phys. Chem. Chem. Phys.*, 2012, **14**, 1330–1338.

499 F. T. Wagner, B. Lakshmanan and M. F. Mathias, *J. Phys. Chem. Lett.*, 2010, **1**, 2204–2219.

500 J. Rossmeisl, J. K. Norskov, C. D. Taylor, M. J. Janik and M. Neurock, *J. Phys. Chem. B*, 2006, **110**, 21833–21839.

501 K. Shiratori and K. Nobusada, *J. Phys. Chem. A*, 2008, **112**, 10681–10688.

502 M. T. M. Koper, *J. Electroanal. Chem.*, 2011, **660**, 254–260.

503 F. Calle-Vallejo and M. T. M. Koper, *Electrochim. Acta*, 2012, **84**, 3–11.

504 S. J. Luo, Y. Zhao and D. G. Truhlar, *J. Phys. Chem. Lett.*, 2012, **3**, 2975–2979.

505 L. K. Bieniasz, G. Maroulis and T. E. Simos, *AIP Conf. Proc.*, 2007, **963**, 481–486.

506 D. H. Evans, *Chem. Rev.*, 2008, **108**, 2113–2144.

507 J. Schneider, H. Jia, J. T. Muckerman and E. Fujita, *Chem. Soc. Rev.*, 2012, **41**, 2036–2051.

508 C. J. Cramer and D. G. Truhlar, *Phys. Chem. Chem. Phys.*, 2009, **11**, 10757–10816.

509 J. P. Perdew, *Phys. Rev. B: Condens. Matter Mater. Phys.*, 1986, **33**, 8822–8824.

510 V. S. Bryantsev, M. S. Diallo, A. C. van Duin and W. A. Goddard, 3rd, *J. Phys. Chem. A*, 2008, **112**, 9104–9112.

511 W. Bottcher, G. M. Brown and N. Sutin, *Inorg. Chem.*, 1979, **18**, 1447–1451.

512 D. T. Richens, *The Chemistry of Aqua Ions*, Wiley, New York, 1997, p. 397.

513 L. Rulisek, *J. Phys. Chem. C*, 2013, **117**, 16871–16877.

514 M. Srnec, J. Chalupsky, M. Fojta, L. Zendlova, L. Havran, M. Hocek, M. Kyvala and L. Rulisek, *J. Am. Chem. Soc.*, 2008, **130**, 10947–10954.

515 H. J. C. Berendsen, J. R. Grigera and T. P. Straatsma, *J. Phys. Chem.*, 1987, **91**, 6269–6271.

516 X. Zeng, H. Hu, X. Hu, A. J. Cohen and W. Yang, *J. Chem. Phys.*, 2008, **128**, 124510.

517 J. Blumberger, *J. Am. Chem. Soc.*, 2008, **130**, 16065–16068.

518 R. Seidel, M. Faubel, B. Winter and J. Blumberger, *J. Am. Chem. Soc.*, 2009, **131**, 16127–16137.

519 J. Moens, R. Seidel, P. Geerlings, M. Faubel, B. Winter and J. Blumberger, *J. Phys. Chem. B*, 2010, **114**, 9173–9182.

520 N. Troullier and J. L. Martins, *Phys. Rev. B: Condens. Matter Mater. Phys.*, 1991, **43**, 1993–2006.

521 M. Jaworska, *Chem. Phys.*, 2007, **332**, 203–210.

522 A. D. Follett, K. A. McNabb, A. A. Peterson, J. D. Scanlon, C. J. Cramer and K. McNeill, *Inorg. Chem.*, 2007, **46**, 1645–1654.

523 M. T. de Groot and M. T. Koper, *Phys. Chem. Chem. Phys.*, 2008, **10**, 1023–1031.

524 M. Kato, S. Izuka, T. Fujihara, A. Nagasawa, S. Kawai, T. Tanaka and T. Takayanagi, *Inorg. Chim. Acta*, 2011, **370**, 304–310.

525 B. F. Gherman, W. B. Tolman and C. J. Cramer, *J. Comput. Chem.*, 2006, **27**, 1950–1961.

526 L. M. R. Hill, B. F. Gherman, N. W. Aboelella, C. J. Cramer and W. B. Tolman, *Dalton Trans.*, 2006, 4944–4953.

527 J. P. Holland, J. C. Green and J. R. Dilworth, *Dalton Trans.*, 2006, 783–794.

528 J. P. Holland, P. J. Barnard, D. Collison, J. R. Dilworth, R. Edge, J. C. Green, J. M. Heslop, E. J. L. McInnes, C. G. Salzmann and A. L. Thompson, *Eur. J. Inorg. Chem.*, 2008, 3549–3560.

529 D. Schultz, F. Biaso, A. R. M. Shahi, M. Geoffroy, K. Rissanen, L. Gagliardi, C. J. Cramer and J. R. Nitschke, *Chem. – Eur. J.*, 2008, **14**, 7180–7185.

530 H. Vazquez-Lima and P. Guadarrama, *Int. J. Quantum Chem.*, 2012, **112**, 1431–1438.

531 T. Lovell, T. Liu, D. A. Case and L. Noodleman, *J. Am. Chem. Soc.*, 2003, **125**, 8377–8383.

532 R. Wang, M. A. Camacho-Fernandez, W. Xu, J. Zhang and L. Li, *Dalton Trans.*, 2009, 777–786.

533 P. Surawatanawong, J. W. Tye, M. Y. Darensbourg and M. B. Hall, *Dalton Trans.*, 2010, **39**, 3093–3104.

534 W. G. Han and L. Noodleman, *Inorg. Chem.*, 2011, **50**, 2302–2320.

535 P. Surawatanawong, S. Sproules, F. Neese and K. Wieghardt, *Inorg. Chem.*, 2011, **50**, 12064–12074.

536 D. A. Khobragade, S. G. Mahamulkar, L. Pospisil, I. Cisarova, L. Rulisek and U. Jahn, *Chem. – Eur. J.*, 2012, **18**, 12267–12277.

537 T. Wondimagegn and A. Rauk, *J. Phys. Chem. B*, 2012, **116**, 10301–10310.
538 G. Gopakumar, P. Belanzoni and E. J. Baerends, *Inorg. Chem.*, 2012, **51**, 63–75.
539 L. E. Grove, J. Xie, E. Yikilmaz, A. F. Miller and T. C. Brunold, *Inorg. Chem.*, 2008, **47**, 3978–3992.
540 A. E. Kuznetsov, Y. V. Geletii, C. L. Hill and D. G. Musaev, *J. Phys. Chem. A*, 2010, **114**, 11417–11424.
541 S. Nandi, D. Bannerjee, J. S. Wu, T. H. Lu, A. M. Z. Slawin, J. D. Woollins, J. Ribas and C. Sinha, *Eur. J. Inorg. Chem.*, 2009, 3972–3981.
542 D. A. Jiao, K. Leung, S. B. Rempe and T. M. Nenoff, *J. Chem. Theory Comput.*, 2011, **7**, 485–495.
543 P. Song, W. Guan, L. Yan, C. Liu, C. Yao and Z. Su, *Dalton Trans.*, 2010, **39**, 3706–3713.
544 N. N. Ma, S. L. Sun, C. G. Liu, X. X. Sun and Y. Q. Qiu, *J. Phys. Chem. A*, 2011, **115**, 13564–13572.
545 M. Buhl, H. Fruchtl and P. Andre, *Chem. Phys. Lett.*, 2011, **509**, 158–161.
546 T. F. Hughes and R. A. Friesner, *J. Chem. Theory Comput.*, 2012, **8**, 442–459.
547 J. J. Berard, G. Schreckenbach, P. L. Arnold, D. Patel and J. B. Love, *Inorg. Chem.*, 2008, **47**, 11583–11592.
548 T. Matsui, Y. Kitagawa, Y. Shigeta and M. Okumurat, *J. Chem. Theory Comput.*, 2013, **9**, 2974–2980.
549 D. E. Haines, D. C. O'Hanlon, J. Manna, M. K. Jones, S. E. Shaner, J. Sun and M. D. Hopkins, *Inorg. Chem.*, 2013, **52**, 9650–9658.
550 G. Saha, K. K. Sarkar, P. Datta, P. Raghavaiah and C. Sinha, *Polyhedron*, 2010, **29**, 2098–2104.
551 S. Masaoka, Y. Mukawa and K. Sakai, *Dalton Trans.*, 2010, **39**, 5868–5876.
552 M. K. Ludlow, A. V. Soudackov and S. Hammes-Schiffer, *J. Am. Chem. Soc.*, 2010, **132**, 1234–1235.
553 B. H. Solis and S. Hammes-Schiffer, *Inorg. Chem.*, 2011, **50**, 11252–11262.
554 H. Lei, A. Han, F. Li, M. Zhang, Y. Han, P. Du, W. Lai and R. Cao, *Phys. Chem. Chem. Phys.*, 2014, **16**, 1883–1893.
555 C. C. Scarborough, S. Sproules, T. Weyhermuller, S. DeBeer and K. Wieghardt, *Inorg. Chem.*, 2011, **50**, 12446–12462.
556 A. M. Khenkin, I. Efremenko, L. Weiner, J. M. Martin and R. Neumann, *Chem. – Eur. J.*, 2010, **16**, 1356–1364.
557 S. Jameh-Bozorghi, M. Darvishpour, S. Mostghiman and Z. Javanshir, *Int. J. Electrochem. Sci.*, 2011, **6**, 4891–4899.
558 E. Mosconi, J. H. Yum, F. Kessler, C. J. Gomez Garcia, C. Zuccaccia, A. Cinti, M. K. Nazeeruddin, M. Gratzel and F. De Angelis, *J. Am. Chem. Soc.*, 2012, **134**, 19438–19453.
559 R. Jono, M. Sumita, Y. Tateyama and K. Yamashita, *J. Phys. Chem. Lett.*, 2012, **3**, 3581–3584.
560 M. Gheidi, N. Safari and M. Zahedi, *Inorg. Chem.*, 2012, **51**, 12857–12866.
561 M. P. Santoni, F. Nastasi, S. Campagna, G. S. Hanan, B. Hasenknopf and I. Ciofini, *Dalton Trans.*, 2013, **42**, 5281–5291.
562 H. Kim, J. Park and Y. S. Lee, *J. Comput. Chem.*, 2013, **34**, 2233–2241.
563 L. Castro and M. Bühl, *J. Chem. Theory Comput.*, 2014, **10**, 243–251.
564 M. Swart, *Chem. Commun.*, 2013, **49**, 6650–6652.
565 T. Lovell, F. Himo, W. G. Han and L. Noodleman, *Coord. Chem. Rev.*, 2003, **238**, 211–232.
566 L. Noodleman, T. Lovell, T. Q. Liu, F. Himo and R. A. Torres, *Curr. Opin. Chem. Biol.*, 2002, **6**, 259–273.
567 M. van den Bosch, M. Swart, J. G. Snijders, H. J. Berendsen, A. E. Mark, C. Oostenbrink, W. F. van Gunsteren and G. W. Canters, *ChemBioChem*, 2005, **6**, 738–746.
568 D. Si and H. Li, *J. Phys. Chem. A*, 2009, **113**, 12979–12987.
569 T. A. Jackson, C. T. Gutman, J. Maliekal, A. F. Miller and T. C. Brunold, *Inorg. Chem.*, 2013, **52**, 3356–3367.
570 W. G. Han, T. Lovell and L. Noodleman, *Inorg. Chem.*, 2002, **41**, 205–218.
571 M. H. Huynh and T. J. Meyer, *Chem. Rev.*, 2007, **107**, 5004–5064.
572 D. R. Weinberg, C. J. Gagliardi, J. F. Hull, C. F. Murphy, C. A. Kent, B. C. Westlake, A. Paul, D. H. Ess, D. G. McCafferty and T. J. Meyer, *Chem. Rev.*, 2012, **112**, 4016–4093.
573 Y. Matsubara, E. Fujita, M. D. Doherty, J. T. Muckerman and C. Creutz, *J. Am. Chem. Soc.*, 2012, **134**, 15743–15757.
574 Y. Hirai, T. Kojima, Y. Mizutani, Y. Shiota, K. Yoshizawa and S. Fukuzumi, *Angew. Chem., Int. Ed.*, 2008, **47**, 5772–5776.
575 J. L. Dempsey, A. J. Esswein, D. R. Manke, J. Rosenthal, J. D. Soper and D. G. Nocera, *Inorg. Chem.*, 2005, **44**, 6879–6892.
576 H. Yamazaki, A. Shouji, M. Kajita and M. Yagi, *Coord. Chem. Rev.*, 2010, **254**, 2483–2491.
577 P. Miró, M. Z. Ertem, L. Gagliardi and C. J. Cramer, in *Molecular Water Oxidation Catalysts*, ed. A. Llobet, John Wiley & Sons, Chichester, 2014, p. 231.
578 M. Z. Ertem and C. J. Cramer, *Dalton Trans.*, 2012, **41**, 12213–12219.
579 S. M. Barnett, K. I. Goldberg and J. M. Mayer, *Nat. Chem.*, 2012, **4**, 498–502.
580 Z. L. Lang, G. C. Yang, N. N. Ma, S. Z. Wen, L. K. Yan, W. Guan and Z. M. Su, *Dalton Trans.*, 2013, **42**, 10617–10625.
581 P. E. Siegbahn, *Biochim. Biophys. Acta*, 2013, **1827**, 1003–1019.
582 D. Hong, S. Mandal, Y. Yamada, Y. M. Lee, W. Nam, A. Llobet and S. Fukuzumi, *Inorg. Chem.*, 2013, **52**, 9522–9531.
583 A. Kazaryan and E. J. Baerends, *J. Comput. Chem.*, 2013, **34**, 870–878.
584 S. Maji, I. Lopez, F. Bozoglian, J. Benet-Buchholz and A. Llobet, *Inorg. Chem.*, 2013, **52**, 3591–3593.
585 M. T. Zhang, Z. Chen, P. Kang and T. J. Meyer, *J. Am. Chem. Soc.*, 2013, **135**, 2048–2051.
586 Z. Chen and T. J. Meyer, *Angew. Chem., Int. Ed.*, 2013, **52**, 700–703.
587 N. Planas, L. Vigara, C. Cady, P. Miro, P. Huang, L. Hammarstrom, S. Styring, N. Leidel, H. Dau, M. Haumann, L. Gagliardi, C. J. Cramer and A. Llobet, *Inorg. Chem.*, 2011, **50**, 11134–11142.

588 K. Tanaka, H. Isobe, S. Yamanaka and K. Yamaguchi, *Proc. Natl. Acad. Sci. U. S. A.*, 2012, **109**, 15600–15605.
589 S. Roeser, M. Z. Ertem, C. Cady, R. Lomoth, J. Benet-Buchholz, L. Hammarstrom, B. Sarkar, W. Kaim, C. J. Cramer and A. Llobet, *Inorg. Chem.*, 2012, **51**, 320–327.
590 L. Vigara, M. Z. Ertem, N. Planas, F. Bozoglian, N. Leidel, H. Dau, M. Haumann, L. Gagliardi, C. J. Cramer and A. Llobet, *Chem. Sci.*, 2012, **3**, 2576–2586.
591 M. Hirahara, M. Z. Ertem, M. Komi, H. Yamazaki, C. J. Cramer and M. Yagi, *Inorg. Chem.*, 2013, **52**, 6354–6364.
592 S. G. Winikoff and C. J. Cramer, *Catal. Sci. Technol.*, DOI: 10.1039/c4cy00500g.
593 A. Singh and L. Spiccia, *Coord. Chem. Rev.*, 2013, **257**, 2607–2622.
594 I. C. Man, H. Y. Su, F. Calle-Vallejo, H. A. Hansen, J. I. Martinez, N. G. Inoglu, J. Kitchin, T. F. Jaramillo, J. K. Norskov and J. Rossmeisl, *ChemCatChem*, 2011, **3**, 1159–1165.
595 M. Bajdich, M. Garcia-Mota, A. Vojvodic, J. K. Norskov and A. T. Bell, *J. Am. Chem. Soc.*, 2013, **135**, 13521–13530.
596 E. J. Sundstrom, X. Yang, V. S. Thoi, H. I. Karunadasa, C. J. Chang, J. R. Long and M. Head-Gordon, *J. Am. Chem. Soc.*, 2012, **134**, 5233–5242.
597 K. P. Jensen and U. Ryde, *J. Phys. Chem. A*, 2003, **107**, 7539–7545.

